Hybrid CFRP-CNT Micro-nanocomposites with Improved Fracture Toughness and Integrated Damage Sensing Capability

SUBMITTED IN PARTIAL FULFILLMENT OF THE REQUIREMENTS

OF THE DEGREE OF DOCTOR OF PHILOSOPHY

August 2015

Han Zhang

School of Engineering and Materials Science

Queen Mary University of London

Mile End Road, London, E1 4NS

Declaration

I declare that the work performed is entirely by myself during the course of my Ph.D studies at the Queen Mary University of London and has not been submitted for a degree at this or any other University.

Han Zhang

Acknowledgements

There are always something you have to experience them yourself to truly understand, and obtaining a PhD is definitely one of these things. Expectation, learning, hardworking, reviewing, struggling, all of these steps were important during my PhD studies, leading me to the next level.

I would like to take this opportunity to first thank my parents for their great support and understanding throughout my life. I know they've been expecting my PhD graduation for a while, but never put pressure on me.

My greatest acknowledgement and appreciation is given to my supervisors and very good friends, Prof. Ton Peijs, and Dr. Emiliano Bilotti. Thank you for not only guiding and sharing me all these knowledge and skills, also mentoring and supporting me in all aspects over these years. It was my great honour to work under Ton and Emiliano's supervision, and I really enjoyed all the time.

I would like to acknowledge European FP7 IMS&CPS project for the financial supports, as well as my collaborators within the project.

Special thanks are given to my lovely girlfriend Lu Zhao. Thank you for your understanding and patience, and your great support throughout my life these years.

I would also like to thank all my talented and hardworking colleagues for all the discussions, knowledge sharing, and all the help. Thanks are given to Dr. Wei Tu, Dr. Jia Ma, Dr. Manabu Kuwata, Dr. Olivier Picot, Dr. Charline Sellam, Dr. Nanayaa Hughes-Brittain, Dr. Jian Yao, Dr. Fang Mai, Ms Anisha Bharti, Mr Zheng Li, and Ms Yi Liu.

Carrying out this PhD has been one of the most important periods in my life, and I do believe this process has helped me to become a better person.

Abstract

This thesis aims to utilize conductive carbon nanotube (CNT) networks in fibre reinforced plastics (FRPs) for integrated damage sensing functionalities. Different routes, including dissolvable thermoplastic carriers and direct spray coating techniques were employed for CNT delivery and localization in damage prone zones in composite laminates. Thermoplastic as well as thermoplastic/thermoset binary systems incorporating CNTs were studied, with a focus on electrical properties of the resulting nanocomposites and dissolution behaviour of the thermoplastic in the thermoset. Nanotube modified thermoplastic interleaves as well as direct CNT spray coating onto fibre preforms showed mechanical property improvement through increased interlaminar toughness.

Percolated sprayed CNT networks have also been used as a sensitive tool for *in-situ* damage detection, and internal crack propagation during a standard composite test has been monitored by electrical sensing signals. Both interlaminar fracture toughness and interlaminar shear strength tests were performed in combination with *in-situ* damage sensing, and an excellent correlation between sensing signals and mechanical response was observed. These sensing signals have been used to determine internal crack propagation as well as damage levels during testing, with the potential for structural health monitoring.

Table of Contents

Chapter 7

List of Tables

List of Figures

Chapter 1

General Introduction

1.1 Fibre reinforced plastics – strength and limitations

As composites generally refer to materials consisting of at least two chemically distinct phases, fibre reinforced plastics (FRPs) refer to those composites consisting of a polymeric matrix and reinforcing fibres. Examples are carbon fibre reinforced plastics (CFRPs) and glass fibre reinforced plastics (GFRPs). Due to their high specific strength and stiffness, lightweight, good corrosion resistance, especially for structural applications, the market demand for FPRs has continuously increased during the last few decades [1] and increasing amounts of CFRPs had been recently employed in aircraft structures, replacing traditional metal components (Fig. 1.1).

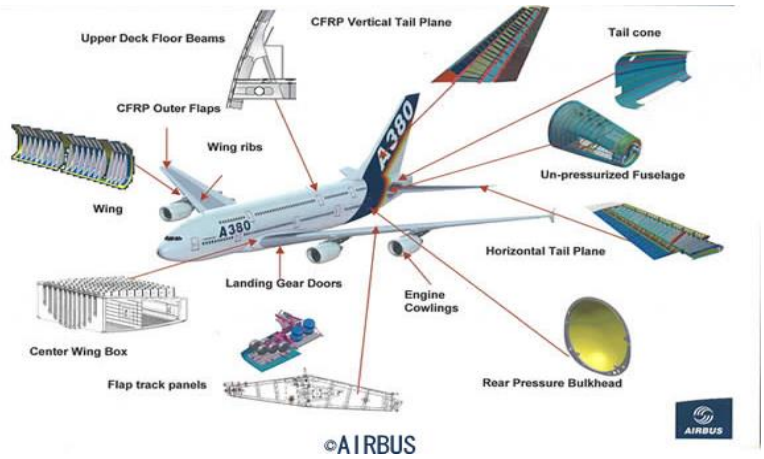

Fig. 1.**1** The use of CFRPs in A380 aircraft (picture source: AIRBUS®) [2], showing major components that using CFRP such as wing sections and fuselage.

However, due to the laminated nature of most FRPs, outstanding in-plane properties are typically accompanied with relatively weak out-of-plane performance. Various interfaces generated by alternating fibre/matrix layers often lead to component failure like delamination, not to mention other early stage failures such as micro-cracking or fibre/matrix debonding. In particular, delaminations severely reduce the strength of FRPs, especially in compression, resulting in reduced performance of components. For this reason, the improvement of out-of-plane properties and damage resistance has been an important aspect for consideration for many years when manufacturing or designing composite materials and structures.

1.2 Nano-engineered hierarchical composites

Nature is always one of the best teachers for the materials scientist. After hundreds of thousands of years of evolution, the bone structure within every human body which consists of hierarchically structured materials with nano- to macro-scale organisations has developed into one of the strongest natural composites in the world. The secret of bone is not only the collagen nanomaterials it possesses, but also the way all these materials are organised, forming one of the best examples of a hierarchical composite (Fig. 1.2). Another good example is wood, where cellulose fibres are acting as reinforcing fibres within lignin matrices, building up optimized layered structures to reach good combinations of strength, stiffness, and toughness.

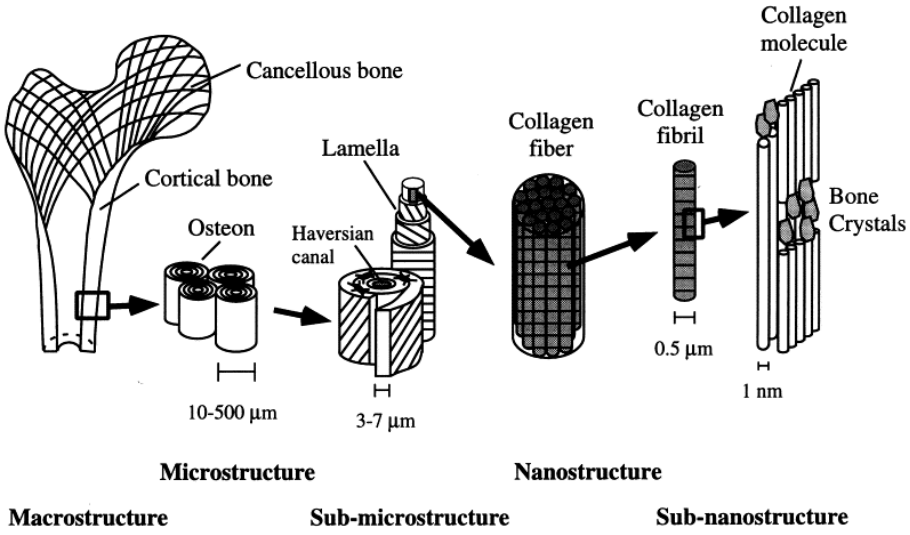

Fig. 1.2 Hierarchical structure of bone [3].

With todays' evolutionary progress in technologies, nanomaterials such as carbon nanotubes (CNTs) have already been commercialized and scaled-up for large production. With the availability of nanomaterials such as CNTs and graphene it becomes possible to develop man-made hierarchical materials with structural organizations from the nano-scale to the macro-scale, mimicking nature derived structural materials with tailored composites properties. Therefore, it is not surprised that various recent research works [4-6] have been focussing on nanoengineered composites by combining CNTs together with traditional reinforcements such as carbon fibres with the aim of property enhancement.

1.3 Structural health monitoring and damage sensing

Since most damage in composites are non-visible, e.g. internal delamination after impact, structural health monitoring (SHM) and damage detection is another very

important issue for large scale acceptance of composites in structural applications such as aerospace and infrastructure where safety standards are always top priority. Over the years, various non-destructive testing (NDT) methods have been developed for the inspection of the internal integrity of composites for quality control as well as in-service maintenance purposes, including ultrasonic testing and acoustic emission. Unfortunately, it is not always feasible to examine each composite part before assembly. For aircraft manufacturers, only limited numbered components can be examined, hence highest repeatability is required for all processes. Not to mention the down-time associated with these NDT methods, raising running costs of aircrafts.

Again, scientists have here also been inspired by nature to overcome this challenge. Efforts on fully integrated SHM systems in next generation aircraft are now being mimicked to the neuron system of humans, as illustrated in Fig. 1.3.

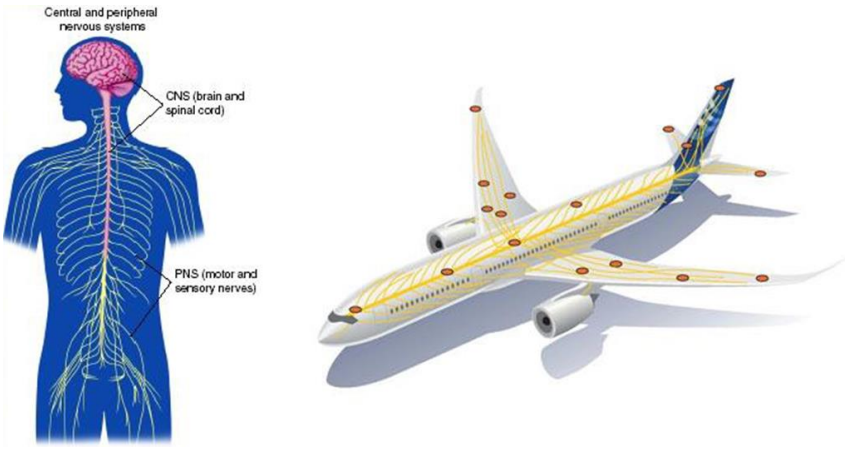

Fig. 1.3 Illustration of human neuron system (left), and fully integrated sensory network in aircraft (right, picture source: *Holger Speckmann, AIRBUS*®) [7].

1.4 Aim and outline of thesis

In this thesis, the aim is to utilize CNTs as nano-scaled reinforcements, to not only improve the mechanical performance of FRPs, but also use their excellent electrical conductivity to develop an integrated damage sensing capability into such nano-engineered composites. To build up such a composite material in the correct hierarchical order similar to nature, two different methods have been employed. The first method is based on the use of a dissolvable thermoplastic carrier, while the second method uses a direct localized deposition method through spraying.

Background knowledge of typical failure modes in composites, with the focus on delamination failure is presented in Chapter 2, together with a detailed review on various toughening methods for composites. Brief information on traditional NDT methods is provided, followed by a comprehensive review on the utilization of CNTs for damage sensing in FRPs.

Phenoxy, an epoxy-dissolvable thermoplastic, was employed to act as a carrier for introducing CNTs in epoxy based laminated composites. Two binary systems of thermoplastic/CNT and thermoplastic/thermoset were studied in Chapter 3 and Chapter 4, respectively. Focus was given on electrical properties of these nanocomposites in Chapter 3, while the dissolution behaviour of thermoplastic in thermoset is studied in Chapter 4.

Chapter 5 focuses on interlaminar toughening using thermoplastic phenoxy interleaves in FRPs. Different forms of thermoplastic interleaves such as electrospun nanofibre non-woven mats and continuous films were incorporated in composite laminates, and their toughening effect was studied and compared. The toughening effect of CNT modified thermoplastic interleaves was also studied.

A simple but innovative spray coating technique for direct CNT deposition into FRPs with controlled localization is presented in Chapter 6, and good toughening effects are reported at extremely low CNT loadings in comparison with previous literature results.

The integrated damage sensing capability of hybrid micro-nanocomposites was examined in Chapter 7 by utilizing an electrical method. *In-situ* damage sensing tests were performed on standard composite tests, providing potential to apply the obtained results to real industrial applications.

In short, enhanced out-of-plane performance and integrated damage sensing capabilities, of nano-engineered hierarchical composite laminates are presented in this thesis with the potential of localized toughening and sensing effects, with the aim to develop multifunctional composite materials capable of in-service damage detection, while at the same time improving out-of-plane laminate properties. Additionally, the enhanced electrical conductivity will also be examined with the objective of partially replacing current copper mesh in aircraft for lighting strike protection purposes.

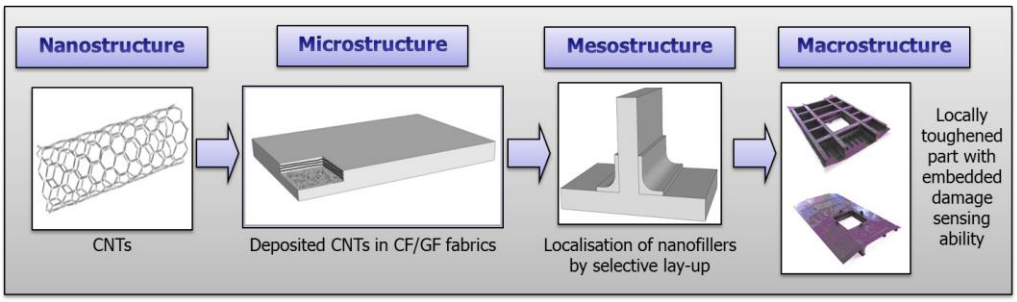

Fig. 1.4 Illustration of nano-engineered hierarchical composites.

Chapter 2

Literature Review

2.1 Introduction

In this chapter, a literature review on the topic of fracture mechanisms in fibre reinforced plastics (FRPs) is presented, with the focus on interlaminar fracture toughness and various toughening routes, including the addition of traditional liquid rubber, thermoplastics and nanofillers. Additionally, traditional non-destructive testing methods have been reviewed and compared, with their specialties and limitations. Special effort on the use of carbon nanotubes as multifunctional fillers for damage sensing and health monitoring of FRPs is made.

2.2 Composite failure modes

Various failure modes can be identified during the usage of composite components, including matrix cracking, delamination, debonding at fibre/matrix interfacial region, fibre pull-out, and fibre breakage. Different failure modes are promoted or combined depending on the load bearing conditions of components. Unlike traditional materials such as metals which possess large ductility and damage or cracks that can often be observed externally, failures in FRPs can be internal and non-visible from the outside. Therefore, a clear understanding of these various failure modes when replacing traditional metals by FRPs is a necessity.

In this section, a brief introduction is presented for the main composite failure mechanisms, with a focus on delamination failure which is the most relevant failure mode to this thesis.

2.2.1 Matrix micro-cracking

In most cases, matrix micro-cracking is the earliest form of damage in composites [8, 9], e.g. in $[0/90]_s$ laminates where matrix cracking is formed within $90°$ plies upon loading. Normally the required critical strain is decreasing with the increased thickness of $90°$ plies [10-13]. Alternative terminology for matrix cracking includes micro-cracking, transverse cracking, and ply cracking, based on their initiation and propagating direction. Although the first micro-crack will only have limited effect on FRPs properties, multiple micro-cracking normally occurs very rapidly after the first crack present, resulting in a more obvious softening effect. Apart from the direct effect of micro-cracking in FRPs on property degradation, this type of damage can also lead to other forms of failure such as delaminations and fibre breakages. Therefore, over the years a large amount of research has been devoted to matrix cracking, and various methods for its analysis have been purposed [8]. A number of detailed reviews on this topic can be found in literature [8, 9, 14, 15].

2.2.2 Interfacial de-bonding

Since FRPs consist of fibres and matrix, the failure occurring at the interface between fibre and matrix is referred to fibre/matrix interfacial debonding [16-19]. Obviously the weakest part within the composites is normally failing earliest upon loading. Hence, when the fibre/matrix interfacial strength is lower than that of matrix (or fibre), debonding will occur at those interfaces.

Interfacial properties can be modified through surface modification of reinforcing fibres, increasing their surface energy and therefore improve the wetting of resin matrix on fibre. The field of fibre surface modification for different resins has been well established over the last few decades [14, 20], and numerous commercialized products could be found in the market. To evaluate the interfacial properties between fibre and matrix, pull-out test, micro-tension test, micro-compression test, and fragmentation test are usually applied.

2.2.3 Fibre pull-out

Fibre pull-out occurs when the transferred load is greater than the interfacial strength of fibre and matrix but smaller than that to cause fibre or matrix failure [12-15, 21]. If numerous fibre pull-outs are present during fractograpy, typically this is an indication that the interfacial bonding between fibre and matrix needs to be improved in order to obtain better stress transfer and tensile strength of composites. However, a too strong interface and too little debonding will lead to brittle fracture of the composites with little fibre pull-out and interfacial sliding failure processes, all capable of absorbing energy and contributing to the toughness of the composites [22]. Single fibre pull-out tests are often been carried out as one of the major characterization of fibre/matrix interfacial adhesion.

2.2.4 Fibre breakage

In multi-directional laminates, fibre breakage is typically occurring in the latter stages of a components life, which can severely reduce both stiffness and strength of composite laminates. Fibre breakage is a cumulative process, with interactions between individual fibre breaks eventually leading to clustering of breaks and final component failure.

2.2.5 Delamination and interlaminar fracture toughness

Due to the laminated nature of FRPs, the in-plane properties which consist of reinforcing fibres are excellent while the mechanical performance in out-of-plane direction which is solely dependent on the bonding between layers is relatively poor. Delamination between plies is one of the most important failure modes that can happen under various loading conditions such as tension, compression, low velocity impact, etc., limiting their service life [23, 24]. Two main routes could be applied to improve the delamination resistance as well as fracture toughness: either improving the mechanical properties of matrix materials or through the modification of fibre architecture [24-26]. Since delamination and interlaminar fracture toughness is the focus of this thesis, a more detailed review on toughening of laminated composites is given in this section.

2.3 Toughening routes for laminate composites

In this section, the concept of interlaminar fracture toughness as well as standard testing methods is described. Various toughening routes including materials property modification and fibre architecture modification are introduced. Interleave toughening as well as micro-nano hybrid composites are reviewed in more detail, due to their relevancy to this thesis.

2.3.1 Interlaminar fracture toughness

Toughness of materials represents the energy required to cause failure. In many situations such as composites under impact, toughness rather than strength is usually been used to determine the suitability of the material [22]. For fracture to occur, the

energy required has to exceed a critical value which is depended on several factors. This critical fracture energy (G_c) for a system with a pre-determined crack size (c) is expressed in Equation 2.1 [22] with the unit of Jm^{-2}, where E is the Young's modulus, and σ_* is the critical stress. The fracture toughness K_c (which also known as critical stress intensity factor) is presented in Equation 2.2 with the unit of $MPa\sqrt{m}$, where σ_* is the critical stress, c is the existing crack size, and G_c is the fracture energy.

$$G_c = \frac{\sigma_*^2 \pi c}{E} \qquad \text{(Equation 2. 1)}$$

$$K_c = \sigma_* \sqrt{\pi c} = \sqrt{E G_c} \qquad \text{(Equation 2. 2)}$$

For tough materials such as metals, the fracture energy is in the order of 100 kJm^{-2}, while for brittle materials like ceramics or glasses, only 0.01 kJm^{-2}. Although both glass fibre and epoxy are very brittle, their composites have a fairly high fracture energy of around 50 kJm^{-2} [22]. This is attributed to the large amount of interface generated between the two phases, as discussed earlier, during fracture such as fibre pull-out, debonding or interfacial sliding, all of these responsible for the large amount of energy that can be absorbed by composites, leading to increased toughness of composites.

For composites which consist of two or more constituents, to determine the fracture toughness is even more complex as different failure modes or surface properties can all contribute. To evaluate the interlaminar fracture toughness of composites, three types of fracture modes can be used: Mode-I (tensile opening mode) which is also known as double beam cantilever (DCB) test, Mode-II (in-plane shear mode), and

Mode-III (out-of-plane shear mode). Illustrations of each fracture mode are shown in Fig. 2.1. As the Mode-II and Mode-III tests are more complex and controversial [27], Mode-I opening mode tests are more widely used to determine the fracture toughness of laminates.

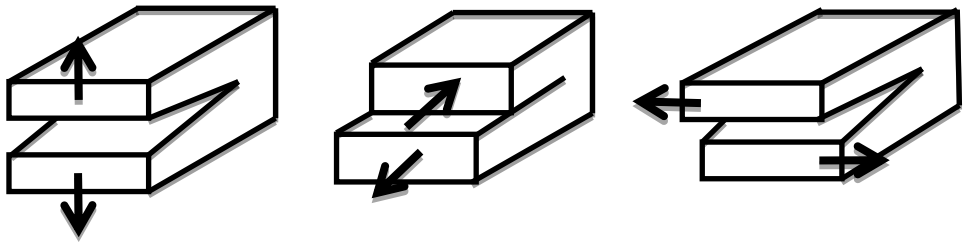

Fig. 2.1 Schematic illustrations on different fracture modes; from left to right: Mode-I, Mode-II, and Mode-III.

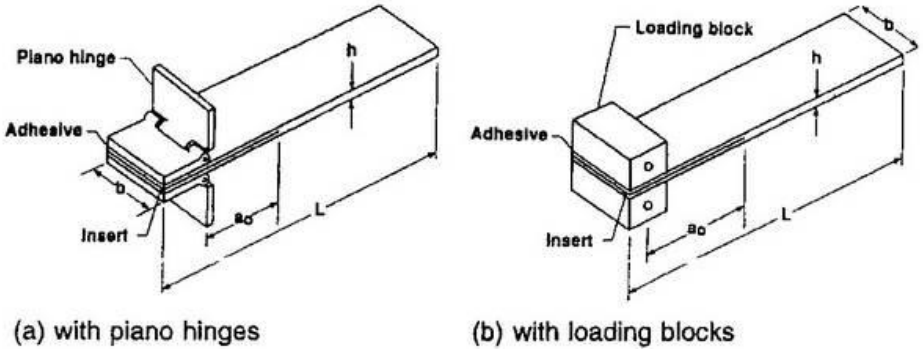

Fig. 2.2 Illustration of Double Cantilever Beam Specimen [29].

Various testing methods for delamination resistance had been reviewed by Davies [27], and testing standards have been provided by both ISO and ASTM [28, 29]. Throughout this work, ASTM D5528 was used to determine the Mode-I interlaminar fracture toughness of laminated composites.

For data calculation and interpretation, three methods have been proposed, including modified beam theory (MBT), compliance calibration method (CC), and modified compliance calibration method (MCC). Due to the very limited variation (less than

3%) in calculated results among above methods, as well as the recommendation from the ASTM standard, here the MBT method was applied to calculate the G_{IC} value.

In beam theory, the fracture toughness G_I is calculated as in Equation 2.3 below:

$$G_I = \frac{3P\delta}{2ba} \qquad \text{(Equation 2. 3)}$$

Where P is applied load, δ is displacement under applied load, b is specimen width, and a is delamination length (crack length).

However, due to possible rotation at the delamination front or other imperfect beam build-in practice, G_I value is normally overestimated. In MBT theory, a slightly longer delamination, $a + |\Delta|$, has been applied to correct this. The value of $|\Delta|$ is determined experimentally as $C^{1/3}$, as showing in Fig. 2.3 below.

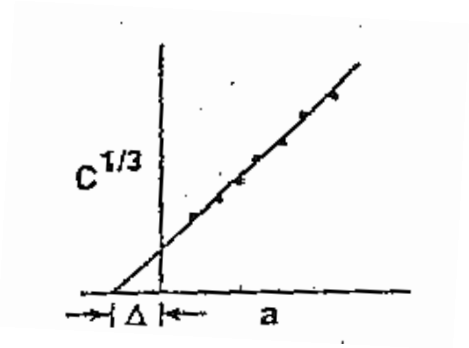

Fig. 2.3 The modified beam theory (MBT) correction for delamination length [29].

Therefore the value of Mode-I interlaminar fracture toughness given by MBT is as follows:

$$G_I = \frac{3P\delta}{2b(a+|\Delta|)} \qquad \text{(Equation 2. 4)}$$

2.3.2 Toughening methods for composites

One of the main routes to improve the fracture toughness of composite laminates is through the improvement of properties of materials, including toughening of the

brittle matrix, fibre coatings or surface treatments. In this section, various material modification routes for toughening are reviewed, including matrix modification (liquid rubber, thermoplastics, nanoparticles), and interface/interleaf modifications.

Matrix modification

As discussed earlier, highly crosslinked thermosetting matrix materials such as epoxies are very brittle and possess relatively low toughness. Because of this, the research topic of adding ductile or rigid fillers into brittle epoxy matrices to improve its toughness has been established for many years. In fact, various materials have been employed in order to toughen epoxy matrices, including liquid rubber or preformed rubber particles [30-38], glass beads [39-43], thermoplastics [44-51], and nanoparticles [52-61].

Two main toughening categories could be identified regardless the added material: the first method involves phase separation processes which take place between the added modifier and uncured epoxy resin during the curing process; while the second method involves the addition of fillers and particles that remain in their initial form and shape upon curing. It worth noting that even for the same material, different categories might be used. For instance, matrix-compatible liquid rubber could lead to phase separation processes upon epoxy curing, while preformed rubber particles will keep their shapes after curing. Therefore, reviewed works here are grouped by materials rather than by those two categories and toughening mechanisms for each are analysed, with a focus on phase separating systems and its associated toughening for rubber and thermoplastic modifications.

Rubber toughening

One of the earliest and most used methods to increase the toughness of epoxy resin is by adding rubber into the epoxy resin, including liquid rubber which phase separates during curing, as well as the use of rubber particles [30, 32, 33, 62, 63]. Numerous works had been performed since the late 1960s [44]. For phase separated rubber, the existence of a rubbery phase within the composite can absorb energy during their deformation upon loading; while for preformed rubber particles, the introduction of these particles can provided multiple crack processes rather than a single crack, which absorbs more energy during the fracture process [62]. Shear yielding of the rubber modified epoxy matrix can also be enhanced by generating cavities which can not only dissipate energy, but also blunt the crack, leading to a larger plastic zone in front of the crack tip [62, 63]. Furthermore, the compatibility between the introduced rubber and epoxy matrix plays a very important role in their toughening effect, which can affect their contribution. Several other factors need to be considered for the introduction of rubber, including volume fraction, molecular weight, crosslink density of epoxy, particle size and shapes.

Chikhi *et al.* introduced liquid amine-terminated butadiene acrylonitrile (ABTN) copolymers to diglycidyl ether of bisphenol A epoxy resin (DGEBA) with various contents. In their results, an increment of 200% in Izod impact strength and 50% of K_{IC} was obtained, which was explained by cavitation of rubber particles and accompanying localized shear yielding [30], although both T_g, stress at break, and tensile modulus decreased. In another study performed by Yan *et al*., both liquid rubber and core-shell rubbers were introduced into a DGEBA matrix to improve not only the fracture toughness of neat epoxy resins but also of fibre reinforced composites. Their results showed that toughened epoxy resins were obtained for both

fillers, although this toughening effect was not fully transferred to laminated composites, especially for rubber particle filled specimens [64].

In short, although obvious toughening effects have been observed for rubber-modified epoxy matrices, the associated drawbacks of these materials such as a lowering of the glass transition temperature (T_g), decrease in yield stress, Young's modulus, and thermal and environmental stability, not fully transferred toughening from matrix to FRPs, as well as the need of large quantities of modifying agents have all driving researchers to find improved or alternative toughening routes for FRPs, especially when localized toughening is desired. Furthermore, the crosslink density of epoxy resin strongly affects the toughening effect of introduced rubbers, since often main successes were obtained for epoxy systems with relatively low crosslink density [44]. For aerospace grade epoxies which normally possess high level of crosslink densities, alternative toughening routes are required.

Thermoplastic toughening

To avoid some of the limitations of rubber toughening for highly crosslinked epoxy resins, relatively high *Tg* thermoplastics have been widely used as an alternative to rubber to improve the fracture toughness of epoxy resins since the late 1980s [44-46, 50, 66]. Various thermoplastics have been introduced into epoxy matrices as toughening agent, including polyether sulfone (PES) [67-69], polyether imide (PEI) [49], polysulfone (PSF) [70], polyphenylene oxide (PPO) [44], polyphenylene ether (PPE) [71, 72], polyethylene terephthalate (PET) [72], and polyhydroxy ether bisphenol A (phenoxy) [73-76]. Similar to liquid rubber toughening concepts initially a homogeneous blend is created in these systems, with the epoxy acting as a solvent for the thermoplastic, which phase separates upon curing. Starting reactant

mixtures are completely miscible and composed of epoxy, thermoplastic and curing agents. Upon curing, reaction induced phase separation takes place resulting in various epoxy/thermoplastic blends, having a two-phase morphology with improved ductility and toughness without significantly losing other mechanical and thermal properties such as modulus, tensile strength, glass transition and heat resistance. Possible toughening mechanisms for introduced thermoplastic phases includes improved energy absorption by plastic deformation upon loading, crack bridging, crack pinning, crack path deflection, shear banding, etc. of which some of them are schematically illustrated in Fig. 2.4 [44]. Several literature reviews had been published on the topic of thermoplastic toughened epoxy resins [44, 50, 77].

After initial studies by Bucknall and Partridge using PES in 1983 with relatively small improvements in fracture toughness [78], various research works have been performed since then. Pearson *et al.* used PPO as a modifier for DGEBA epoxy systems, and obtained an almost linear relationship between increased fracture toughness and increasing amount of PPO added [44]. Micro-cracking was believed the main toughening mechanism for their results. Crack bridging is another widely accepted toughening mechanism in thermoplastic modified epoxy resins, which has been confirmed by fractography of the specimen [44, 79-81]. Wong *et al.* used phenoxy in DGEBA epoxy resin and improved the G_{IC} to ten-fold with only 10 wt.% loadings, with clear phase separation being observed at the fracture surface [76].

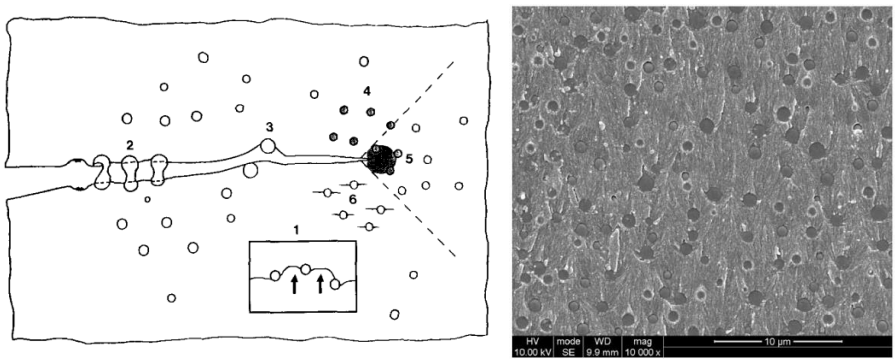

Fig. 2.4 Left: Schematic illustration of different toughening mechanism for thermoplastic modified epoxy: (1) crack pinning; (2) bridging; (3) crack path deflection; (4) particle yielding; (5) shear banding; (6) micro-craking [44], and right: SEM image of phenoxy modified epoxy [76].

Many factors are believed to affect the toughening of epoxy matrices, including morphology, end-groups of thermoplastics, crosslink density, etc. [50]. Although the effect of functionalized end-groups remains controversial [47, 50, 67, 81, 82], a co-continuous phase morphology, and higher crosslink density are generally regarded as more favourable for optimized toughening. For more detailed reading about the subject the reader is referred to several reviews on the topic [44, 50, 66, 77].

Nanoparticle toughening

Nanoparticles as fillers in composites for improved properties have been extensively studied over the last two decades. For instance, carbon nanotubes (CNTs), first discovered by Iijima in 1991 [83], have been widely used as reinforcing filler in polymer matrices due to their excellent mechanical, electrical, and thermal properties [59, 84-90]. Furthermore, their large aspect ratio provides the possibility of introducing percolated networks at extremely low loadings, which greatly preserve

the original properties of the matrix material. Besides CNTs, various other nanoparticles such as layered silicates like montmorillonite (MMT) and silica and ceramic nanoparticles (TiO_2, Al_2O_3, etc.), have also been introduced into epoxy resins, in order to improve their fracture toughness and other properties.

Becker *et al*. used octadecyl ammonium ion-modified MMT into DGEBA epoxy resins, and found a linear relationship between fracture toughness K_{IC} increment and increasing amount of clay loading [91, 92]. Pluart *et al.* found a similar improvement in stiffness and fracture toughness by addition of clay into DGEBA resins [93]. From their SEM observations, evidence of nanoclay platelets deflecting crack propagating pathways can be seen clearly.

The main toughening mechanisms for nanoparticles filled epoxy composites include crack deflection, crack pinning, matrix plastic deformation along interfacial regions, and/or debonding [54-56, 59, 91-93, 95]. Similarly, Zhang *et al.* used a special sol-gel process to produce SiO_2/epoxy nanocomposites with increased mechanical performance [55]. They found that apart from the homogeneous dispersion which is very important and necessary for mechanical reinforcement, the distance between each nanoparticle also playing an important role. Significant reinforcement was found when the distance between nanoparticles is smaller than the radius of filled nanoparticles [55].

Deng *et al.* applied halloysite nanotubes into epoxy resins with different concentration (5 wt.% and 10 wt.%), and obtained increased the K_{IC} by 50% and G_{IC} by 127%. The main mechanism is believed to be crack bridging, crack deflection, and matrix plastic deformation around those nanoparticles [95]. Kinloch and his colleagues obtained increased fracture energy from 100 J/m^2 to 460 J/m^2 by adding

13 vol.% of nanosilica into epoxy resin, and found main mechanisms were not crack deflection but debonding of nanofillers and plastic void growth [56]. Similar theories were proposed by Hsieh *et al*. [58, 96]. According to research performed by Zhao *et al.* [97], this difference in mechanisms might depend on the interfacial properties between filled nanoparticles and epoxy matrix. In their work, the effect of interfacial properties between alumina nanoparticles with bisphenol A based epoxy matrix, on their reinforcing mechanisms was studied. Results showed that relatively weak interfaces led to crack deflection, debonding, and matrix plastic deformation as reinforcing mechanism, while greater interfacial strengths led to enhanced crack deflection and microcracking which provided a better mechanical improvement [97]. This was found consistent with previous introduced fracture mechanism in FRPs but at a different scale from micro- to nano-level.

After those works of using nanoparticles in epoxy resins for improved fracture toughness, these studies were extended to FRPs. Although it is more complex when analysing toughening mechanism for FRPs since various failure modes can occur as discussed earlier, improvements have been obtained in this research field. Haque *et al.* examined the fracture toughness of S2-glass/epoxy/clay composites using a notched bending test (NBT) method, and obtained an increase of 20-23% in fracture toughness with 1-2 wt.% of nanoclay particles. The fracture surface showed clear matrix agglomeration and matrix cracking which indicates strong interfacial bonding [98]. In a study performed by Hsieh and his colleagues, fracture energy G_C for carbon fibre composites was increased from 439 J/m^2 to 489 J/m^2 with the addition of 12 wt.% silica, which was significantly less than improvements of their bulk epoxy resins system (from 77 J/m^2 to 212 J/m^2 by adding 20 wt.% of silica nanoparticles) [58]. This is believed due to constrained plastic zone between plies in

composite laminates, as illustrated in Fig. 2. 7. Gojny *et al.* [99] improved fracture toughness of glass fibre reinforced composites by about 19% using 0.1 wt.% of DWCNT-NH_2. In another work, Zhou *et al.* [100] showed an improvement of 30% in fracture toughness with 2 wt.% CNTs introduced into a satin woven carbon fibre composite system.

It has to be admitted that most fracture toughness improvements of using nanoparticles compared to previously introduced rubber or thermoplastic toughening are relatively low. For most of nano-toughened composite laminates, the fracture toughness increment was below 50%, which is much lower than thermoplastic-toughened system. However, the new functionalities introduced by nanoparticles such as electrical conductivity have shown potential to create multifunctional composites, while mechanical properties also been maintained or improved.

One of the major challenges of using CNTs in polymer matrices is their dispersion since CNTs always tend to agglomerate during processing [101]. Different processing and manufacturing techniques have been performed in order to improve both dispersion and interfacial properties between nanofiller and matrix. For instance, high shear force generated during mixing could assist the dispersion but also might reduce the length of CNTs and therefore lower their reinforcing efficiency. As mentioned earlier, as processing is not the main topic of this section, a detailed comparison between different processing methods as well as their toughening effects will be presented in a later chapter, alongside some experimental results and discussion.

Interface and interleaf toughening

Apart from dispersion, the localization of CNTs in desired regions within composites is another major concern when using them for material toughening. Similarly, localized toughening by other materials such as thermoplastics is also desired. Since the relatively weak out-of-plane properties are limited by the laminated nature of FRPs, various types of interleaves have been proposed with the aim of increasing the interlaminar fracture toughness in a localized manner, including toughened epoxy films, different forms of thermoplastic, and CNTs [102-109]. Interleaving also provides another advantage over miscible blend systems, as it retains the low viscosity of epoxy resins for subsequent liquid moulding processing, while normally for blend systems a significant increase in viscosity is obtained.

The idea of incorporating interleaves was first patented by Evans and Hirschbuehler in 1984 for the American Cyanamid Company [110], and involved the incorporating of a layer of ductile epoxy with high toughness into the laminates to improve the fracture toughness. The same matrix resin was used as toughening interleaves due to their compatibility and ease of processing (Fig. 2.5). The increased resin region relieved the plastic zone restrains and therefore increasing the fracture toughness of composites (Fig. 2.6) [104]. Singh and Partridge used similar matrix resins as interleaves placing them at the mid-plane of laminates, with a thickness of 50 μm and 200 μm. G_{IC} was increased from 213 J/m^2 to 310 J/m^2 and 369 J/m^2, for 50 μm and 200 μm interleaved specimen, respectively [102]. The relief of plastic constrains by introducing epoxy interleaves was also believed to be the main toughening mechanism. Normally, with increasing thickness of resin interleaves, the fracture toughness would be increase. This was confirmed by several research works [23, 105, 111].

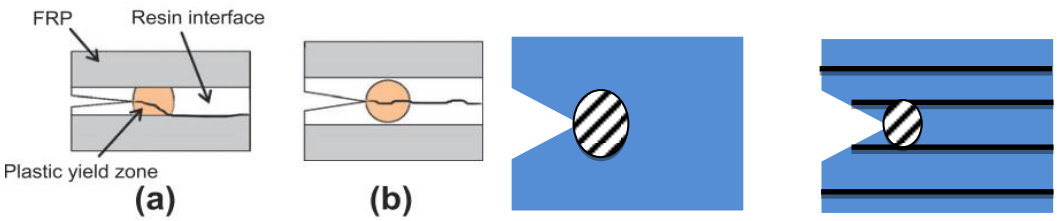

Fig. 2.5 Top: illustration of plastic yield zone interaction with different epoxy resin thickness, cited from [113]; and bottom: schematic illustration of constrained plastic zone in neat resin and composite laminates.

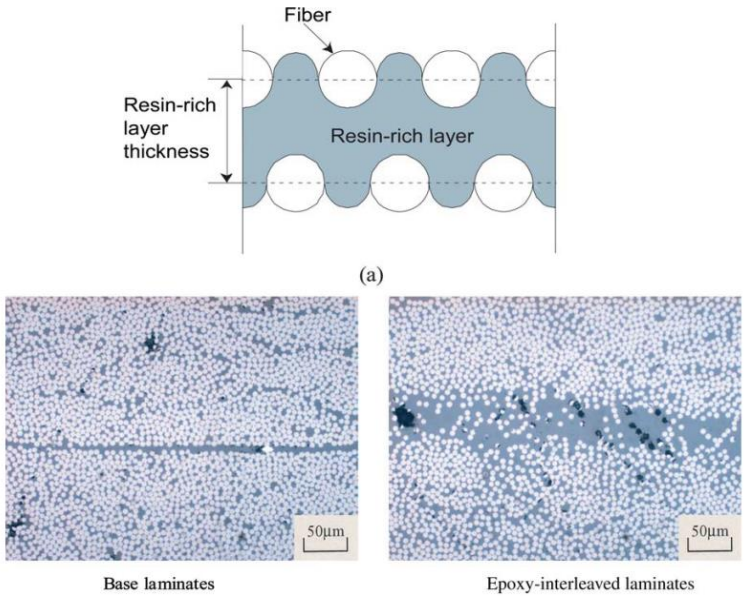

Fig. 2.6 Optical micrographs of transverse section for base and epoxy-interleaved specimen [104].

However, with increased thickness of resin layers, the overall volume fraction of reinforcing fibres is decreased, lowering the in-plane properties of composite laminates as well as the compressive strength.

Thermoplastics have also been used as interleaves for toughening of composites, including PEI, PSF, PEEK, etc., and in various forms such as film [114], microfibers [115], or electrospun nanofibre mats [106, 116]. Apart from localized toughening,

another advantage of interleaving over miscible thermoplastic/thermoset blend is the improved processability in subsequent composite manufacturing. With miscible blend systems, the high molecular weight of thermoplastics will normally lead to an increase in system viscosity hence interfering with liquid moulding process such as resin infusion or resin transfer moulding, all of which becoming increasingly important in the manufacturing of large composite parts.

Different toughening mechanisms are involved, including plastic deformation and crack bridging, depending on the form of introduced interleaves. Various thermoplastics were employed as interleaves and promising toughening results have been obtained for some systems [74, 76, 115, 117-119]. Dzenis and Reneker patented the use of electrospun nanofibres as interleaves for toughening in 2001 [120], while several research works on this topic have been performed since then [106, 116, 119, 121-124]. Zhang *et al.* used electrospun polyetherketone cardo (PEK-C) nanofibres as interleaves in CF/epoxy composites, and an increase in fracture toughness was obtained with interleave loadings as low as 0.4 wt.% [121]. They also examined the effect of electrospun nanofibre diameter, and found a more stable crack propagation for finer fibres [121]. Apart from nanofibres, microfibres in the form of non-woven mat have also been used as interleaves in FRPs. Kuwata and Hogg examined different non-woven mat interleaves in fibre reinforced composites using immiscible thermoplastics such as polyester and polyamide, and found that the main mechanism was fibre bridging at the fracture surface [122, 123]. Li *et al.* introduced a PET film into GF/epoxy composites and found a 40% increase in G_{IC} for thick film (0.2 mm) interleaved specimens and reduced fibre bridging for thinner interleaves (0.1 mm) [119]. Gao *et al.* introduced thermoplastic particles as interleaves in CFRPs, leading to enhanced fracture toughness and toughening effects

by crack deflection, and energy absorption during the thermoplastic deformation [106].

An important issue need to be addressed is how to define the thermoplastic interleaf loading in these studies. Most of toughening was achieved by introducing a single interleaf at the laminate mid-plane, which clearly leads to unrealistic low thermoplastic concentrations as thermoplastic is only introduced between two plies of a multi-ply laminate. Before compare to epoxy/thermoplastic blend system, interleaf loadings need to be calculated accordingly.

CNTs were not only used to improve the interlaminar fracture toughness by localized toughening at the interlaminar region, but have also been used to improve interfacial properties of reinforcing microfibres and fibre/matrix interfaces, although several challenges exist such as processing, dispersion, localization, and cost, comparing to other forms of interleaves.

Great progress had been obtained in this research field in last few years. In the research work performed by Veedu *et al.* at 2006, CNTs were grown vertically on microfibers and significant improvements in interlaminar fracture toughness were shown due to the interlocking of CNT forests [128]. Here SiC woven fabrics were used for growing CNTs perpendicular to microfibres to form CNT reinforcement in the through-thickness direction. Wardle's group at MIT successfully introduced aligned CNTs onto advanced fibre surfaces, providing three-dimensional reinforcements (Fig. 2.8), especially for increased out-of-plane properties such as interlaminar fracture toughness [108, 109]. The G_{IC} value of CNT grown alumina fibre composites ("fuzzy fibres") increased by 67% with the volume fraction of CNTs ranging between 1 to 2% [108]. The use of alumina fibre was due to their

compatibility with CNT growth, and detailed manufacturing processes can be found in their publication [109].

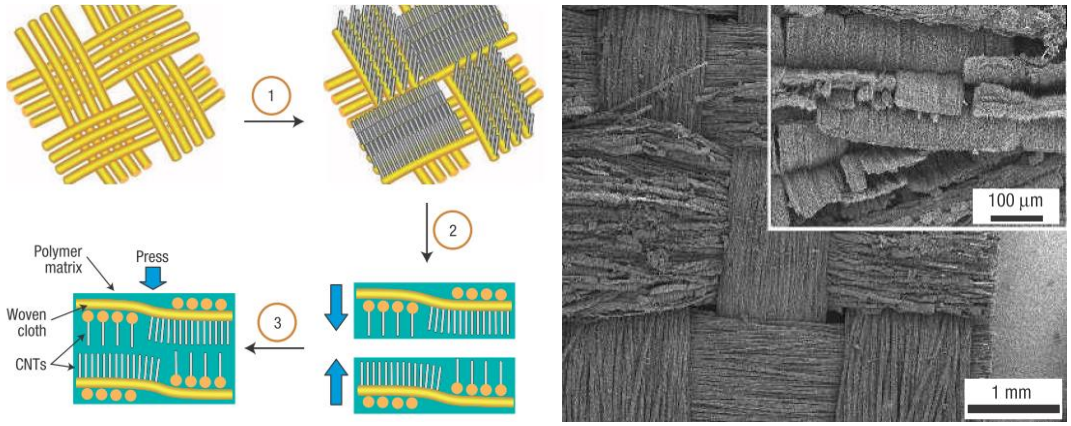

Fig. 2.7 Illustration and of in-situ forest grown CNTs on SiC micro-fibre based woven fabrics [128].

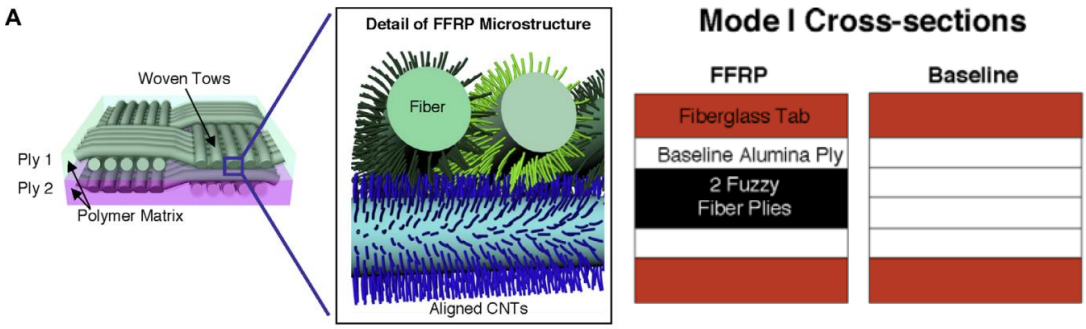

Fig. 2.8 Schematic illustration of "fuzzy fibre" reinforced composite concept [108].

Recently, Hamer *et al*. successfully demonstrated the possibility of combining thermoplastics with nanoparticles in nanofibres, which increased the G_{IC} by three times with interleaved Nylon/MWCNT nanofibril mats [132]. White *et al.* also combined thermoplastics with nanoparticles as interlayers for FRPs, and obtained increased fracture toughness from these multi-scale composites [133].

Although the relatively complex procedures, limited scales, as well as questions of how to apply these methods into more widely used carbon fibre composites without sacrificing fibre strength remain challenging, those first inspiring results have shown

great potential of using CNTs as interleaves and/or interfacial reinforcements for composites.

2.3.3 Fibre architecture toughening

To improve out-of-plane properties such as interlaminar fracture toughness, modification through fibre architecture has also been studied. Obviously, the existence of reinforcing fibres in the through-thickness direction could carry load and therefore improve out-of-plane properties. In this section, various forms of fibre architecture modifications with the aim of improving interlaminar fracture toughness are briefly reviewed, including effects of cross-ply, weaving, braiding, and stitching.

When non-crimp fabrics are placed in [0/90] or [90/90] for ply orientation, the G_{IC} propagation values are normally higher than those for [0/0] laminates [24]. During failure, delamination tends to propagate along adjacent plies. Higher values also can be attributed to matrix crack branching and deviation for angle-ply laminates [24]. For propagation values, [+45/-45], [90/90], and [0/0] are ranging from highest to lowest, although G_{IC} initiation has not been obviously affected by orientation [134].

Unlike unidirectional (UD) or non-crimp fabrics which contain parallel fibre tows within each ply, woven fabrics contain fibre tows that are interlacing between each other in warp and weft direction in a certain order. The categories of woven fabrics, such as plain weave, twill weave, or satin weave, are determined by their interlacing order within the ply. For instance, if the fibre tow in weft (latitudinal) direction is going alternatingly above and underneath the fibre tow in warp (longitudinal) direction one by one (or vice versa), then it is named plain weave (1 x 1); similarly, if the weft fibre tows go above and underneath warp tows two by two, then it is

called 2 x 2 twill weave. In the case of weft direction tows going above warp direction tows more than four in a row, it is been categorized as satin weave.

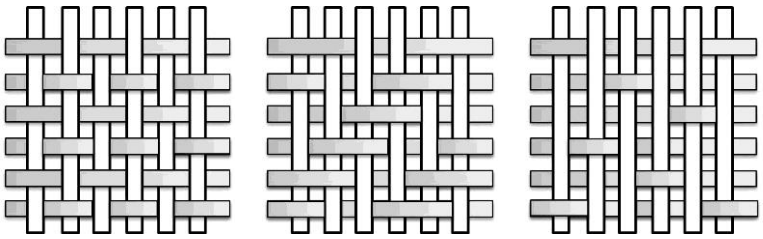

Fig. 2.9 The illustration of plain, twill, and satin weave (from left to right).

Normally for woven fabrics with various weave structures, the interlaminar properties improve compared to those of UD composites [24, 135-138]. One reason is that crack propagation is being diverted as mentioned earlier, the other reason is the roughness which generates the plastic zone between fibres at crack tip front (Fig. 2.12) [24, 136, 139-142]. The restricted plastic zone as shown for non-crimp fabrics also explains why an increase in matrix toughness cannot be fully transferred to the UD or non-crimp composites. However, it is worth to note that in-plane properties are affected as weaving disrupts the in-plain fibre continuity (compared to UD). In general, waviness lowers the in-plane properties. Other architecture modifications to improve interlaminar properties of composites include stitching, knitting, braiding, z-pinning, and through-thickness weaving. Successes to different extent were obtained by various researchers, with the main toughening mechanisms being extensive crack branching, and crack bridging.

Unfortunately, the main limitation of these techniques is that in-plane properties are compromised such as strength, tensile fatigue life, and compressive strength [128, 143]. Although some of the research claims that stitching did not degrade in-plane properties, it is believed to depend on several factors such as the nature of the matrix,

compatibility between fibre and matrix, and way of introducing stitching [144]. A detailed review on the effect of stitching on in-plane properties can be found in Mouritz *et al.* from [143].

2.4 Non-destructive testing (NDT) methods for composites

Due to the strict requirements on safety and reliability in aerospace applications (especially for civil aircraft), current composite parts and structures within aircraft are typically overdesigned to offset the possibility of unexpected internal failures, which in fact works against the weight reduction purpose of using them in the first place. A promising way to better utilize the potential of FRPs is by being able to detect and monitor the internal damage state, hence to setup proper safety thresholds and reduce the risk of catastrophic failures. The concept of structural health monitoring (SHM) is not new, but has been more integrated into the composites' industry in recent years. Several health monitoring concepts have been proposed, including novel non-destructive testing (NDT) technologies, embedded sensors, and self-sensing systems, etc.

Non-destructive testing (NDT) refers to those testing methods that can be used to detect composite damage without further damaging the components, which is very necessary for quality control and constantly increasing safety standards. During manufacturing or subsequent processing and installation, composites may have flaws which potentially may affect properties of the materials. Therefore, NDT is extremely important for composites all the way from production, to installation, service life, until the end of a components service life. Several NDT methods have

been widely used in composites industries, and different methods have advantages in detecting specific defects in composites.

Table 2.1 Comparison table cited from ASTM E2533-09 listing the possible application of NDT method [147].

NDT method	**Application**
Acoustic Emission	Used for quality control of production and fabrication processes, proof-testing of pressure vessels after fabrication, and for periodic in-service and health monitoring inspections prior to failure.
Computed Tomography	Used as a post-fabrication metrological method to verify engineering tolerances.
Leak Testing	Used to validate leak tightness following fabrication, and in-service re-qualification of pressure vessels.
Radiography and Radioscopy	Used during fabrication inspection to evaluate honeycomb core imperfections or discontinuities such as node debonds, core-to-core splices, porosity, included materials as well as verification of structural placement.
Shearography	Used in quality assurance, materials optimization, and manufacturing process control.
Strain Measurement	Used during proof testing, or during periodic re-qualification.
Thermography	Used to follow imperfections, delaminations or discontinuity growth during service.
Ultrasound	Automatic recording systems allow parts to be removed from a processing line when defect severity exceeds established limits. Most common method applied for laminar oriented defect detection such as impact damage caused delamination, fibre fracture, and porosity.
Visual	Used primarily for quality inspections of composite materials and components upon receipt.

Unlike traditional materials such as metals which consist of a homogeneous phase, composites materials are often non-homogeneous and anisotropic in their properties, leading to more specific requirements for NDT. In this section, some of the major NDT methods are briefly introduced and described, with their applications to the composites industries, as well as their limitations.

Table 2.2 summarizes the possible applications of various NDT methods for composites. Although traditional NDT is widely used in composite industries, most of these NDT tests not only require special equipment to perform damage detection,

but also strongly depend on the experience of engineers to interpret data as well as involves additional assembly time, costs and difficulties of monitoring the health of FRPs continuously. The down-time nature of many of these NDT methods, which often requires that examinations are performed during out-of-service periods, increases the life cycle costs even further. Because of this reason there is a clear need for cost-effective SHM systems that are fully integrated into the composite structure.

Table 2.2 Application of NDT for FRPs cited from ASTM standard E2533-09 [147].

Defect	Product and process design and optimization	In-line process control	Post manufacture inspection	In-service inspection	Health monitoring
Acoustic Emission	√	√	√	√	√
Computed Tomography			√		
Radiography & Radioscopy	√	√	√	√	
Thermography			√	√	
Ultrasound	√	√	√	√	√
Visual	√	√	√	√	√

2.5 The use of CNTs in FRPs for damage sensing and health monitoring

Carbon nanotubes were first introduced into FRPs as sensors for SHM purposes by Fiedler *et al*. in 2004 [148], since then, several studies exploring the use of CNTs for damage sensing in FRPs have been conducted, particularly in the last five years. Because of their extraordinary mechanical and electrical properties, CNTs have become the nanofiller of choice for many multifunctional applications over the last decade [83, 89, 149-153]. With respect to electrical properties their high aspect ratio guarantees a very low percolation threshold which does not compromises the

original resin properties. By introducing CNTs into insulating polymer matrices, various matrix-dominated failure modes can be sensed and detected, providing a promising route for next generation SHM systems. The use of CNTs in FRPs also provides the possibility of in-service health monitoring, without complicated equipment and intensive labour requirements. In-service damage detection can greatly save aircraft or wind turbine down-time, in other words, providing more in-service time, improving efficiency and reducing costs.

Although a large amount of research works have been conducted in this field, a systematic understanding of using CNTs in FRPs for damage sensing and health monitoring purposes remains lacking. Not to mention the gap between lab-scale results and real industrial applications, and how to interpreting existed knowledge to real uses in structural components. In the present work, up to date research on using CNT networks for FRPs damage sensing are reviewed and compared, in the aim of build up a better understanding and systematic comparison of this research field. Apart from those, special efforts have been made to analyse and conclude the existed knowledge from end-user point of view, to classify various works and data, trying to reduce the gap between lab work results and real composite application.

2.5.1 Model studies on single fibre damage sensing

Single fibre composites are often chosen as model systems to study interfacial properties of composites and for this reason they have also been used to study the effect of CNT sensory networks within interfacial regions. Various research works have been conducted to understand how conductive interfacial networks behave during loading which is an important aspect of damage sensing in FRPs, especially for loading situations where interfacial debonding is likely to occur.

Park *et al.* [154, 155] have combined an electrical sensing method together with traditional acoustic emission, in order to obtain damage sensing results. In this study, CNTs were dispersed in epoxy using a solvent and after solvent evaporation, composites with carbon fibre (CF) positioned at the mid-plane were manufactured, as illustrated in Fig. 2.10 [155]. During tensile loading along the fibre direction, fibre breakage occurred and electrical sensing signals as well as AE signals were collected. For the specimen with extremely low CNT content (0.1 wt.%), electrical signals were obtained until the first fibre fracture when electrical resistance suddenly jumped to insulating level (Fig. 2.10a). This jump was due to the low amount of CNTs which could not build up a stable electrically conductive network. The insulating nature of the surrounding matrix made that only the carbon fibre could transfer electrons, and once broken this also shuts off the pathway for electrons, leading to an immediate increase in resistivity. Specimen with relatively high CNT loadings (0.5 wt.%) possessed a percolating CNT network within the matrix. Therefore after initial fibre fracture, the electrical signals still progressively increased with increasing strain, revealing more internal damage information which could be confirmed by AE data (Fig. 2.10b). This was attributed to the existence of a percolating network of CNTs in the matrix that maintains conductivity after the first fibre breakage. At higher CNT loadings (2.0 wt.%), the measured resistance change during the test was obviously lower than that of the 0.5 wt.% specimen, although the sensing signals still increased progressively after the first fibre break. This was due to more possible contact points for this percolated CNT network were with increasing strain and deformation electrons can still pass through the specimen via remaining CNT pathways.

These model studies showed some promise of the use of CNTs into FRPs. Even in combination with conductive carbon fibre, CNTs showed their potential for damage sensing, not to mention their benefits through additional multi-scale mechanical reinforcement. After the establishment of a percolating network, larger amounts of CNTs reduce the sensitivity of the electrical damage sensing signal, which was also confirmed by other sensing works based on CNT networks [156-159].

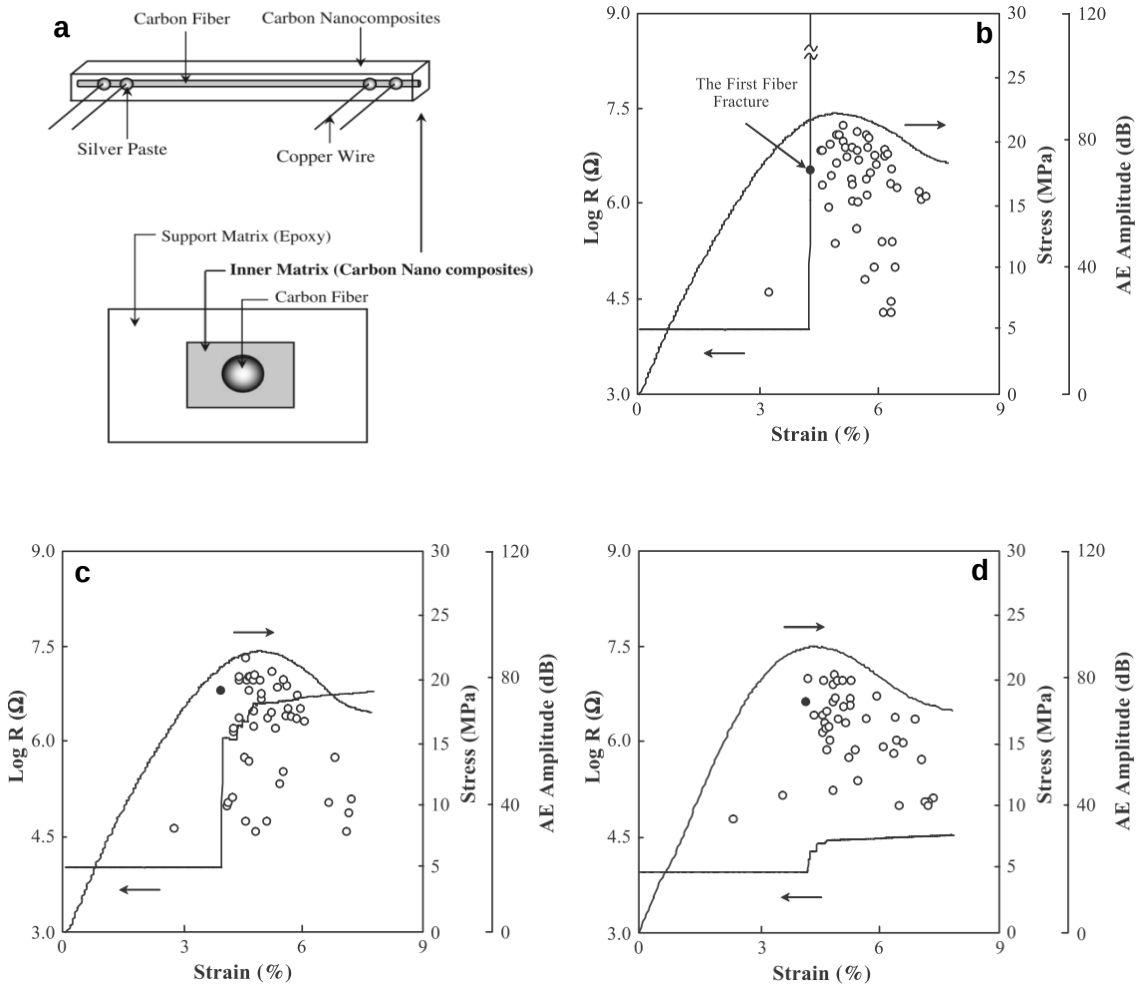

Fig. 2.10 Park et al.'s single carbon fibre model composite results [155].

With the aim of highlighting the effect of percolated CNT networks as sensory systems, insulating glass fibre was also used in similar model composite studies. Zhang *et al.* [161] used both electrophoretic deposition (EPD) and dip-coating to

produce multifunctional glass fibre interfaces to be evaluated in single fibre fragmentation tests. EPD showed improved dispersion of CNTs on glass fibre (GF) surfaces compared to dip-coating, and a more than 30% increment in interfacial shear strength compared to the reference system. The EPD specimens were chosen to perform in-situ electrical resistance measurements, as shown in Fig. 2.11. The sensing curve showed three stages with a linear, non-linear, and abrupt change, indicating the possibility of using this multi-functional layer as a mechanical sensor. It is worth to mention that a large scatter in electrical resistivity was measured for specimens with similar CNT loadings, while dip-coating also led to a reduction in single fibre tensile strength.

Apart from depositing CNTs directly onto carbon or glass fibre surfaces for sensing functionalities, polymer/CNT sizings and coatings have also been studied as interface sensors. Rausch and Mäder [163, 164] introduced an alternative route to incorporate CNTs into FRPs at the fibre/matrix interface by sizing or coating a CNT/polymer film former onto glass fibre. For their CNT/GF/PP model composites, 0.5 wt.% CNT/PP film was coated onto glass fibre surfaces, followed by an annealing process to achieve a more homogeneous coating. The CNT/polymer coating enabled the localization of the sensory network at the interfacial region rather than being distributed throughout the matrix. However, for such a coating to be effective it needs to be continuous and homogeneous (> 10 wt.%). During tensile loading, interface failure as well as glass fibre breakage could be identified [154-158, 160].

Based on these single fibre model studies, the use of CNT networks as a sensor have shown great potential for the detection of interfacial damage in both conductive and insulating reinforcing fibres. Localized CNT sensory networks on fibre surfaces can

make insulating glass fibre multifunctional in the composites, regardless of polymer or interface.

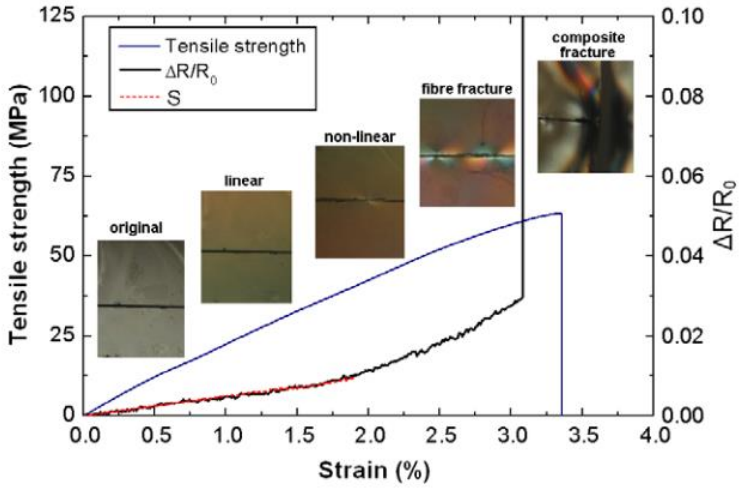

Fig. 2.11 In-situ damage sensing on single glass fibre with CNT coating via EPD. Different stages of fibre under tensile loading are shown in the graph together with the corresponding electrical sensing signals [161].

2.5.2 Model study on laminates with CNTs

After the initial idea of using CNTs as multifunctional sensors for FRPs [148, 165, 166], numerous research works based on GF/CNT (or CF/CNT) hybrid multi-scale composites had been conducted [131, 167-182] in order to further explore the potential of this damage sensing methodology in laminated composites. The introduction of CNT networks within an insulating matrix acts like a neuron sensory networks for FRPs, enabling the detection of micro-crack initiation and propagation, with the possibility of identifying the damage stage under certain conditions. Both static and cyclic loading conditions have been studied and are reported below, while also different manufacturing processes such as calendering or solution-based

processes as well as specific specimen preparation methods will be described briefly for each work.

Static loading condition

Thostenson and Chou [171] used high shear mixing methods (calendaring and three-roll mill) to disperse MWCNTs in epoxy phase, creating a percolating network for the onset of damage detection and evolution in GFRPs. During their specifically designed mechanical tests, interlaminar delamination and transverse microcracking were evaluated in unidirectional and cross-ply laminates, respectively. In the delamination tests (Fig. 2.12a), the electrical resistance increased significantly when delamination started and then progressively increased until the specimen failed. On the other hand, for microcraking detection (Fig. 2.12b), the electrical resistance increased step-wise after initiation. This difference in sensing signals opened up the possibility to identify different failure modes by using CNT networks.

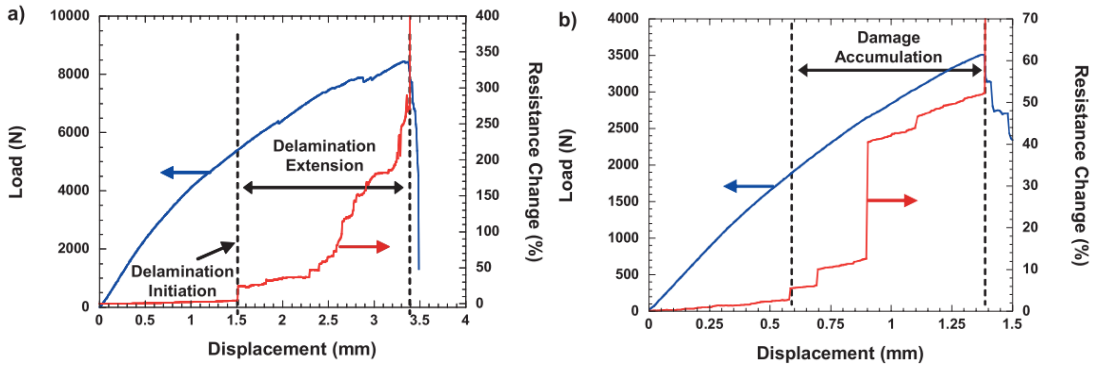

Fig. 2.12 In-situ sensing for: (a) mid-ply delamination (b) micro-cracking [171].

Cyclic loading conditions

Apart from static testing conditions, cyclic loading was performed with the aim of evaluating damage progression as well as identifying the failure stages during the composites' usage.

Thostenson and Chou [185] examined microstructural damage evolution under cyclic loading with CNTs dispersed in epoxy via a calendering method. Cracks initiated within the 90° mid-plies with the applied load increasing until crack saturation occurred in this ply. For cyclic sensing (Fig. 2.13), the strains of the first two cycles were lower than the critical first ply failure strain of transverse cracking and therefore the resistance followed the strain curve like in the case of strain sensing [185]. As the strain increased, cracks were initiated and the resistance clearly started to deviate from the strain curve, leaving a permanent resistance change after unloading. After crack initiation, for each incremental strain applied, three types of sensing signals were captured (Fig. 2.13b); (i) crack re-opening, (ii) elastic deformation (which did not lead to no new crack formation) and (iii) new crack accumulation, although this slope change was only clearly shown in the fifth cycle and not that obvious in later cycles which might be due to a too large applied strain. Similar to sensing test results under quasi-static conditions, the difference in nature between electrical sensing method and AE has been confirmed under incremental cyclic loading conditions. AE data together with electrical sensing results indicate that AE can only detect new crack formation during each incremental loading cycle, while electrical sensing are continuously increasing throughout the test [183].

In short, the existence of CNT networks within an insulating polymer matrix that establishes itself as a nerve-like sensory network to sense deformation and damage initiation and propagation, can provide a useful tool for health monitoring of composite laminates. By analysing the sensing data, different failure modes and stages can potentially be identified. Regardless the great difficulties in data interpretation on real components or coupon tests, all of these results have shown

great potential on the use of CNTs for damage sensing purposes in both CFRPs and GFRPs.

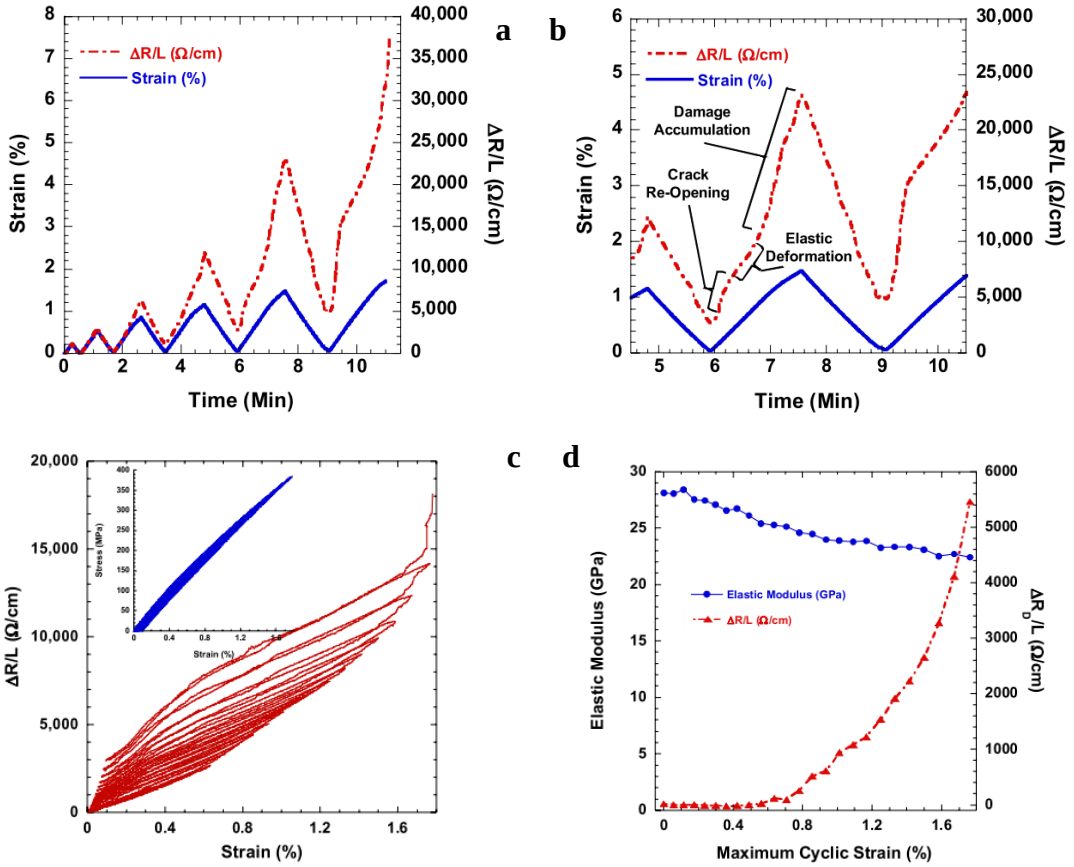

Fig. 2.13 Damage initiation and evolution study under incremental cyclic loading on 90 °mid-ply composites [185].

2.5.3 Established damage sensing system on standard test

In the previous sections it was shown that the use of CNTs in the FRPs, especially in the case of insulating fibres like glass fibre, can lead to hierarchical composites with damage sensing capability. Various stages of failure initiation and propagation, under both static and dynamic loadings could be identified and analysed. However, in order to replace existing embedded sensors in FRPs, improved sensitivity and reliability remains a challenge. Most of the research in this area are performed on

model systems or specially designed tests on laminates aiming to promote specific failure modes and prove the concept. Few works have tried to transfer existed know-how of the use of CNT networks as integrated sensor in real composite applications. The first step to fulfil this gap, would be to apply the technique to standard composite tests which are more closely related to realistic loading conditions. In the following section, up to date damage sensing studies for various composite tests are introduced and analysed, with the aim to build up a systematic understanding on how to transfer existed knowledge on sensing to real composite components.

Impact damage sensing

Impact damage is one of the major concerns in health monitoring of FRPs [24, 186]. Normally the electrical sensing signals are correlated to the impact energy during the data analysis. Yesil *et al.* [187] compared different treated CNTs for dispersion as well as impact damage sensing properties. Better dispersion gave better electrical sensing signals which correlated to the impact energy applied. Similar findings were reported in other research works [184, 188]. It is worth mentioning that impact works listed below were not performed under ASTM D7136 for drop-weight impact, although the potential of using electrical signals for impact damage sensing was shown. Gao *et al.* [186] examined electrical sensing signals during repeated impact loadings, in combination with AE to confirm the damage (Fig. 2.14). Monti *et al.* [190] also observed an increase in electrical resistivity for specimen after impact, which again was due to break down of internal CNT networks.

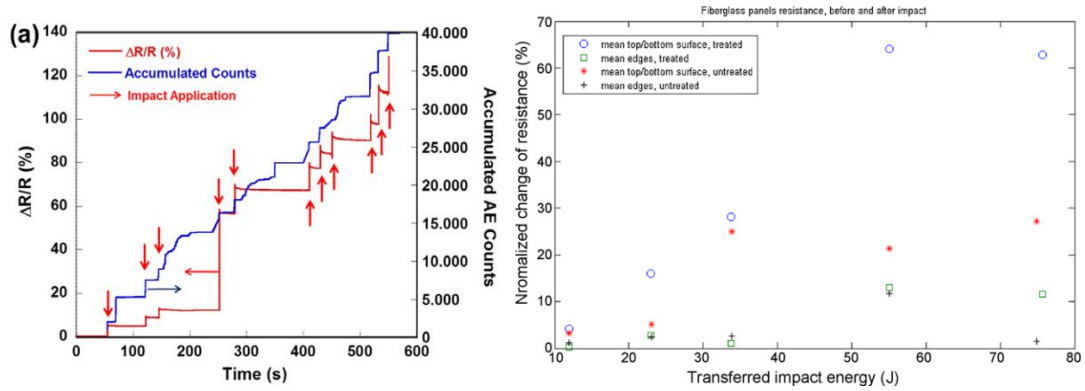

Fig. 2.14 *In-situ* impact damage sensing via CNT percolated networks in FRP [186].

Fatigue and cyclic loading

It is well known that the fatigue life of composites is strongly affected by matrix-dominated properties [172, 194, 195]. In fatigue, residual strain is often used as an indicator for the internal health of a composite laminate. Hence, by comparing the resistance change and number of cycles together with residual strain, the internal health conditions of laminates can be revealed by electrical signals. Yesil *et al.* [187] followed ASTM D3039 to produce tensile specimen for fatigue testing, with various treated CNTs introduced in the GFRP laminates. Among their results, the largest sensing signals were obtained for treated CNTs which gave better dispersion and interaction within the matrix. Other sensing works on fatigue or under cyclic loading conditions were excluded from this section or are discussed elsewhere if the test was not according to standards.

Flexural loadings

Thostenson and Chou [171] used two different spans to promote different failure modes in three point bending tests (Fig. 2.15). For short beam shear conditions, i.e. a short span-to-depth ration of 4, electrical signals increased by several orders at the point of shear failure, indicating abrupt delamination. Subsequent reloading did

establish some new electrical contacts but still resulted in a much greater resistance than its initial value. For a longer span-to-depth ratio of 8, i.e. more towards bending conditions, a more incremental resistance change was observed, which corresponded to matrix cracking and damage accumulation.

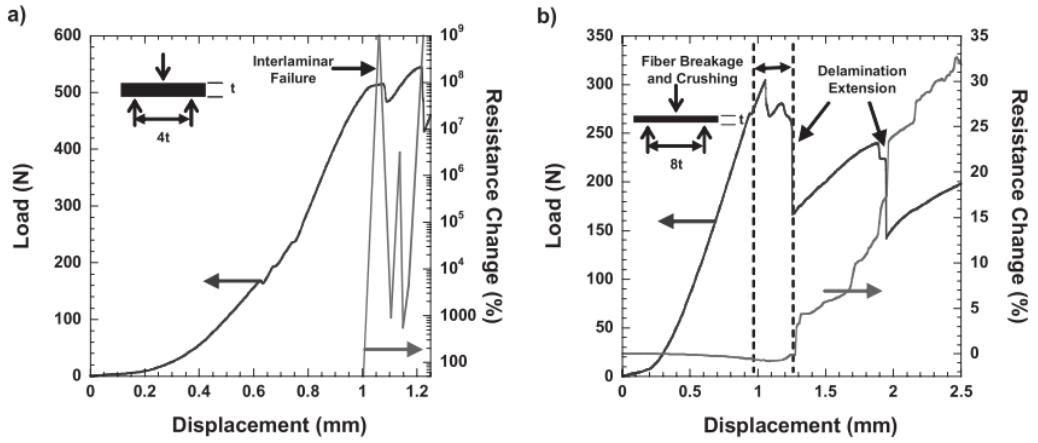

Fig. 2.15 *In-situ* damage sensing results from [171], showing different span ratios.

2.5.4 Summary of composites damage sensing works based on CNTs

A summary table was presented in Table 2.3, with the majority of research works on the topic of damage sensing in FRPs based on CNTs. The materials used, manufacturing processes applied, as well as main results were concluded. More importantly, the table indicates whether the damage sensing works were performed based on standard composite testing method. Unfortunately, no previous literature can be found based on damage sensing of Mode-I interlaminar fracture toughness test where delamination is one of the most important failure mode in composite laminates.

Table 2.3 Summarized results of composites damage sensing works based on CNT networks:

Fibre/Matrix	**Nanofillers (loadings) and location**	**Manufacturing processes**	**Detected failure and damages**	**Main results**	**Standard test* (ASTM or ISO)**	**Author, year [Ref. no.]**
GF/Epoxy	MWCNT (0.5 wt.%) in epoxy matrix	Three-roll mill	Delamination; micro-cracking	Showed possibility of using CNTs to identify different failure modes	No	Thostenson and Chou, 2006 [171]
GF/Epoxy	MWCNT on GF surface	Electrophoresis deposition (EPD)	Micro-cracking	Coated single GF as in-situ sensor for tracking micro-cracks	No	Zhang, 2011 [196]
GF/Epoxy	CNT (0.5 wt.%) in epoxy matrix	Calendering	Crack initiation during static and incremental tensile loading	Used CNT networks to identify different failure stages	No	Thostenson, 2008 [185, 197]
GF/Vinyl ester	CNT (0.5 wt.%) in matrix	Calendering approach	Crack initiation during static and incremental tensile loading	Combined with AE, showing advantages of electrical sensing method	No	Gao LM, 2009 [183]
GF/Epoxy	MWCNT (0.3 wt.%) in epoxy matrix	Calendering	Crack initiation during tensile loading	Used CNTs to identify damage initiation	No	Böger, 2010 [173]
GF/Epoxy	SWCNT on GF surface	Spray coating	Micro-crack initiation and propagation under tensile loading	Embedded SWCNT coated fibre sensor provided in situ resin curing information, and strain-stress state under loading	No	Luo, 2014 [180]
GF/Epoxy	MWCNT (1.0 wt.%) in matrix	Three roll mill	Localization of failure under tensile loading	Localized failure by placing electrodes at different positions	No	Nofar, 2007 [195]
GF/Epoxy	MWCNT (0.5 wt.%) in epoxy	Three roll mill and sizing-agent	Sensing under tensile loading	Compared effect of dispersion and CNT localization on sensing results	No	Gao LM, 2010 [184]
CF/Epoxy	CNT (0.1/0.5/1.0 wt.%) in epoxy	Calendering approach	Sensing under tensile loading	Improved sensing signals for CNT modified specimen	No	Kostopoulos, 2009 [168]
CF/Epoxy	MWCNT (0.5 wt.%)	Sonication	Sensing under tensile	Improved sensitivity for CNT	Yes (Tensile)	Grammatikos

	in epoxy matrix		loading	modified CFRPs compared to neat CFRPs	ASTM D3039	, 2012 [198]
GF/PP	MWCNT (0.5 wt.%) in polymer film coated on GF	Sizing or coating CNTs/polymer film onto GF	Interface strain sensing under tensile loading	Alternative route utilizing aqueous CNT/polymer coating on GF for sensing	No	Rausch and Mäder, 2008 [199-201]
CF/Epoxy	CNT (0.1 to 2.0 wt.%) in epoxy	Solution-based processing	Fibre breakages in dual-matrix composites	Use of CNT networks to detect fibre breakage in model sample	No	Park JM, 2003 [154, 155]
CF/Epoxy	CNT (0.5 wt.%) in epoxy	Solution-based processing	Fibre breakages in dual-matrix composites	Showed effect of CNT dispersion on sensing results	No	Park JM, 2008 [160]
GF/Epoxy	MWCNT (0.3 wt.%) in epoxy	Three roll mill	Sensing during interlaminar shear strength test (ILSS)	In-plane sensing signals gave sudden increase at failure, while through-thickness signals showed no obvious changes during testing	Yes (ILSS) ASTM D2344	Böger, 2008 [172]
GF/Epoxy	CNT in PVA fibre	CNT/PVA fibre strain sensor	Strain sensing under tensile and three point bending test	Use of an CNT/PVA fibre as strain sensor in GFRPs	Yes (Tensile) ASTM D3039	Alexopoulos, 2010 [202-204]
GF/Epoxy	MWCNT in epoxy matrix	Dispersed in epoxy using sizing agent	Impact damage	Showed potential of electrical sensing method for impact	No	Gao LM, 2011 [186]
GF/Epoxy	CNT (0.1 to 0.5 wt.%) in epoxy matrix	Mechanical stirring and sonication	Impact damage	Showed increased resistance after impact	No	Monti, 2011 [190]
GF/Epoxy	MWCNT (0.5 wt.%) in epoxy matrix	As received	Impact damage	Four probes measurement provided better sensing results compared to two probes method	Yes (Impact) ASTM D7136	Arronche, 2013 [189]
GF/Epoxy	CNT (0.1 to 1.0 wt.%) in epoxy matrix	Three roll mill	Open hole and impact damage	Apply electrical sensing method to large composites plate	No	Naghashpour , 2013 [191]
GF/Epoxy	MWCNT in epoxy	Solution-based	Sensing under tensile,	Compared effect of sizing and	Yes (Impact)	Yesil S, 2010

		processing	cyclic tensile fatigue, and impact	treatment of CNTs with improved dispersion leading to better sensing signals	ASTM D7136	[187]
GF/Epoxy	MWCNT (0.5 wt.%) on GF surface	Dip coating	Single glass fibre with coated CNTs as multi-functional sensor	First time coating of CNTs onto GF for sensing rather than mixing into matrix	No	Gao SL, 2010 [162]
GF/Epoxy	CNT thread	Embedded	Matrix cracking	Use of CNT thread as embedded sensor in GFRPs for damage detection	No	Hehr, 2014 [179]
CF/Epoxy	CNT (0.5 wt.%)	Sonication	Fatigue	Correlation between electrical sensing results and AE signals under fatigue mechanical testing	No	Grammatikos , 2014 [205]
GF/Epoxy	CNT/Al_2O_3 (0.5 wt.%)	Three roll mill	Sensing under tensile loading	Use of CNT/Al_2O_3 as conductive filler in epoxy to detect damage	Yes (Tensile) ASTM D3039	Li, 2014 [181]
CF/Epoxy	CNT growth on GF	Embedded	Sensing under tensile loading	Use of fuzzy glass fibre as strain sensor in CF prepreg	No	Sebastian, 2013 [182]

*Note: Standard test in this table means both performed test and specimen dimension was following testing standards.

2.6 Conclusions

Fibre reinforced composites have been used extensively to replace traditional materials like metals in many fields. To improve the reliability of these materials, integrated health monitoring systems have been the topic of numerous studies for many years. In the last decade the use of CNTs to create sensory networks that are able to detect various stages of internal damage and failure modes in composites have been studied. Percolated networks of electrically conductive CNTs allow electrons to pass through the material or structure and provide the possibility to monitor internal deformation and damage in composites using an electrical method. Recent advances in both model composite studies as well as laminates have been discussed. The effect of CNT concentration and dispersion on electrical sensing behaviour has also been compared and analysed.

It is worth noting that different manufacturing and dispersion processes can have a significant effect on the feasibility of industrial scale-up. Each processing route has its pros and cons, which might be suitable for a certain application. For instance, directly mixing CNTs into low viscosity epoxy resin may seem easy from a logistics point of view, but may result in poor dispersion and filtering effects by fibre preforms during liquid moulding processes or to high viscosity resin systems. To achieve good CNT dispersion (and localization), in-situ growth of CNTs directly onto the reinforcing fibre surface or electrophoresis deposition can be performed. Unfortunately, such nano-functionalization processes are relatively complex and costly procedures that could limit industrial applications. Spray coating on the other hand is an easy industrial scalable process which has shown to create good CNT dispersion and localization. However, when spraying nanomaterials care needs to be

taken that safety precautions are taken and that solvents are recovered in order to reduce the risk on personnel and environment. Apart from technological issues related to dispersion and localization of CNTs in composites, easy scale-up, relatively simple procedures, safety and environmental issues are among the most important aspects when considering technology transfer from the lab into an industrial environment.

Apart from good dispersion and localization which provides the multi-functionalities of composites, easy scale-up, relatively simple procedures, safety and environmental friendly are the most important aspect when considering transfer the knowledge from lab research into industrial applications.

Damage sensing concepts for composites based on CNTs to detect damage has now been around for a couple of years. Since then a number of studies have examined the potential of CNT sensing in composites, as well as interpreting obtained data to identify different failure modes. After some promising results which confirmed the potential of CNTs as an effective nanomaterial to detect damage in laminated composite the question remains how to transfer this technology into real industrial components.

Chapter 3

Electrical Properties of Phenoxy/CNT Composites

3.1 Introduction

As reviewed in Chapter 2, the incorporation of CNTs in FRPs has shown great potential for integrated damage sensing and health monitoring. However, the dispersion and delivery of CNTs into composites on an industrial scale production remains challenging, especially for high temperature epoxy systems, which are characterized by a relatively high viscosity. Using epoxy-dissolvable thermoplastic materials as carrier materials to deliver CNTs at desired locations within FRPs might prove to be an interesting route that overcomes some of these problems. The use of thermoplastics has additional advantages as it may improve the toughness of composites [69, 71, 72, 206-209].

In present work, high performance thermoplastic polyhydroxy bisphenol A (phenoxy) is employed as matrix material. This thermoplastic possesses ease of processing, good mechanical properties, and a relatively high glass transition temperature. In particular, thermoplastic phenoxy has been proven to be an interesting toughening agent for carbon fibre (CF) reinforced epoxy systems [76, 115], improving the damage tolerance of carbon/epoxy composites without compromising their processability. Furthermore, by embedding nanofillers like CNTs into phenoxy films or fibres such systems can be used for the localized delivery of these nanofillers in epoxy based composites, which might offer new routes for nanoengineered

hierarchical composites. Such an approach would at the same time also overcome current challenges associated with such hybrid systems like increased viscosity by CNTs, poor spatial control, and filtering effects during resin infusion processes. Therefore, before studying such a ternary system, it is important to understand the binary systems, including previously studied CNT/epoxy [210, 211], and the current phenoxy/CNT system.

In this chapter, thermal, morphological and electrical properties of the phenoxy/CNT nanocomposites are characterized and analysed, and a systematic study of its static and dynamic percolation behaviour is conducted and presented, providing a basis of utilizing this system for further composite applications. For example, the addition of CNTs to these phenoxy systems can lead to electrically conductive percolating networks that can be used for damage sensing and health monitoring, creating intelligent composites materials and structures. The solution-based process produced phenoxy film with various amounts of CNTs will be used as interleaves for CNT delivery in FRPs, and results will be discussed in Chapter 6 and Chapter 7.

3.2 Experimental

3.2.1 Materials and sample preparation

Non-functionalized, high aspect ratio (>150) multi-walled carbon nanotubes (MWCNTs) produced by chemical vapour deposition (CVD) were used as received from Nanocyl S.A. (Product No. NC7000). Polyhydroxy ether bisphenol A (phenoxy) was supplied by InChem® (PKHH) with an average molecular weight (M_w) of

52,000, and a glass transition temperature (T_g) of 92 ℃. Chemical formula and other properties can be found in Table 3.1.

Table 3.1 Summary on main properties of phenoxy.

Chemical formula [212]	Specific gravity	Average M_w	T_g (℃)
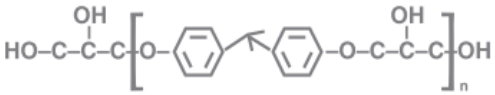	1.18	52,000	92

Melt processing

Phenoxy/MWCNT composites, with various CNT concentrations were compounded in a DSM X'plore 15 ml mini twin-screw extruder. Typical processing conditions were 260 ℃ under a nitrogen environment for 4.5 min at an initial speed of 150 rpm, and then reduced to 50 rpm for 30 sec before collection. This processing condition was selected after a number of preliminary experiments which compared different mixing temperatures (220 ℃ to 260 ℃) and times to optimize the final electrical conductivity of the extruded strands. Melt draw-down upon collection was avoided in order not to disturb the formation of a conductive CNT network. The collected extruded strand with a diameter of 3 mm, was pelletized, and subsequently compression moulded into 100 μm films at 240 ℃. For this, pellets were placed into a mould for 5 min in a hot-press to soften before a pressure of 30 bar was applied for another 2 min. Circular specimens with a thickness of 1.6 mm and a diameter of 30 mm were also produced by hot-pressing for rheological studies.

Fig. 3.1 DSM X'plore 15 ml mini-extruder used for phenoxy/CNT composites compounding.

Solution-based processes

Simple bar-coating was also used to produce large sized thermoplastic/CNT composite film to be used as interleaves for composite laminates. Pre-dried phenoxy pellets were dissolved in a mixture of chloroform and DMF, at a weight ratio of 8 to 2. For phenoxy/CNT specimen, CNTs were first added into the mixed solvent and dispersed using probe sonication (model GEX 750 for controller, and model CV33 for probe, 25 % of maximum amplitude, 1000 J). Next, phenoxy was added into this solution and gently stirred for 2 hrs at 50 °C using a magnetic stirrer. The solution was then again sonicated (25 % of maximum amplitude, 500 J) to enhance dispersion of CNTs. Thickness and weight of the final film depends on many parameters including, the depth of the wire bar as well as the concentration of phenoxy. Therefore, in order to obtain films of different thicknesses, different bars and phenoxy concentrations were used. The produced film was left for solvent evaporation before cutting and measuring the weight, unfortunately, no

measurements were made to examine the residual solvents. The weight of the produced phenoxy films after cutting into a size of 150 mm by 150 mm, were 0.2 g, 0.7 g, and 1.4 g, respectively, while the phenoxy/CNT film weighted 0.7 g, at a CNT concentration of 1.0 wt.%. These films will be used as interleaves for composites in a later chapter.

3.2.2 Characterization techniques

SEM

The scanning electron microscope (SEM) used in this work is an Inspect F model from FEI®. Before inspection, the extruded strands from the mini-extruder were cold fractured in liquid nitrogen. The fracture surface was gold coated before examination. An accelerating voltage of 10 kV was applied during SEM observation.

Rheology

Rheological properties of phenoxy were measured by an AR 2000 Rheometer from TA Instruments. Frequency sweeps from 1 Hz to 10 Hz in the linear viscoelastic region were performed at different temperatures, ranging from 170 ℃ to 270 ℃ with increments of 5 ℃. Oscillatory rheometry was applied, with a frequency sweep for each temperature. Storage modulus, loss modulus, and viscosity were recorded.

DSC

Differential scanning calorimetry (DSC) was performed using a Mettler-Toledo Model number 822e for the characterization of the glass transition temperature (T_g) of phenoxy. All samples were heated from 25 ℃ to 300 ℃ at a rate of 10 ℃/min, held at 300 ℃ for 3 min and then cooled to 25 ℃ at the same rate. After an isothermal period of 1 min at 25 ℃, the specimen was heated again at 10 ℃/min to 300 ℃. First heating cycle was used to remove any thermal processing history, while the second heating cycle was used to characterize the materials.

Electrical conductivity

The electrical conductivity of both extruded strands and hot-pressed films were measured by two-point measurement using a voltage power source (Agilent, 6614C) and a picometer (Keithley, 6485). The extruded strand samples were cut into 35 mm long rods with diameter of 3 mm, and silver paint was applied to both ends in order to minimize contact resistance. Conductive silver paint was also applied to film samples which were cut to the dimension of 60 mm x 5 mm with thicknesses ranging from 100 to 120 μm. Subsequently, metallic electrodes were connected to both ends for measurement. For each concentration, five specimens were tested and average value with standard deviation was used for discussion.

Electrical conductivity calculation

The resistivity of specimen is calculated using equation:

$$\rho = R * A/L = R * \pi r^2/L \qquad \text{(Equation 3. 1)}$$

Where *R* is measured resistance, *A* is the cross-sectional area of the specimen, *r* is the radius of the extruded strand, and *L* is the length. Due to the relationship between resistivity and conductivity ($\sigma = 1/\rho$), the conductivity was calculated for different filament and film samples for further data analysis.

Dynamic percolation

The in-situ conductivity test during the heating of polymer melts was set up according to previous dynamic percolation studies performed in our group [213]. Another layer of silver paint was used before an insulating epoxy layer was applied, avoiding any direct contact between epoxy and the phenoxy, which is prone to swelling and dissolution by the epoxy. The length of the strand samples was 10 mm with diameters of about 3 mm. Different heating profiles were applied and recorded. Temperature, time, and conductivity were monitored simultaneously throughout the test.

3.3 Results and discussion

3.3.1 Thermal properties

DSC

DSC was used to confirm the T_g of as received phenoxy pellets. As shown in Fig. 3.2, the glass transition endothermic peak for phenoxy was present at around 95 to 100 ℃, with a measured value for T_g of 100.4 ℃, which is close to the reported value from the phenoxy data sheet.

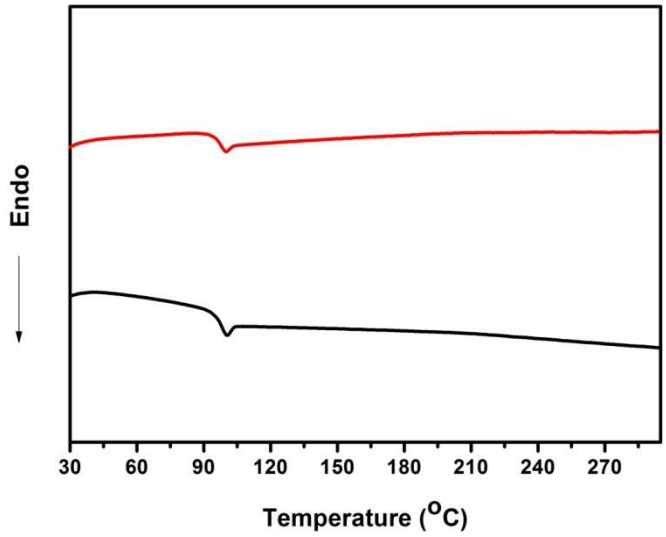

Fig. 3.2 DSC results for as received phenoxy.

Rheology

Rheological results are presented in Fig. 3.3, where storage modulus and loss modulus are plotted against frequency (Fig. 3.3a) to confirm the viscous-like behaviour of the phenoxy, as well as a temperature scan at different frequencies (Fig. 3.3b and 3.3c). Frequency scans in Fig. 3.3a were performed at relatively low temperatures of 170 ℃. Under these conditions loss modulus was higher than storage modulus for all frequencies, indicating the viscous-like behaviour in this region. Temperature scans were performed above this region without any signs of solid-like behaviour.

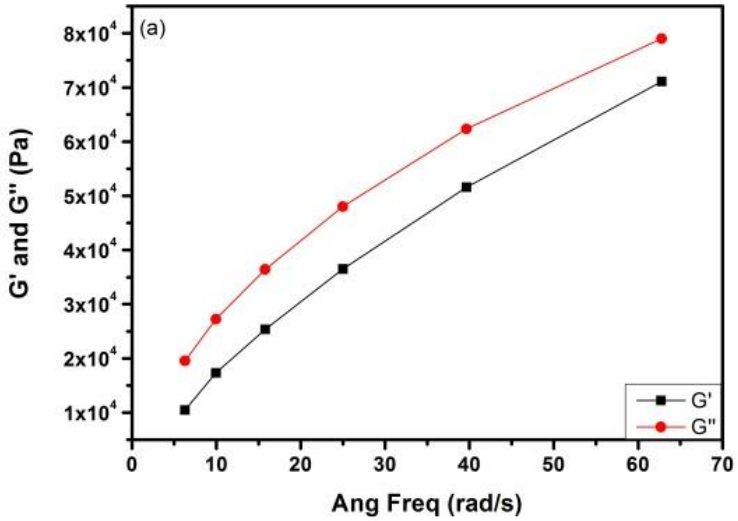
(a)
G' and G'' (Pa)
Ang Freq (rad/s)
G'
G''

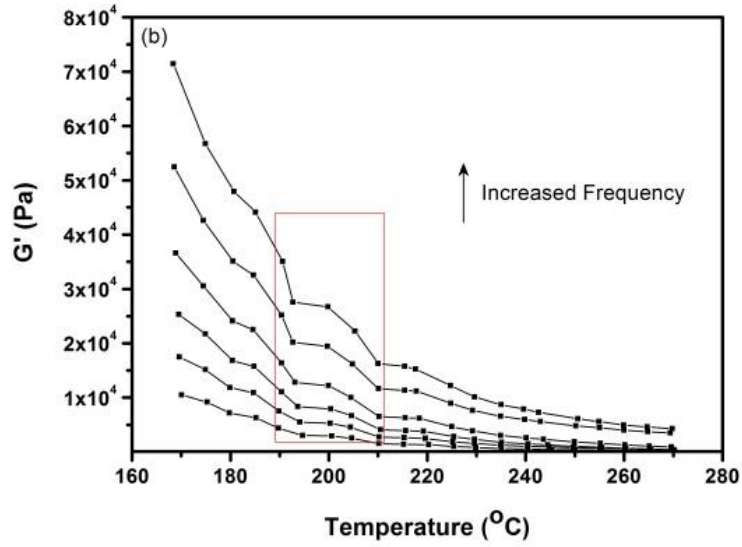
(b)
G' (Pa)
Temperature (°C)
Increased Frequency

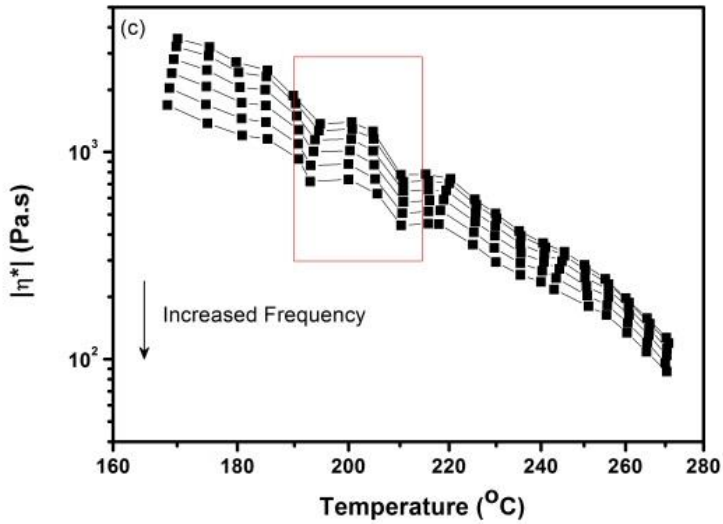
(c)
|η*| (Pa.s)
Temperature (°C)
Increased Frequency

Fig. 3.3 Rheological data for neat phenoxy: (a) Storage modulus and loss modulus at 170 ℃ as a function of frequencies; (b) Storage modulus as a function of temperature for different frequencies ranging from 1 Hz to 10 Hz; (c) Viscosity as a function of temperature for different frequencies ranging from 1 Hz to 10 Hz.

With increasing frequencies from 1 Hz (6.28 rad/s) to 10 Hz (62.8 rad/s), the slopes of the storage moduli changed at a temperature range around 200 ℃. Similar trends were found for viscosity plots using a temperature scan. These observations indicate a transition from rubbery state to liquid state of phenoxy, indicating the suitable processing temperature range.

3.3.2 Optimization of processing parameters

In order to obtain electrically conductive nanocomposites, processing parameters such as residence time, mixing speed, and mixing temperature were optimized after various trials. Theoretically, higher processing temperatures, longer processing times, and higher mixing speeds should break-down CNT agglomerates, leading to better dispersion of nanoparticles in the polymer matrix. However, the final processing window is limited as too high temperature, shear force and too long processing times may lead to degradation of the polymer matrix, lowering its mechanical and electrical properties.

Therefore, the influence of processing temperatures, processing time and mixing speed on electrical conductivity of the extruded strands was investigated for

phenoxy/CNT nanocomposites with a fixed CNT loading (1 wt.%). Main results are presented in Fig. 3.4.

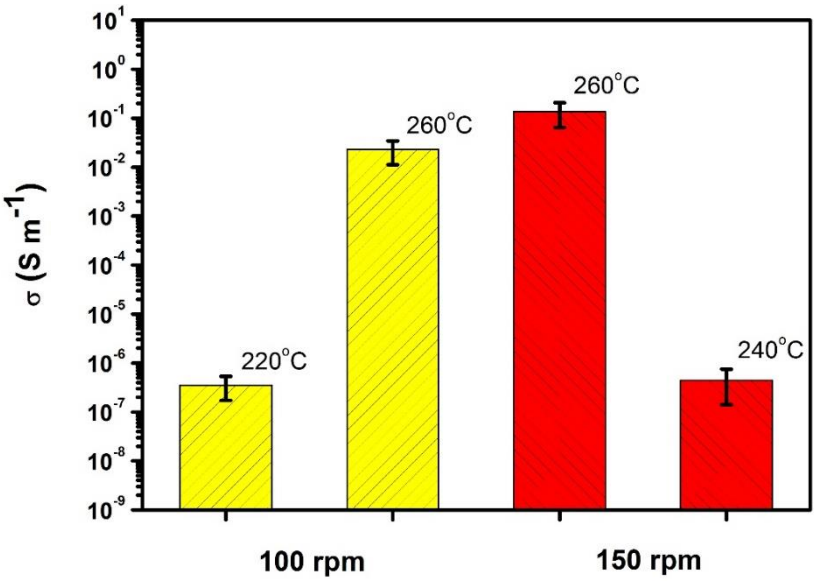

Fig. 3.4 Electrical conductivity comparison between different processing conditions.

It can be seen that a combination of a high processing temperature and mixing speed, results in the highest electrical conductivity. Although in theory, even higher temperatures might result in better electrical properties, the processing temperature was limited to 260 ℃ in order to avoid degradation of the polymer, while for the same reason the processing time was limited to 5 min for all specimens and was carried out under nitrogen environment (condition 3).

3.3.3 Morphological observations

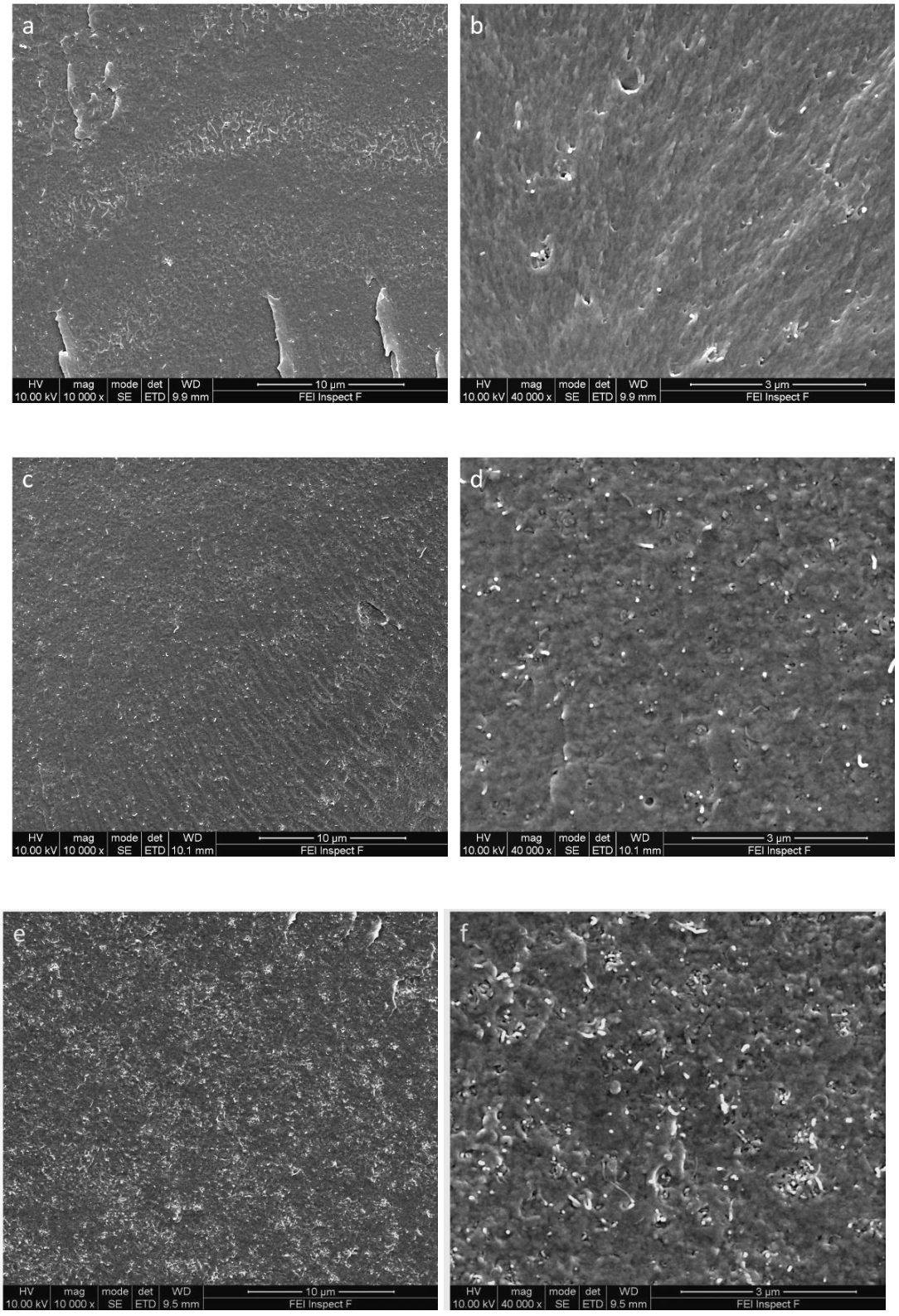

Fig. 3.5 SEM images of fracture surface of extruded strands of phenoxy/CNT composites with different CNT loadings at different magnifications: (a)-(b) 0.5 wt.% CNT; (c)-(d) 1.0 wt.% CNT; and (e)-(f) 1.5 wt.% CNT.

CNT dispersion in nanocomposites was examined under SEM and morphological observations are presented in Fig. 3.5. The bright dots and rod-like particles show dispersed CNTs within the polymer matrix, with few of those been pulled-out during cold-fracture. Relatively well dispersed CNTs can be observed in most images, although it is difficult to have quantitative measurements on nanofiller dispersion. With increasing loading of CNTs, more CNTs become visible at the same magnification, but no large agglomerates were observed. Since the CNTs employed in this work are not functionalized, this good dispersion is mainly attributed to the processing, and good compatibility between filler and matrix. First, at optimized processing temperature, the fluidity of the polymer melt allows the CNTs to be dispersed. Secondly, the high shear force applied during mixing breaks down any large agglomerates and bundles of CNTs, leading to well dispersed nanocomposites.

3.3.4 Electrical properties

Static percolation for phenoxy extruded strand and hot-pressed film specimen

Fig. 3.6 shows the electrical conductivity of the phenoxy/CNT nanocomposites, with different CNT concentrations for both extruded strand and hot-pressed film. With the addition of only 1 wt.% of CNTs into phenoxy, the electrical conductivity of the

extruded strand specimens was increased in excess of 10 order of magnitudes up to conductivity levels of 10^{-1} S/m.

For extruded strand samples in Fig. 6a, the conductivity increased almost four orders of magnitude from 6×10^{-5} S/m to 6×10^{-1} S/m when the CNT concentration is increased from 0.5 wt.% to 1.17 wt.%.

Percolation theory [214] was applied to analyse the electrical properties of the specimens, fitting Equation 3.2, valid for concentrations above the percolation threshold.

$$\boldsymbol{\sigma = \sigma_0 (p - p_c)^t} \qquad \text{(Equation 3. 2)}$$

Where σ is electrical conductivity, σ_0 is a scaling factor, p_c is the critical concentration, and t is an exponent that depends on dimensionality of the formed network where t larger than 2 normally refers to a three-dimensional network [215, 216]. Fitting extruded strand data (Fig. 3.6a) with Equation 1 gives a percolation threshold of 0.46 wt.% (0.28 vol.%) which is very low for melt processed thermoplastic nanocomposites [217]. This is partly attributed to the good CNT dispersion in the phenoxy matrix. The extracted value for critical exponent t from this fit was 6.2, indicating a three-dimensional network within the nanocomposites [215, 218]. It worth noting that this obtained static percolation threshold value is slightly lower than previous reported (0.58 wt.%) for a similar system [219], mainly due to the very limited CNT orientation within the extruded strand. In fact, it is generally believed that the highest conductivity is obtained in oriented systems where the CNTs are slightly misaligned along the extruded direction [220].

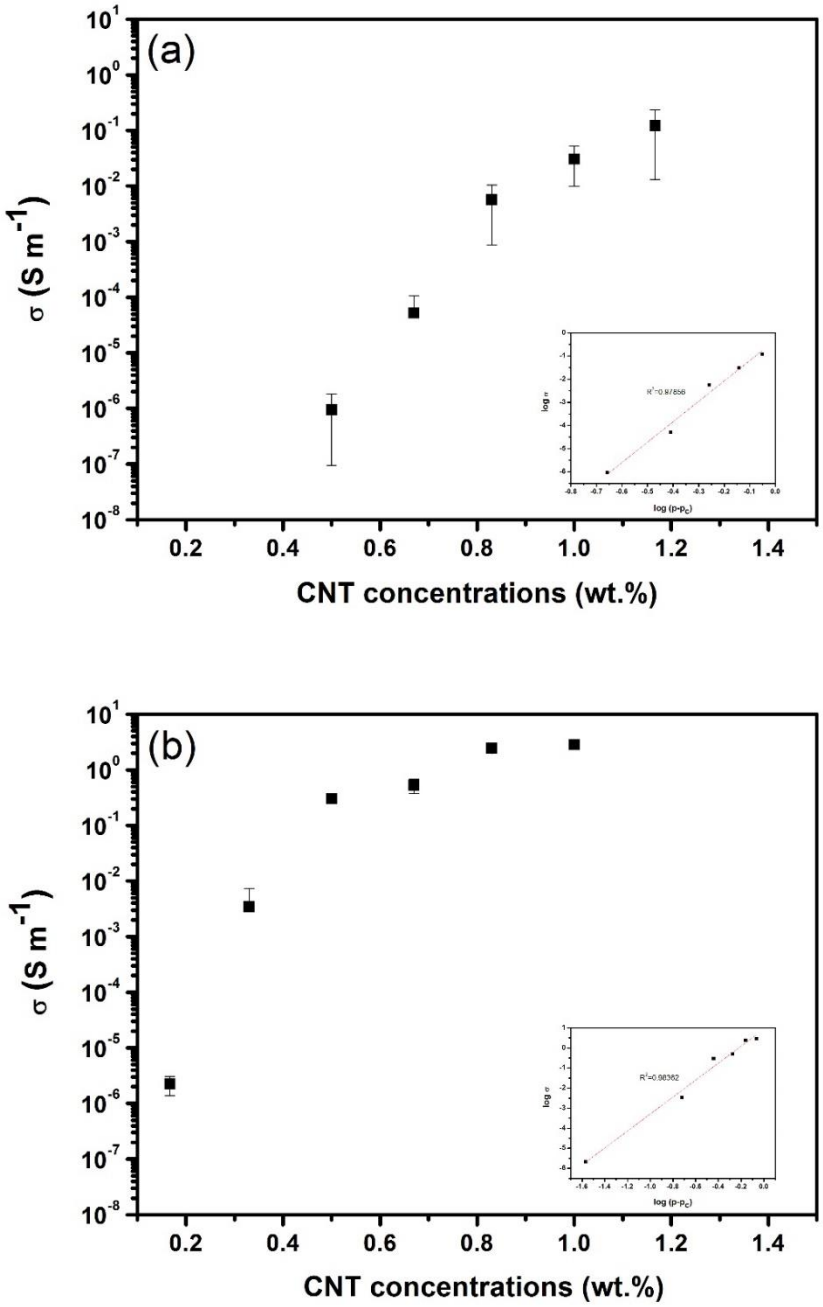

Fig. 3.6 Electrical conductivity as a function of CNT concentration for: (a) extruded strand samples, (b) hot-pressed film samples.

Fig. 3.6b shows the electrical conductivity for hot-pressed films with increasing CNT loading. A percolation threshold of 0.20 wt.% (0.12 vol.%) CNT was

calculated from this graph, which is clearly lower than that of extruded strands. It is worth mentioning that the obtained percolation threshold value is among the lowest values for melt-processed thermoplastic systems [217]. The value of critical exponent *t* was here 5.0. At a CNT concentration of 0.5 wt.%, the conductivity of pressed films is 3×10^{-1} S/m which is over four orders of magnitude higher than that of extruded strands (6×10^{-5} S/m). The reason for such a large increase in conductivity with hot-pressing has been well reported in our previous works and is believed the result of a dynamic percolation process within the composites [157, 213, 221, 222]. As mentioned earlier, the formation of a conductive filler network is a time and temperature dependent process which requires certain energy. Raising temperature during hot-pressing allows the CNTs within the polymer matrix to re-agglomerate and establish particle-particle contacts, leading to a four orders of magnitude increment in conductivity. Therefore, the understanding of relationship between temperature, time, and filler loading is essential for the understanding of network formation in CPCs as well as the further optimization of processing conditions.

Dynamic percolation in phenoxy/CNT nanocomposites

Fig. 3.7a shows the electrical conductivity of extruded strand specimen when subjected to the temperature profile specified in Fig. 3.7b. Clear dynamic percolation behaviour, with an up to seven orders of magnitude increase in conductivity, can be observed from the graph. This observation has great technological implications as with exactly the same conductive filler content, electrical properties can show very large variations depending on the thermal history of the sample. This phenomenon

has previously been reported by other researchers for other systems [156, 157, 213], and is as mentioned before explained by a dynamic process of filler re-agglomeration.

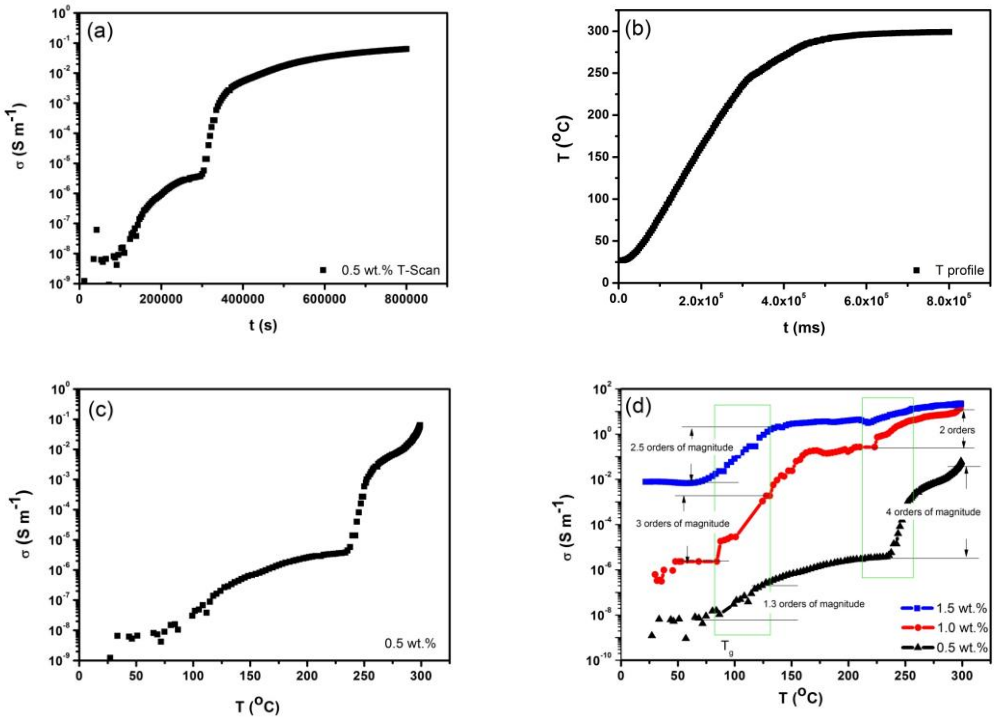

Fig. 3.7 Dynamic percolation behaviour of phenoxy/CNT nanocomposites, showing (a) electrical conductivity with time; (b) applied temperature profile; (c) electrical conductivity with temperature; (d) analysis on three concentrations of CNT with increasing temperature.

Fig. 3.7c shows the electrical conductivity as a function of temperature. A fixed concentration of 0.5 wt.% CNT was chosen, i.e. close to the static percolation threshold. Upon reaching the phenoxy's T_g (92 ℃), electrical conductivity increased slightly due to the relaxation of macromolecules and increased mobility of the CNTs in the phenoxy. As heating continued, a plateau of conductivity is reached until the next transition (rubbery to liquid) is encountered. When the polymer is in the liquid

state (i.e. from 220 ℃) the CNT network is re-establishing itself, and a sharp increase in conductivity of several orders of magnitude is observed. It is worth noting that the starting temperature at this sharp increment depends on the conductive filler content, since it is related to possible connected pathways. However, for filler content around the percolation threshold, this temperature range relates to the transition (rubbery to liquid) observed from rheological results (Fig. 3.2). This phenomenon can be explained by dynamic percolation theory of nanocomposites as mentioned earlier. Since the formation of a conductive network requires a certain time and energy, with CNTs re-agglomerating, the original network might be affected, resulting in a slight reduction in conductivity. After initial CNT network reformation, the conductivity of the composites increased rapidly, finally reaching a much higher conductivity level compared to the original value.

To get more of an insight into the effect of CNT concentration on the dynamic percolation process, as well as the onset and peak temperature of the re-agglomeration process, the electrical conductivity as a function of temperature was plotted for different CNT loadings in Fig. 3.7d. The small variations in electrical conductivity at the beginning of heating as shown in the graph are probably due to a competition between thermal expansion of the polymer which increases the distances between conductive fillers, and temperature dependence tunnelling effect [213].

Two stages of conductivity increment can be seen for all specimens, with the first increment taking place in correspondence with T_g, and the second increment in correspondence of with the rubber-liquid transition. At 0.5 wt.% CNT loading, the conductivity increment during the first stage is not very obvious, due to the limited amount of conductive filler within the matrix. When the CNT loading increased to 1.0 wt.%, a three orders of magnitude increment is observed during the first stage,

confirming a re-agglomeration process above T_g. A slightly lower increase of around 2.5 orders of magnitude is observed for higher CNT loading (1.5 wt.%) but it is believed that this is mainly due to the relatively high initial value of these composites. A summary is presented in Table 3.2 below.

Table 3.2 Summary of dynamic percolation behaviour at different CNT loadings.

CNT concentration (wt.%)	0.5	1.0	1.5
Orders of magnitude increase @ 1st increment	1.3	3	2.5
Orders of magnitude increase @ 2nd increment	4	2	1

A plateau in conductivity was found for all specimens when they are in the rubbery state. For lower CNT concentrations, this plateau lasts longer than for higher CNT loadings. Since processing conditions and testing parameters are identical for all samples, this observation is mainly attributed to the difference in CNT loading. The higher the CNT loading, the easier for the conductive network to re-form, and the shorter the time and lower the temperature required for the dynamic percolation process. Clearly, at lower CNT concentrations a higher activation temperature is required for dynamic percolation. With CNT loading increasing from 0.5 to 1.0 wt.%, the dynamic percolation process shifts to lower temperatures, which indicates that at higher CNT concentrations the dynamic percolation process is able to operate at lower temperatures. When the CNT concentration is well above the percolation threshold, for instance at 1.5 wt.%, the electrical conductivity is already high at room temperature, which does not lead to an obvious increase in conductivity with increasing temperature.

Isothermal conditions

Isothermal dynamic percolation tests are performed and presented in this section. Since the dynamic process of conductive network formation is less obvious for high CNT concentrations, a relatively low CNT loading (0.5 wt.%) was selected for the isothermal tests at different temperatures.

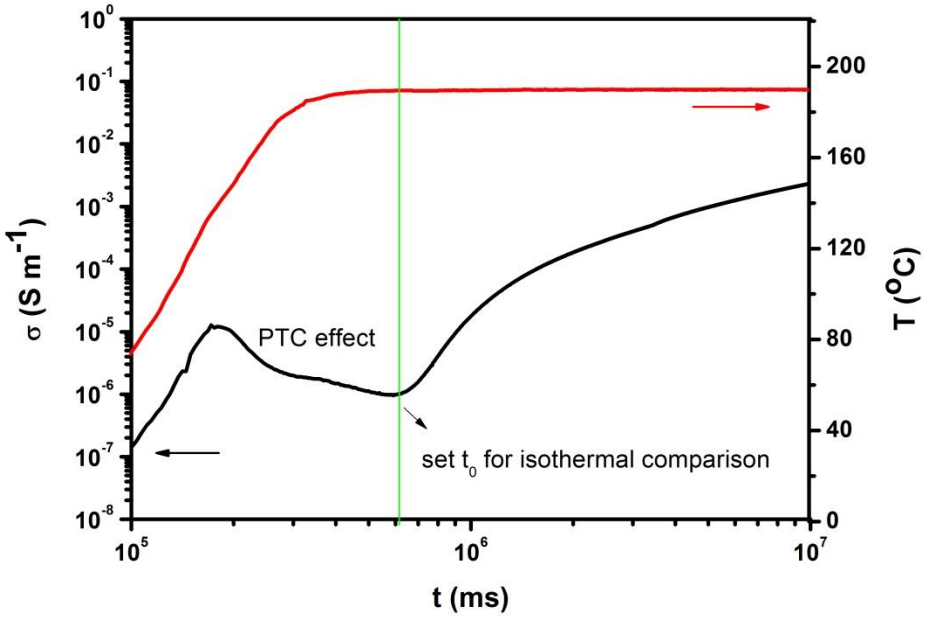

Fig. 3.8 Representative curve of electrical conductivity as a function of time under 190 ℃ isothermal conditions.

Fig. 3.8 shows a representative curve of electrical conductivity at 190 ℃ together with the temperature profile. Interestingly, a positive temperature coefficient (PTC) effect is observed, with this effect being more obvious for lower isothermal temperatures, which cannot be explained by the variation in heating rate. It is believed that two main processes are taking place: (i) thermal expansion which increases the gaps between conductive CNT fillers hence reducing the electrical

conductivity; and (ii) dynamic percolation which allows for the re-agglomeration of CNTs hence increasing the electrical conductivity. At relatively low temperatures, for instance 190 ℃, thermal expansion is taken place while the viscosity of the polymer is not low enough for CNTs to re-agglomerate. Therefore, after initial softening of the polymer matrix the electrical conductivity is reduced. Once the specimen remains under isothermal conditions for a certain time, the thermal energy accumulated within the composites allow CNTs to re-establish conductive networks, leading to the final increment of electrical conductivity.

To eliminate other factors and demonstrate only the re-agglomeration processes under isothermal conditions, the starting time was set when the PTC effect is finished and the temperature is stabilized, as indicated in Fig. 3.8.

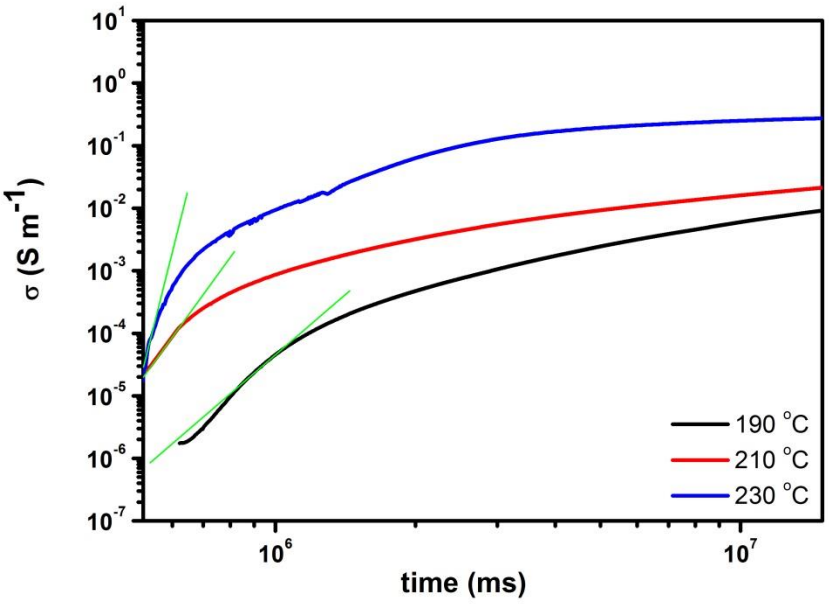

Fig. 3.9 Electrical conductivity of phenoxy/0.5wt.% CNT composites under different isothermal temperatures.

Fig. 3.9 shows the results of isothermal electrical conductivity tests for phenoxy/0.5 wt.% CNT composites at different temperatures. It can be seen that for the same CNT concentration, the slope of the conductivity curves increases with temperature, while the time required to reach a certain conductivity level is also greatly affected by this temperature. In other words, the time required for CNTs to re-establish a percolated pathway greatly depends on the given energy. For instance, to reach a conductivity level of 10^{-4} S/m, a specimen at 190 ℃ takes about 26 min, whilst at 230 ℃ a much shorter time of only 9 min is required.

Table 3.3 Summary of isothermal dynamic percolation results

	170 ℃	190 ℃	210 ℃	230 ℃
Time required to reach conductivity of 1×10^{-2} S/m (min)	807.8	345.8	91.0	16.6
Conductivity reached after 15 min (S/m)	4.6×10^{-7}	9.8×10^{-6}	6.5×10^{-4}	0.7×10^{-2}
Time period of PTC effect (min)	24.5	7.1	3.8	2.6

The results of the isothermal dynamic percolation tests at different temperatures are summarized in Table 3.3. With higher temperatures less time is required for CNTs to re-establish a network. This phenomenon was found consistent with previous dynamic percolation studies on other polymers [156, 157, 213]. These results further confirm that by selecting an optimal processing temperature, the processing time of conductive polymer composites can be significantly shortened, as required electrical properties can be reached at shorter times through a tailored heating process.

These results also indicate that thermal history greatly affects the electrical properties of samples, even after the effective initial dispersion of conductive nanofillers in the polymer matrix. Therefore, applying a post-treatment may be an interesting approach to improve the final electrical properties of such materials. To obtain higher levels of electrical conductivity at the same CNT concentration, higher annealing temperatures or longer annealing times are required, although care should be taken to avoid thermal degradation of the polymer matrix during such a process.

3.4 Conclusions

Electrical percolation curves were obtained for both extruded strands and hot-pressed films of phenoxy/CNT nanocomposites. Morphological studies showed good CNT dispersion without aggregates. The difference in electrical properties at the same conductive filler content between strand and film specimens confirmed the importance of post-treatments on electrical properties of conductive polymer composites. After annealing a percolation threshold value as low as 0.20 wt.% (0.12 vol%) was achieved, which is among the lowest ever reported for any melt-processed thermoplastic systems. For the first time the dynamic percolation process of CNT in phenoxy has been studied, demonstrating that CNT network formation within the phenoxy matrix is a time-dependent, energy activated process. The different isothermal conditions studied could be instrumental in optimizing processing and post-processing parameters (time/temperature) for different CNT loadings and required final properties.

Chapter 4

Dissolution Behaviour of Phenoxy in Epoxy

4.1 Introduction

In order to enable the use of thermoplastics as carriers for the delivery and localization of CNTs in FRPs, the time required for thermoplastic phenoxy to dissolve within a thermoset epoxy needs to be identified, providing guidelines and fundamental knowledge for subsequent processing as well as relevant toughening mechanism in FRPs.

As the dissolution behaviour of the thermoplastic depends on the area of this thermoplastic in contact with the epoxy solvent. To obtain thermoplastics with different surface-to-volume ratio various techniques are applied to produce phenoxy fibres with different diameters, including traditional melt extrusion, as well as electrospinning. Electrospinning has been widely used to produce polymer nanofibres in last two decades [223-227]. Compared to conventional melt-spinning, electrospinning usually leads to much smaller diameters and as a result much higher specific surface areas, together with high porosity non-woven mat.

In this chapter, phenoxy fibres produced by both melt-spinning and electrospinning have been introduced in epoxy resins, and their dissolution time has been recorded, together with morphological studies using microscopy. A heating stage was

employed to mimic the temperature profile during the infusion process and subsequent curing cycles.

4.2 Experimental

4.1.1 Materials

Polyhydroxy ether bisphenol A (phenoxy) was supplied by InChem (PKHH) with an average molecular weight (Mw) of 52,000, and a glass transition temperature (T_g) of 92 ℃. The composite system employed consists of high strength 2 × 2 twill carbon fibre fabrics, with an areal weight of 286 g/m^2, and RTM6-2 which is a two components aerospace grade epoxy, both from Hexcel. The RTM6-2 was chosen due to its high performance and wide applications in current aerospace applications. After mixing this two component system, the formulation of the RTM6-2 is similar to RTM6, consisting of tetraglycidyl diamino-diphenyl-methane (TGDDM) and diamino-diphenyl sulphone (DDS). Chloroform and N,N-Dimethylformamide (DMF) was purchased from Fisher Scientific and Sigma-Aldrich, respectively.

4.1.2 Electrospinning

As illustrated in Fig. 4.1, in the electrospinning process a high voltage is applied to a polymer solution to generate a potential difference between polymer solution and grounded collector. Polymer solution is pumped at a controlled feeding rate from syringe, and formed a Taylor cone at the end of needle due to the electrostatic repulsion forces from charges in the solution [228]. After the repulsion force overcomes the surface tension of the solution at the spinneret, solution will be

ejected toward a collecting substrate, whilst the organic solvent will evaporate during this flight, resulting in a solid nanofibre depositing onto the substrate.

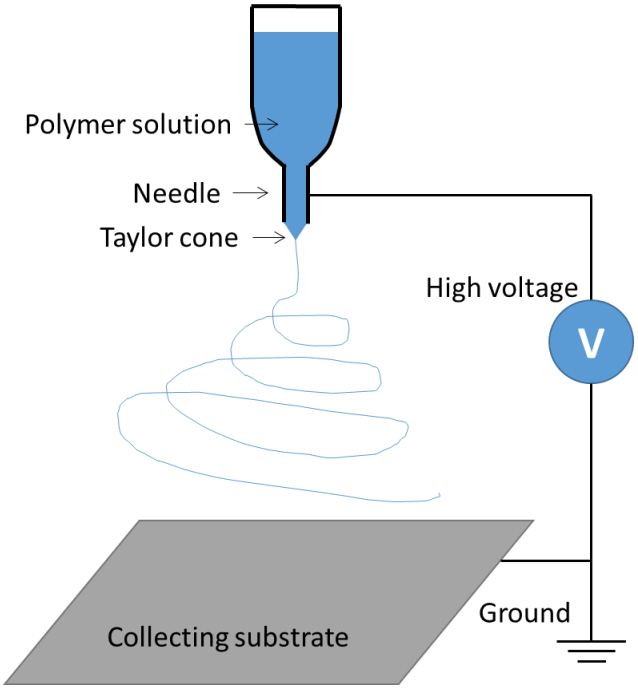

Fig. 4.1 Schematic illustration of the electrospinning process.

4.1.3 Optical microscopy

Optical microscopy (Olympus BX60F) was used to examine the morphology of the extruded and electrospun fibres. Electrospun fibres with different diameters were collected on glass slides and observed under an optical microscope equipped with a digital camera.

4.1.4 Hot stage microscopy

To study the dissolution behaviour of phenoxy fibre in epoxy resin, a Linkam HFS600 heating stage was fitted to an Olympus BX60 optical microscope. The temperature of the heating stage was controlled by LinkSys32 software, while optical microscopy images were processed using Image-Pro Express software. Phenoxy fibres (with diameters ranging from 1 μm to 200 μm) were placed on a glass slide and positioned under the optical microscope, with both heating stage and epoxy resin pre-heated to 80 ℃ before a droplet of epoxy (RTM6-2) was placed on the glass slide. A thin glass cover slide was then positioned on top of the epoxy droplet before observation. The same procedure was used for temperatures of 90 ℃ and 100 ℃, as well as different fibre diameters (1 - 200 μm).

4.3 Results and discussion

4.3.1 Optimization of electrospinning parameters

Several parameters are affecting the quality of the produced nanofibres, including applied voltage, polymer concentration in solution, feeding rate of solution, humidity, temperature of solution, and the distance between needle and collecting substrate. For instance, a higher polymer concentration in solution results in a higher fibre diameter, while a higher voltage applied normally leads to thinner fibres, etc. Therefore, to obtain continuous phenoxy nanofibres, an optimization of processing conditions has been employed.

The solvents involved were chloroform and DMF, both polar solvents with a solubility parameter of 9.3 and 12.1, respectively. Phenoxy as a polar polymer with a

solubility parameter of 10.7 can be easily dissolved in either of these two solvents. The combination of two was mainly for balancing the evaporation time during the electrospinning processes.

Fig. 4.2 shows the effect of polymer concentration in solution for electrospun fibres with other parameters kept the same: 1.2 ml/hr, 24 kV, 26 cm, 22 % for feeding rate, applied voltage, distance, and relative humidity, respectively. From top to bottom, the solution concentration was increased from 12 wt.% to 15 wt.%, then finally reaching 18 wt.%. At a low polymer concentration of 12 wt.%, the solution was "spinnable" and evidence of fibres is observed. However, beads are formed throughout the fibre mats, resulting in inconsistent fibre morphologies. With increased polymer concentration in solution (15 wt.%), the fibres became more continuous, while their diameter also becomes more consistent. No obvious beads are observed at this concentration level. When the solution was further increased to 18 wt.%, the diameter of the electrospun fibres becomes inconsistent again, while the average diameter was also increased from previous results.

In fact, none of these parameters can be isolated, and both applied voltage, concentration, feeding rate as well as distance need to be balanced in order to produce continuous fibres with consistent diameters. Although some defects were observed for 15 wt.% solution concentration fibres, the overall quality of the produced fibres was acceptable. Therefore the concentration chosen for final phenoxy nanofibre production was 15 wt.%, and other parameters such as feeding rate and voltage were accommodated depending on required fibre diameters.

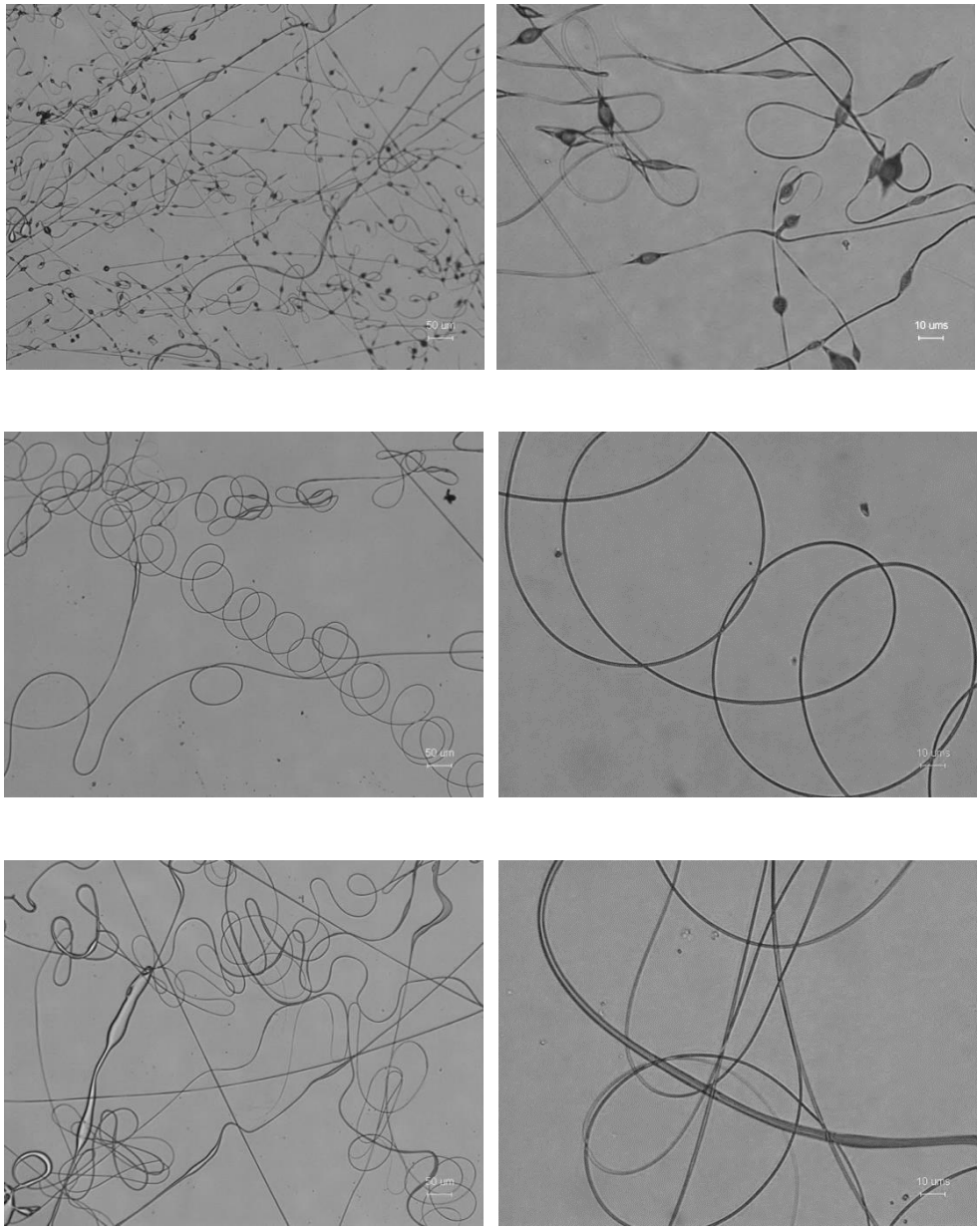

Fig. 4.2 The effect of polymer solution concentrations on morphology of electrospun nanofibres. From top to bottom: 12 wt.%; 15 wt.%; and 18 wt.%.

After the optimization of the electrospinning parameters, a non-woven veil was produced which can be used as interleaves for the manufacturing of composite laminates.

4.3.2 Dissolution behaviour of phenoxy fibres in epoxy resins

Phenoxy fibres with different diameters were placed in epoxy resins under isothermal conditions, and dissolution time was recorded. The diameter was measured by microscope images throughout the dissolution, and the data points were used to plot the diameter change with time under different isothermal conditions.

Fig. 4.3 shows optical microscopy images of phenoxy fibres at 90 ℃ isothermal condition. The measured phenoxy fibre diameter was 111 μm. After the epoxy resins were placed onto the glass slide, images were taken with minute intervals up to one hour. The interval in Fig. 4.3 is 10 min from top to bottom, with the measured diameter being clearly reduced with time, from 111 μm to 69 μm at 30 min, and 46 μm at 60 min.

The measured diameter with dissolution time was recorded and plotted in Fig. 4.4, in order to have a better insight into the dissolution process as well as a guide to predict the required time for complete dissolution. To examine the effect of temperature on dissolution behaviour, isothermal dissolution studies were performed at 80 ℃, 90 ℃ and 100 ℃.

Apparently, although the starting diameter of the phenoxy fibres is the same for all three specimens, their dissolution behaviour is clearly affected by the resin temperature. At a resin temperature of 80 ℃, the diameter was only reduced to 70 μm after 60 min. At 90 ℃ the diameter decreased to 45 μm, while at 100 ℃ the phenoxy fibre was completely dissolved in epoxy resin.

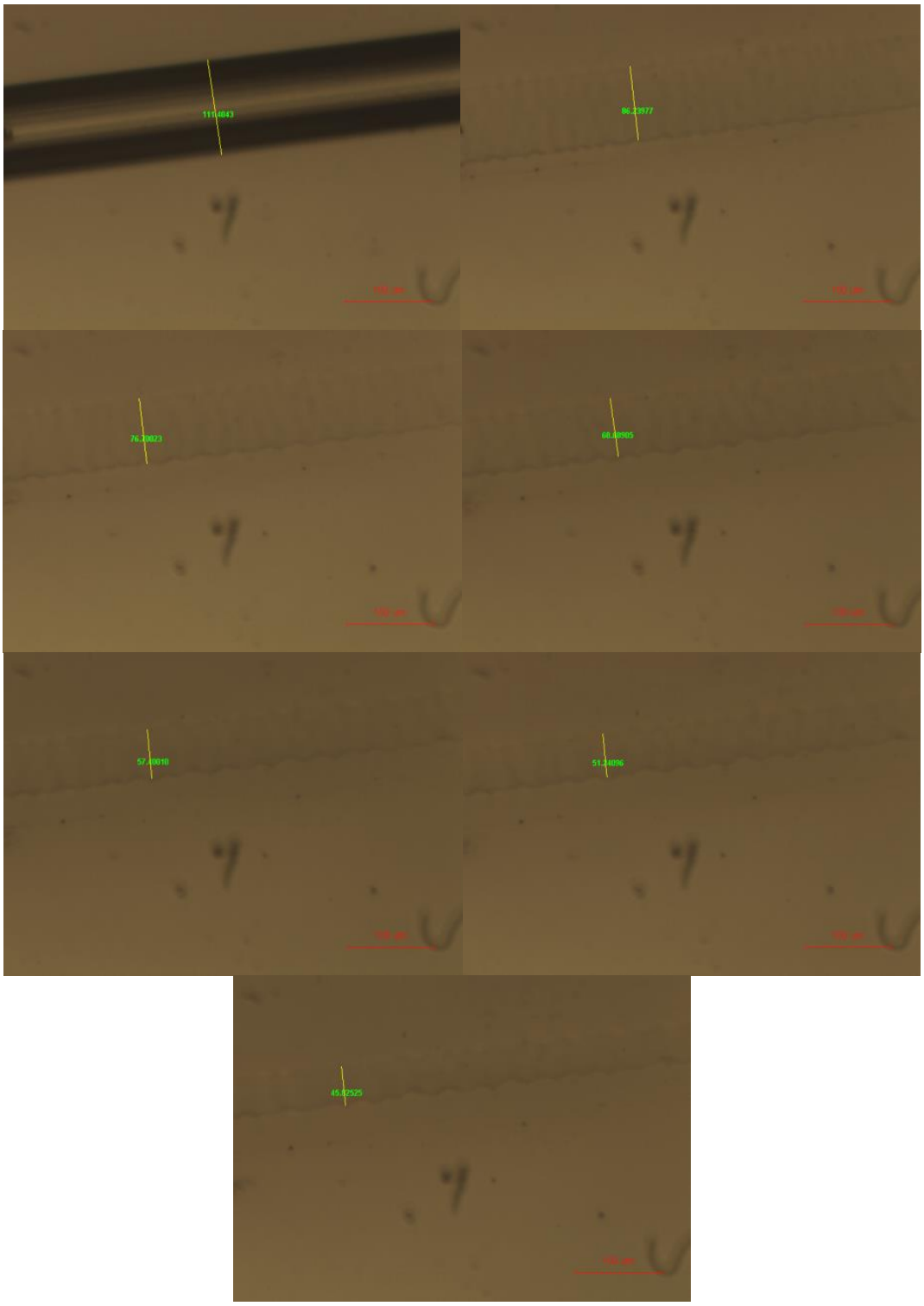

Fig. 4.3 Optical microscopy images of phenoxy fibres in epoxy at 90 ℃, from top to bottom: without epoxy, and from 0 min to 60 min with 10 min intervals.

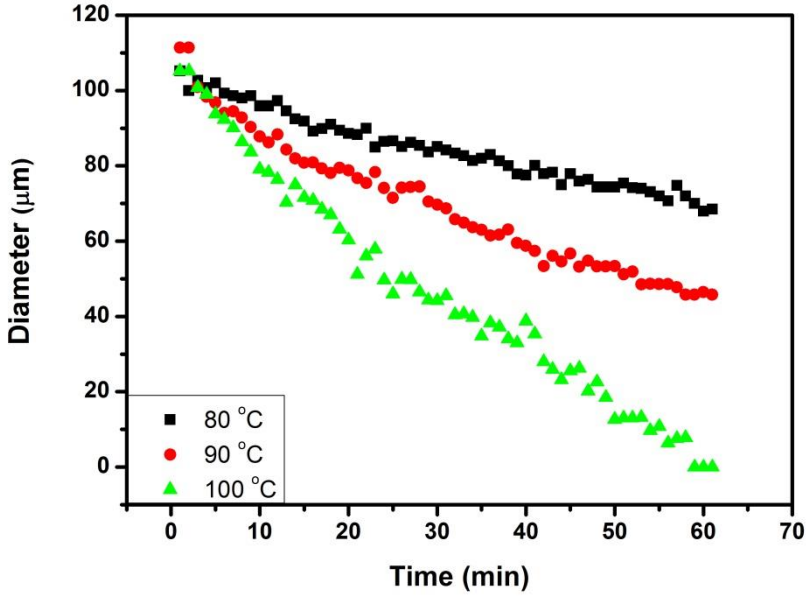

Fig. 4.4 The dissolution behaviour of phenoxy fibres in epoxy resins under different isothermal conditions.

Since the main aim of this dissolution studies was to provide some further insight and guidelines for the required dissolution times under various conditions, a simple linear fitting was chosen to simplify the equation. After applying a linear fit to these data, the slope of each curve is -0.533, -0.932, and -1.623, for temperatures of 80 ℃, 90 ℃, and 100 ℃, respectively. To predict the dissolution time of phenoxy fibre in epoxy resin, a simple relationship is proposed (Equation 4.1), where d is diameter of fibre, d_0 is the original fibre diameter, a is the slope of the dissolution curve, and t is the time. To have d reaching zero value for a fixed d_0, slope a needs to be negative and large enough.

$$d = d_0 + at \qquad \text{(Equation 4. 1)}$$

Based on the obtained dissolution time under different isothermal conditions, a table was presented together with the predicted times based on this equation (Table 4.1). To completely dissolve a phenoxy fibre with a diameter of 100 μm in epoxy resin, theoretically three hours are required at 80 ℃, while one hour is needed if the temperature is raised to 100 ℃. However, it worth noting that the actual dissolution process will be slower than predicted using Equation 4.1, as during the phenoxy dissolution processes, the surrounding concentration of phenoxy in the epoxy resin keeps increasing, reducing the rate of dissolution.

Table 4.1 Summary of dissolution time under different isothermal conditions.

Temperature (℃)	80	90	100
Initial diameter (μm)	105	111	105
Slope from linear fit	-0.533	-0.932	-1.623
Predicted time (min)	197	120	65

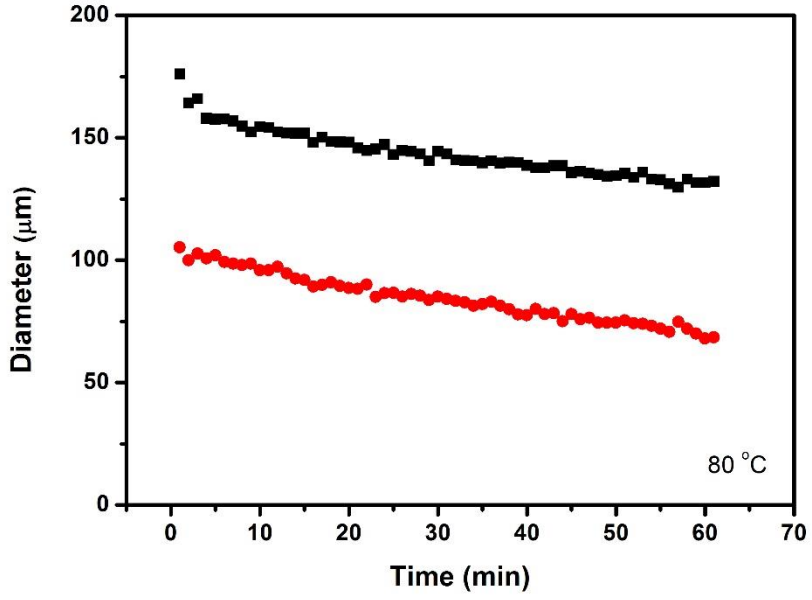

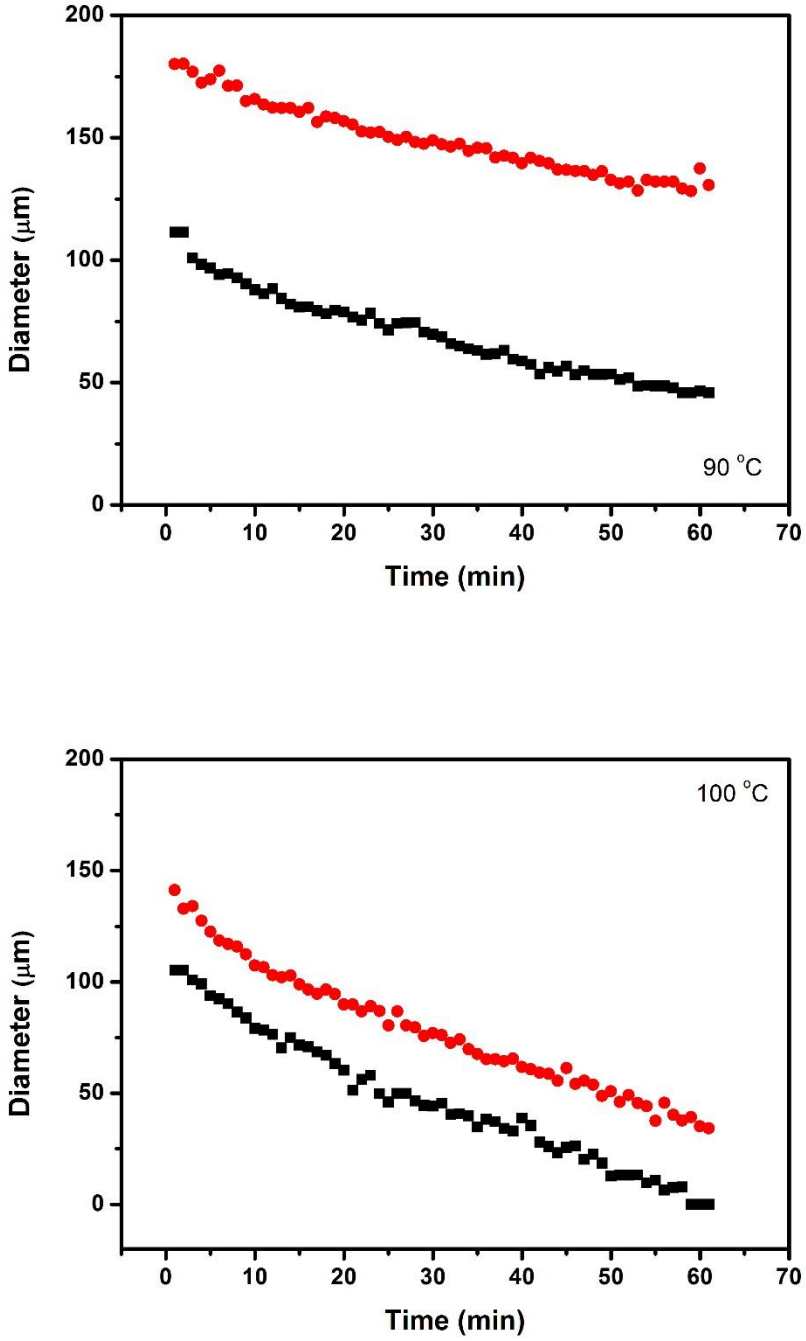

Fig. 4.5 Dissolution time for different phenoxy fibre diameters in epoxy, from top to bottom: 80 ℃, 90 ℃, and 100 ℃.

To confirm this proposed dissolution time relationship, phenoxy fibres with different diameters were placed into epoxy resin, and diameter changes were monitored and recorded (Fig. 4.5). As expected, larger diameter phenoxy fibres, having lower surface-to-volume ratio, require longer dissolution times. To facilitate the dissolution process of phenoxy fibres in epoxy resin, fibres with smaller diameter are therefore desirable.

Based on the proposed equation, the dissolution time for phenoxy fibres with a diameter of 1 μm at 80 ℃ and 90 ℃ should be less than 1.9 min and 1.1 min, respectively. Fig. 4.6 shows the optical observations for phenoxy fibre at 80 ℃. Some of the phenoxy fibres with smaller diameters have become invisible after 30 sec, while fibres with larger diameters still remained visible. After 60 sec, most of the phenoxy fibres have been dissolved in the epoxy, while no obvious trace of phenoxy can be found after 90 sec. This dissolution time provides supports to the predictions based on Equation 1. It is worth pointing out that in the performed dissolution model studies, phenoxy fibres are individually examined, while during subsequent composite manufacturing, interleaves are compressed between carbon fabrics plies, which may slightly affect their dissolution time.

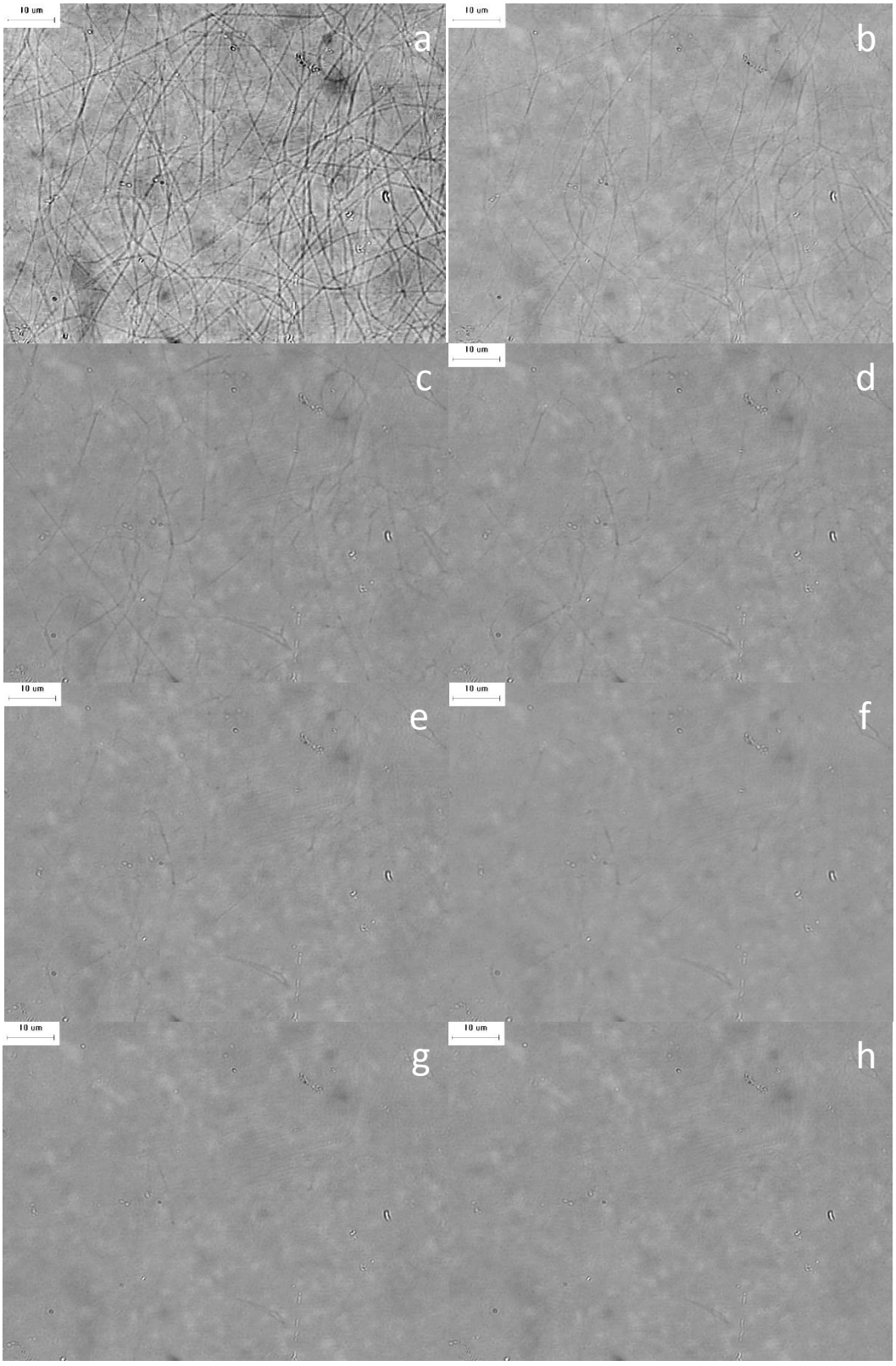

Fig. 4.6 Optical observations of phenoxy fibre with a diameter of 1 μm at 80 ℃, time interval between each image is 10 sec (from a to h).

4.4 Conclusions

The dissolution behaviour of phenoxy fibres in epoxy resin has been studied. Fibres with different diameters were produced via melt extrusion and electrospinning, and examined under various isothermal conditions. Parameters of electrospinning processes were optimised for continuous fibre production.

A simple relationship was purposed based on observed dissolution times, and various slopes were calculated for phenoxy fibres with diameters of 100 μm under different isothermal conditions. It is expected that for larger diameters, this slope will become less steep, hence increasing the dissolution time, and vice versa. The proposed relationship was used to predict phenoxy fibre dissolution times for 1 μm diameter fibres, and experimental data have shown good agreement with predicted times.

These dissolution studies have provided guidelines for subsequent composite manufacturing processes, such as resin infusion processes and curing of epoxy resins. Furthermore, the observed dissolution time scales can provide insight into toughening effects from dissolvable interleaves of different surface-to-volume ratios.

Chapter 5

Toughening of Laminated Composites by Phenoxy and Phenoxy/CNT Interleaves

5.1 Introduction

In previous chapters, the binary systems of thermoplastic/CNT and thermoplastic/thermoset were studied, with the focus on electrical properties and dissolution behaviour, respectively. Suitable processing conditions for optimized electrical properties, as well as dynamic percolation behaviour was observed and analysed. The dissolution process of thermoplastic phenoxy fibres of different diameter in epoxy was also studied under optical microscopy, in order to obtain guidelines for optimized composite laminate manufacturing. The produced thermoplastics in the form of electrospun fibres mats, solution cast films, and compression moulded films were used in this chapter, as interleave materials for laminated composites.

In this chapter, the interlaminar fracture toughness of interleaved composites is evaluated, and toughening effects as well as toughening mechanisms of various forms of interleaves are compared and analysed. First, the manufacturing process of composite laminates and thermoplastic interleaves is presented. Secondly, the effect of these thermoplastic interleaves on composite morphology is studied, with the aim

to unravel their toughening mechanism. Finally, the toughening effects of various interleaved specimens are discussed, together with toughening mechanisms and comparison to previous literatures.

5.2 Experimental

5.2.1 Materials and sample preparation

Materials

The composite system employed consist of high strength, PAN based carbon fibre in the form of 2 × 2 twill fabrics (G0986), with an areal weight of 286 g/m^2, and RTM6-2 two component aerospace grade epoxy, both from Hexcel®. The PTFE copolymer release film with a thickness of 12 μm (A6000®) was supplied by Aerovac Systems Ltd. The mould release agent was purchased from Frekote®, and an adhesive spray was purchased from 3M®.

Sample preparation

A steel plate was used as a substrate to create a resin infusion mould. This plate was cleaned first with acetone, and subsequently treated three times with mould release agent. Tacky tape was used to create the mould, with inlet and outlet tubes placed at both ends of the mould to facilitate resin flow. Tacky tape was used to create the mould, with inlet and outlet tubes placed at both ends of the mould to facilitate resin flow. Then fabrics with desired dimensions were placed into the mould, with a release film embedded at the mid-plane for crack initiation. Peel-ply was placed on

top of the fabrics, and wrapped both springs with the aid of adhesive spray. To facilitate resin flow during the infusion processes, flow media was applied on top of the peel-ply and attached with tacky tape to the inlet side. Extra tacky tapes might be applied during the manufacturing of mould, with the aim to improve the sealing of the system under vacuum.

In the case of interleaved specimens, the produced interleaf in the form of film or veil was placed in between the 5th and 6th ply of carbon fibre fabrics. The interleaf covered the total area of the fabrics, including the area with the PTFE release film.

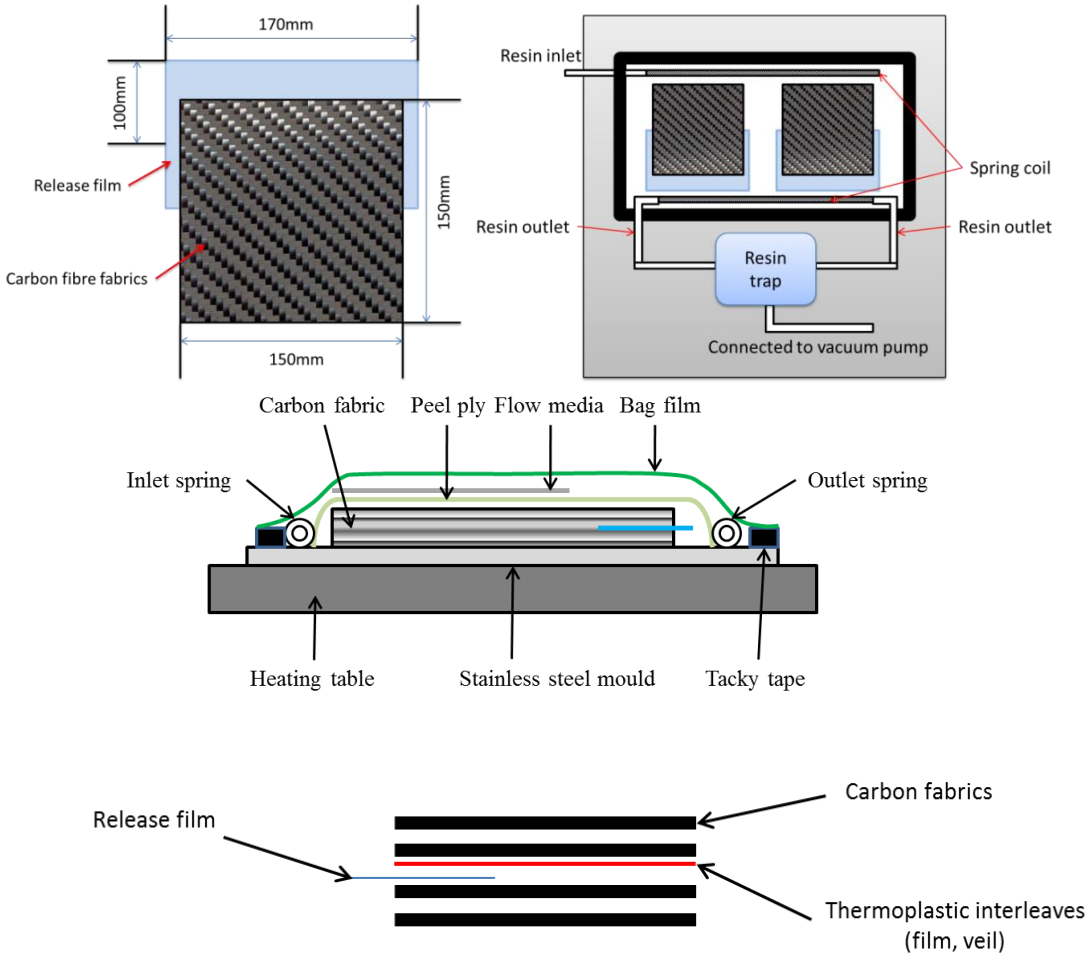

Fig. 5.1 Schematic illustration of composites mould manufacturing and interleaves placement.

Two types of phenoxy interleaves were produced and applied: continuous film and non-woven electrospun nanofibre veils. Phenoxy films produced by bar coating with various thicknesses were used as interleaf materials in composite laminates. The details of the produced laminates can be found in Table 5.1. For each concentration, three to five specimens were tested to obtain the average value.

Table 5.1 Summarized information for produced phenoxy film interleaved specimen.

Description	Weight fraction (volume fraction) to final panel	Interleaves (weight)	wt.% of interleaves in composites	vol.% of interleaves in composites	Thickness (mm)
Carbon fibre reference	66.4 (56.2)	n/a	n/a	n/a	3.08 (±0.02)
Carbon fibre reference	64.8 (54.4)	n/a	n/a	n/a	3.17 (±0.01)
Phenoxy film	53.3 (42.5)	0.171 g (5.7 μm)	0.15	0.17	3.15 (±0.03)
Phenoxy film	53.1 (42.3)	0.765 g (29 μm)	0.58	0.62	4.16 (±0.01)
Phenoxy film	53.3 (42.5)	0.83 g (32 μm)	0.63	0.67	4.30 (±0.02)
Phenoxy film	57.6 (46.8)	1.395 g (62 μm)	1.13	1.10	3.95 (±0.05)

The phenoxy nanofibre veils produced via electrospinning have been inserted in composites laminates, as another form of interleaves for mechanical toughening purposes. As described in Chapter 4, all parameters during the electrospinning process were optimized in order to produce continuous electrospun nanofibres with

stabilized fibre diameters of around 700 nm. Table 5.2 shows the summarized information regarding to the produced laminates with nanofibre veil interleaves.

Table 5.2 Summarized information for phenoxy veil interleaved specimen.

Description	Weight fraction (volume fraction) to final panel	Interleaves weight (g) and thickness (μm)	wt.% of interleaves in composites	vol.% of interleaves in composites	Thickness (mm)
Carbon fibre reference	66.4 (56.2)	n/a	n/a	n/a	3.08 (±0.02)
Carbon fibre reference	64.8 (54.4)	n/a	n/a	n/a	3.17 (±0.01)
Phenoxy fibre mat	66.7 (56.4)	0.19 (35)	0.18	0.22	3.67 (±0.03)
Phenoxy fibre mat	67.2 (57.0)	0.38 (50)	0.37	0.43	3.03 (±0.05)
Phenoxy fibre mat	59.6 (48.9)	1.31 (106)	1.14	1.11	3.65 (±0.05)
Phenoxy fibre mat	68.8 (58.8)	1.69 (150)	1.66	1.45	3.03 (±0.01)

From the table above, it can be seen that the thickness of some of the interleaved laminates are slightly greater than others, which might be due to certain levels of mould leakage during curing. However, all specimens are within the dimension requirements for standardized testing.

The RTM6-2 resin part A and part B were taken from the freezer and left at room temperature for 2 hrs, and then pre-heated in an oven to 80 ℃ prior to infusion. Measured quantities of part A and part B with weight ratios 59.5 to 40.5 were mixed under vacuum for degassing, which took 30 min.

The mould was placed on a heated table and vacuum was first applied with closed resin inlet and outlet clamps for at least 30 min before infusion to check for any leakage. Then the table was heated to 90 ℃ prior to the infusion process, which lasted 10-15 min.

Fig. 5.2 Resin infusion mould under vacuum prior to infusion.

After filling of the mould, the clamps at both the resin inlet and outlet side were closed, and the whole set-up was placed into an oven with a pre-set curing cycle (Fig. 5.3). In case of two laminates being produced within the same mould in order to minimise experimental error, two outlets at each side of the spring were used, as shown in Fig. 5.2 above.

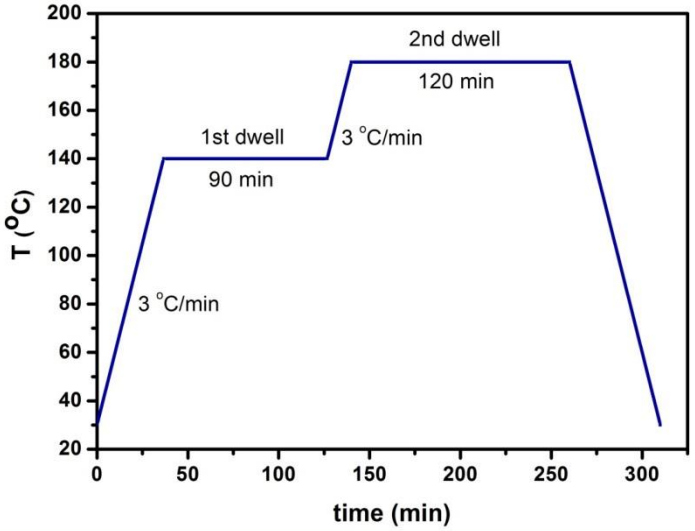

Fig. 5.3 Curing cycle applied for RTM6-2 resin systems.

Test specimens were cut from the laminates using a diamond cutting wheel, with dimensions of 135 x 20 mm in accordance with ASTM D5528 [29]. One side of the specimens was painted and in order to draw a scale in mm for crack length recording during the test. Piano hinges were attached with epoxy adhesive (Hysol HY932) on both sides of the specimen for mounting it into a universal testing machine, as illustrated in Fig. 5.4.

5.2.2 Mechanical testing

The DCB tests were performed with an Instron 5566 universal testing machine equipped with a 1 kN load cell and test speed of 1 mm/min. Crack length was visually observed from the specimens marked side. For each specimen, the crack length was allowed to reach 3-5 mm after the first loading cycle, and then the

crosshead was stopped and unloaded at a speed of 10 mm/min. Thereafter the specimens were loaded at the same test speed of 1 mm/min until the crack length reached 50-60 mm for final delamination. Load-displacement data and delamination crack propagation length was recorded by microscopy and used for the calculation of the interlaminar fracture toughness. No permanent set has been found on tested specimens after unloading.

5.2.3 SEM

Scanning electron microscopy was used to explore the fracture surface of the specimen after DCB test. Specimens were cut into desired dimensions, and attached onto a conductive substrate. A thin layer of gold was sputter coated on the exposed fracture surface prior to SEM imaging. Vacuum was applied throughout the SEM examination process, and accelerating voltage was set to 20 kV, but might be varied during the test in order to obtain images of good quality. All parameters such as magnification were recorded and presented at the bottom of each SEM image.

5.2.4 Data interpretation and G_{IC} calculation

As illustrated in Chapter 2, the DCB specimen was produced and tested in accordance to ASTM D5528 [29] in order to characterize the interlaminar fracture toughness.

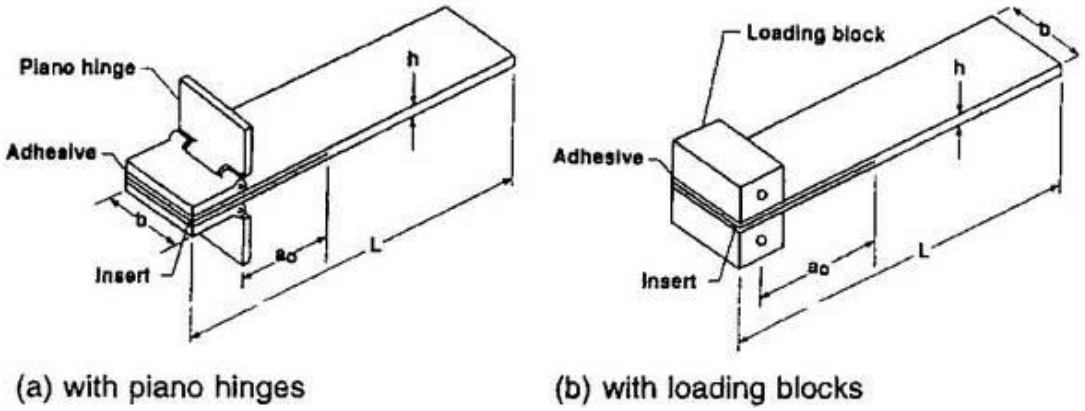

Fig. 5.4 Illustration of Double Cantilever Beam Specimen [29].

Two main values of interlaminar fracture toughness (G_{IC}): G_{IC} non-linear (nl) and G_{IC} propagation (prop) were calculated based on the Modified Beam Theory (MBT) (see Chapter 2, Equation 2.4). Details of data interpretation can also be found in Chapter 2.

5.3 Results and discussion

5.3.1 Interlaminar toughening using continuous film

The toughening results have been divided into two sections depending on the type of dissolvable phenoxy interleaf: (1) continuous films with a low surface area of 4.5×10^{-2} m^2; and (2) electrospun fibre mats with high surface areas up to 8.2 m^2. For each dissolvable interleaf system, morphological and mechanical properties are discussed.

5.3.1.1 Solution processed interleave films

Morphology

The fracture surface of mode-I tested specimens examined by SEM is presented here. The reference specimen without interleaves (Fig. 5.5a and b), shows relatively good bonding between carbon fibres and epoxy matrix, with little evidence of debonding. As expected, a smooth fracture surface was observed for the reference specimen, indicating brittle failure during the interlaminar toughness test. This is attributed to the high stiffness of the carbon fibres which limits the size of the plastic deformation zone in the epoxy at the front of crack tip during the crack-opening [23].

In case of phenoxy interleaved specimen, good compatibility was found between the phenoxy phase and the epoxy phase. With the introduction of thicker phenoxy interleaves, the fracture morphology changed from brittle to more ductile, as shown in Fig. 5.5c to 5.5h. In the case of relatively thick phenoxy films (> 30 μm), phase inversion occurred within certain regions, creating a continuous thermoplastic phase in the interlaminar region between fabric plies. The occurrence of phase inversion is probably due to the continuous nature of the interleaf films applied here, leading to higher local phenoxy concentrations within the interlaminar region. Continuous films also take relatively long to dissolve and become miscible with epoxy resin and once this dissolution time is longer than the infusion time the thermoplastic phase will remain within the interlaminar region between plies with little possibility to migrate due to the absence of resin flow. Based on previous studies, the dissolution time for phenoxy fibre with a diameter of 100 μm was already more than one hour at 80 °C. In the case of a continuous film the surface-to-volume ratio is much lower than of fibre mats and dissolution and phase separation is likely to take place well after the infusion process.

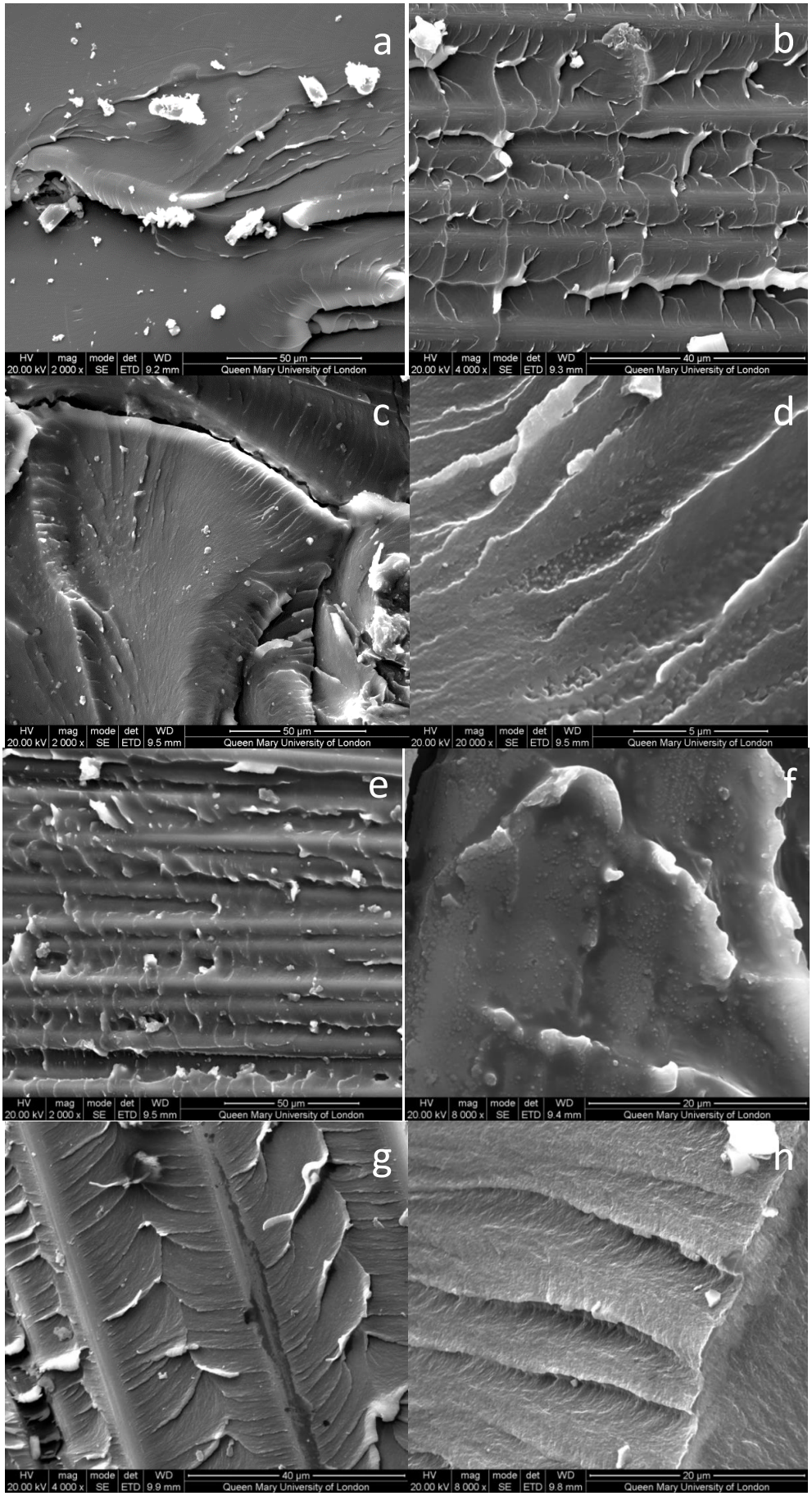
a
HV 20.00 kV | mag 2 000 x | mode SE | det ETD | WD 9.2 mm | 50 µm | Queen Mary University of London
b
HV 20.00 kV | mag 4 000 x | mode SE | det ETD | WD 9.3 mm | 40 µm | Queen Mary University of London
c
HV 20.00 kV | mag 2 000 x | mode SE | det ETD | WD 9.5 mm | 50 µm | Queen Mary University of London
d
HV 20.00 kV | mag 20 000 x | mode SE | det ETD | WD 9.5 mm | 5 µm | Queen Mary University of London
e
HV 20.00 kV | mag 2 000 x | mode SE | det ETD | WD 9.5 mm | 50 µm | Queen Mary University of London
f
HV 20.00 kV | mag 8 000 x | mode SE | det ETD | WD 9.4 mm | 20 µm | Queen Mary University of London
g
HV 20.00 kV | mag 4 000 x | mode SE | det ETD | WD 9.9 mm | 40 µm | Queen Mary University of London
h
HV 20.00 kV | mag 8 000 x | mode SE | det ETD | WD 9.8 mm | 20 µm | Queen Mary University of London

Fig. 5.5 Mode-I interlaminar fracture surfaces under SEM: (a)-(b) carbon fibre/epoxy reference specimen; and phenoxy film interleaved specimens with different film thicknesses (concentration in composite): (c)-(d) 6 μm (0.15 wt.%); (e)-(f) 30 μm (0.58 wt.%); and (g)-(h) 62 μm (1.13 wt.%).

Ten and Chang [73] showed that curing kinetics greatly affects the phase separation process of phenoxy/epoxy blends with spinodal decomposition being the dominant mechanism for phase separated morphologies. The morphological features observed in the current fracture surfaces confirm such a phase separation process, while the resulting thermoplastic-rich zones enable shear yielding around the crack tip and blunting of the crack tip during mode-I delamination, increasing the overall fracture toughness of the composite laminates.

Load-displacement curves and resistance (R) curves

Representative load-displacement curves and R-curves of reference as well as film interleaved specimens are plotted in Fig. 5.6, with the aim of understand the fracture behaviour during the DCB test. The effect of phenoxy film interleaves on crack initiation and propagation is discussed.

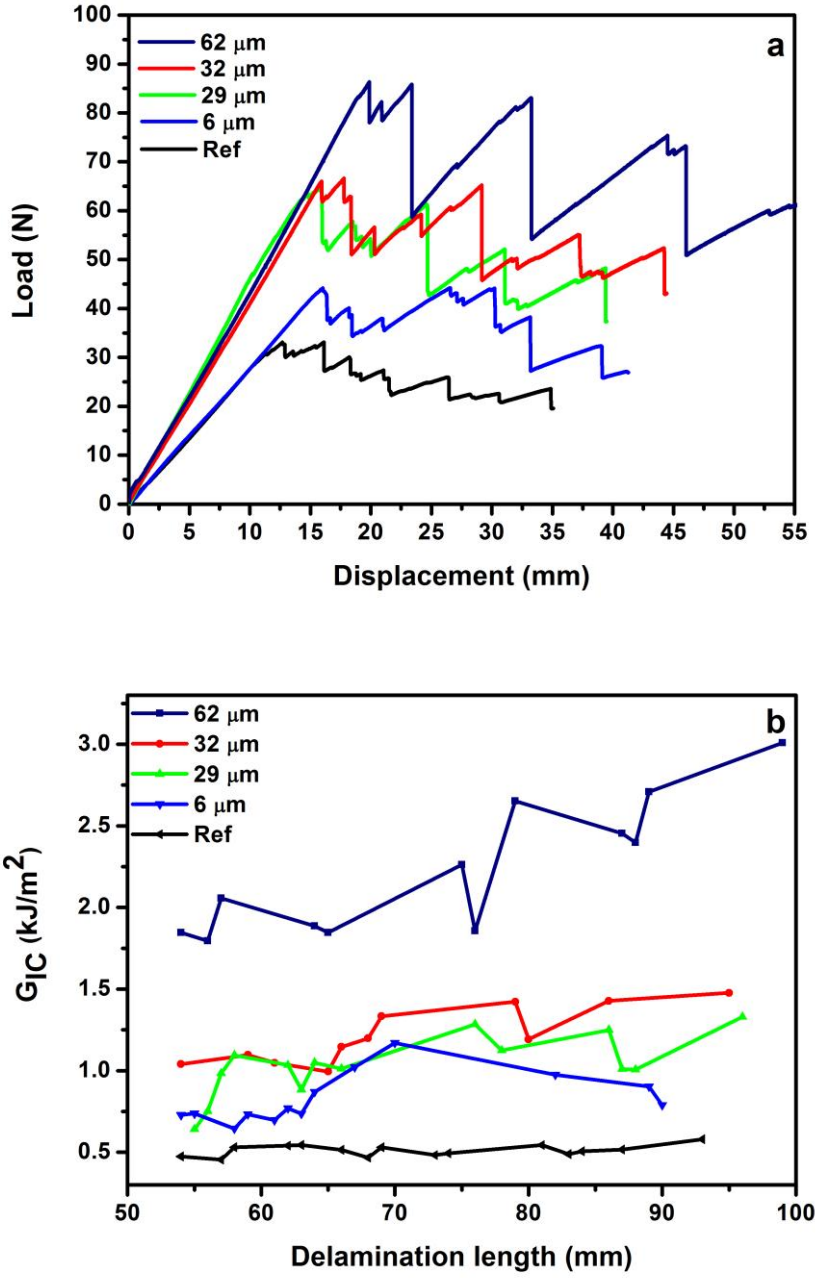

Fig. 5.6 Representative load-displacement curves (a) and R-curves (b) for phenoxy film interleaved carbon/epoxy laminates with interleaves of different thickness.

For reference specimen, relatively small and unstable load fluctuations were observed in the load-displacement curve, confirming the brittle failure mode of

epoxy based laminates. The maximum load sustained is about 35 N. Increasing load steps can be observed in the load-displacement curves with increasing phenoxy concentration. The introduction of thermoplastic phenoxy in the interlaminar region leads to increased plasticity and energy dissipation. The maximum load obtained for a laminate with a 62 μm (1.13 wt.%) phenoxy interleaf was about 85 N, which is more than twice the reference value. This is mainly due to large phenoxy-rich regions which promote shear yielding around the crack-tip, and which is consistent with fractographic observations.

The R-curves of the interleaved systems also confirm enhanced energy absorption with increasing phenoxy content. A plateau is found for both reference and low phenoxy content specimens, indicating steady crack propagation during the DCB tests. For the thickest phenoxy films (62 μm), the initiation value of fracture toughness was already high, leading to no obvious plateau. Again this may be due to the thermoplastic-rich phenoxy phase ahead of the crack-tip, as well as local phase inversion leading to a continuous phenoxy phase morphology.

Difference in stiffness of specimens can be seen from Fig. 5.6, with two groups of stiffness values. This is believed due to the difference in thickness between panels, as listed in Table 5.1. The flexural modulus of specimen was calculated and listed in Table 5.3, together with stiffness calculated from the linear section of each curve. Clearly the standard deviations of all specimens are within the required range from standard, while after considering the thickness difference, the stiffness values are also within the same range for all specimens. It worth mentioning that the dimensions of all specimens were within the standard requirements.

Table 5. 3 Calculated flexural modulus and stiffness for produced phenoxy film interleaved specimen.

Description	Flexural modulus E_{1f} (GPa)	Slope from L-D curve linear section	Thickness (mm)	Slope per unit thickness
Carbon fibre reference	68.91 (±4.9)	2.76	3.08 (±0.02)	0.896
Ph 6 µm	86.78 (±6.8)	2.80	3.15 (±0.03)	0.880
Ph 29 µm	62.20 (±5.9)	4.62	4.16 (±0.01)	1.113
Ph 32 µm	82.66 (±7.5)	4.08	4.30 (±0.02)	0.959
Ph 62 µm	118.34 (±10.1)	4.33	3.95 (±0.05)	1.070

Interlaminar fracture toughness

Fig. 5.7 shows the critical strain energy release rate G_{IC} for specimens with various interleaf thicknesses. The increasing trend of both G_{IC} non-linear (nl) and G_{IC} propagate (prop) values with increasing film thickness, confirms the effectiveness of phenoxy interleaf toughening. The relatively low G_{IC} value for the unmodified reference laminates is again due to the brittle nature of the highly cross-linked RTM6-2 epoxy matrix, although the obtained values for the composite laminate are higher than for the neat epoxy (0.17 kJ/m^2), which is mainly due to crack deviation and typical for woven fabric based laminates.

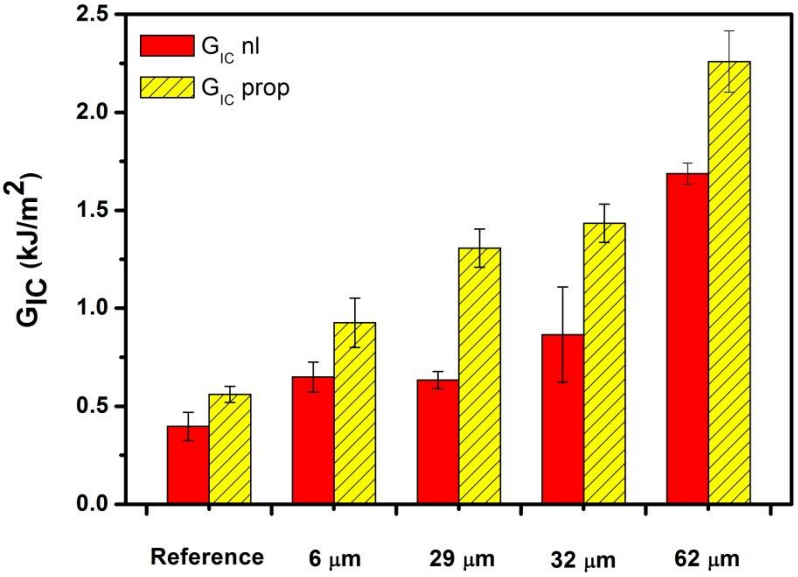

Fig. 5.7 Interlaminar fracture toughness of CFRP laminates with dissolvable phenoxy film interleaves of different thickness.

With the addition of a 6 μm thick (0.15 wt.%) phenoxy interleaf, the G_{IC}-nl value of the composite has already increased from 0.40 kJ/m^2 to 0.65 kJ/m^2, while G_{IC}-prop values increased from 0.56 kJ/m^2 to 0.93 kJ/m^2. For the thickest phenoxy films of 62 μm (1.13 wt.%) in this work, the G_{IC}-nl value increased by 325 % to 1.69 kJ/m^2. It is easy to see from these graphs that the G_{IC}-prop values with increasing phenoxy film thickness are also significantly improved, as they show a four-fold increase compared to the reference laminate. To eliminate the effect of overall thickness and possible increased thickness between plies, optical microscopy was used to examine the cross-sectional areas of panels after polishing. As shown in Fig. 5.8, although the overall thickness between plies was increased from reference to 62 μm film interleaved specimen, no obvious resin layer was found. It was consistent with

calculated fibre volume fraction that 62 μm film interleaved specimen has lower fibre content than reference specimen. Compared to previous research [102] on using same resin interleaves (200 μm) to increase the mid-ply thickness hence improved fracture toughness (70 %), this significantly enhanced toughness is more attributed to the good adhesion level between phenoxy and epoxy phases after phase separation, and the appearance of a co-continuous phase as well as some phenoxy-rich phases, providing regions for plastic deformation and energy dissipation during crack propagation. In previous miscible film interleaf studies, Li *et al.* used polysulfone (PSF) film to increase the interlaminar toughness of carbon/epoxy laminates, and obtained an increase in G_{IC} by 19 %, 74 %, and 100 %, for PSF concentrations of 1 wt.%, 3 wt.%, and 5 wt.%, respectively [229, 230]. In another study Yun *et al.* inserted 21 wt.% of PSF film into composite laminates and improved the fracture toughness by 170 % [114]. As such the obtained increase in fracture toughness as reported here is among the highest at similar interleaf loadings at the laminate mid-plane.

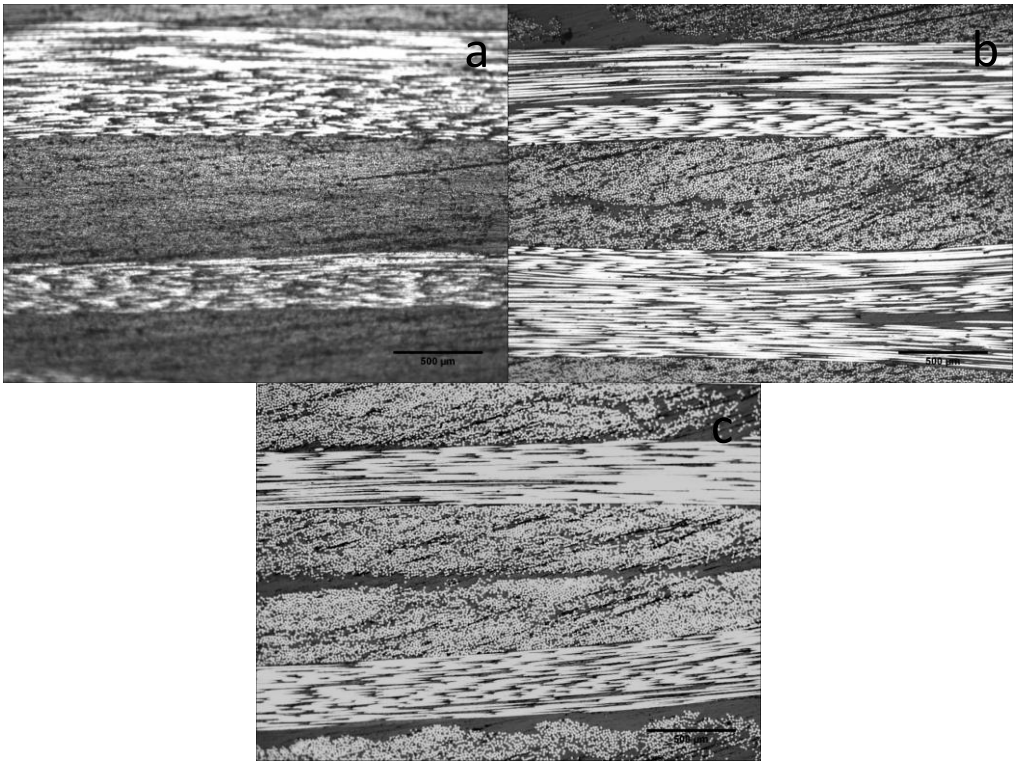

Fig. 5. 8 a reference with thickness between plies of 689.7 (±22.1) μm; (b) 6 μm phenoxy film interleaved specimen, with thickness between plies of 629.1 (±5.1) μm and resin rich regions of 38.7 (±3.2) μm; (c) 62 μm phenoxy film interleaved specimen, with thickness between plies of 840.6 (±32.0) μm and resin rich regions of 69.4 (±36.3) μm.

5.3.1.2 Melt-processed interleave films

To explore melt-processing routes to produce phenoxy interleave film, pre-dried pellets were directly hot-pressed into film. To reach a homogeneous thickness distribution, the produced film was relatively thick (between 250 and 300 μm). The weight fraction of the phenoxy interleaves in the composites was therefore 1.9 wt.%, which was much higher than for solution processed films. The same procedure was applied to produce phenoxy/CNT films as interleaves, with 3 wt.% of CNT in the

film. The phenoxy/CNT interleave film specimen are only briefly discussed in this section, but will be discussed in more detail together with all other thermoplastic/CNT interleave specimen in section 3.3.

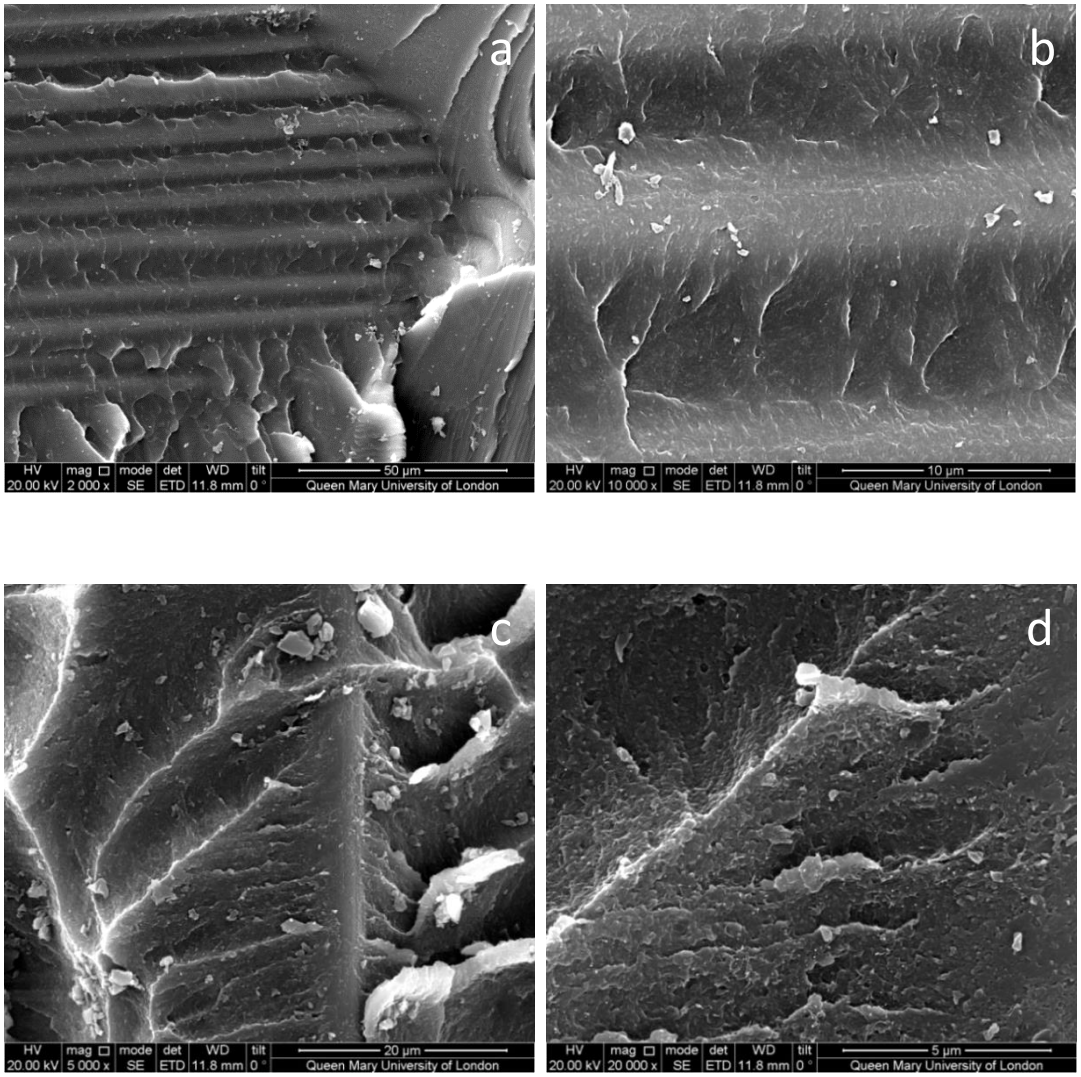

Fig. 5.9 SEM images of fracture surfaces of melt-processed phenoxy film interleaved specimen (a)-(b), and melt-processed phenoxy/CNT film interleaved specimen (c)-(d).

As expected, due to the high concentration of phenoxy, especially near the interfacial region, the fracture surface consisted mainly of a phenoxy phase, with phase inverted morphologies. The phenoxy/CNT film interleaved specimen also showed similar morphologies, with traces of CNTs dispersed within the phenoxy-rich regions. Evidence of CNT pulled-out can be found.

The fracture toughness of these two laminates was examined and presented in Fig. 5.10. With relatively high phenoxy loading, the fracture toughness values were increased by 178% and 313% for G_{IC}-nl and G_{IC}-prop, respectively. Although relatively large variations were observed for G_{IC}-prop values, the existence of a phenoxy-rich zone apparently increased the energy required to propagate the crack. Regarding to the laminate interleaved with phenoxy/CNT film, although an improvement of 60% was obtained to reference specimen, the G_{IC} values were obviously decreased comparing to phenoxy film specimen without CNTs. This decrement was believed mainly due to the high initial CNT loading within the phenoxy films, which had introduced nanoparticles agglomerates. Another possible reason is the difference in processing history, as comparing to phenoxy film which was directly hot-pressed into film, the phenoxy/CNT specimen was firstly compounded via extrusion processes. Although the complete process was under nitrogen environment and the oxidation as well as degradation should be already minimized, this might still affecting the ultimate properties of composites.

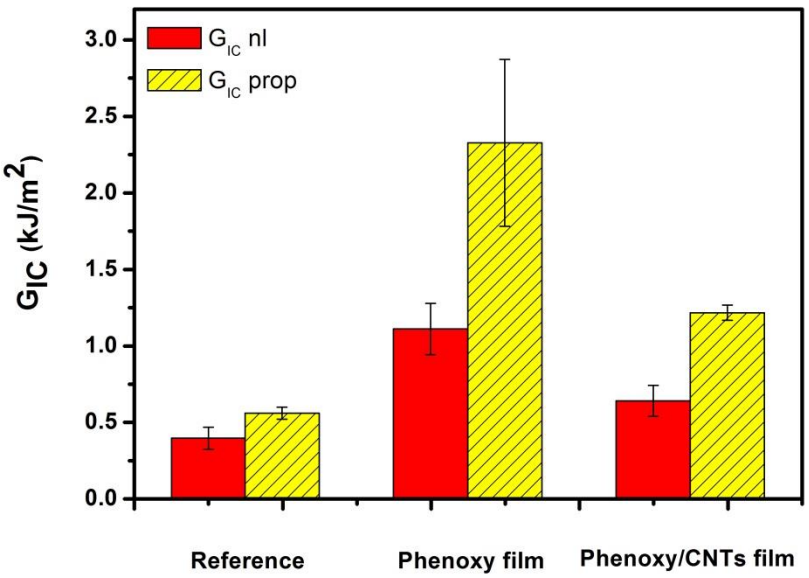

Fig. 5.10 Comparison of interlaminar fracture toughness of melt-processed phenoxy film and phenoxy/CNTs film interleaved specimens.

Although the concentration of phenoxy interleaves was higher than solution processed films, the obtained fracture toughness value was not improved much comparing to 1.12 wt.% film interleaved specimen. In fact, the G_{IC}-nl values were obviously lowered. There are several factors affecting the toughening effect from dissolvable thermoplastics, including thermodynamics, cure kinetics, and crystallinity of thermoplastics. The difference in processing history might also affect the crystallinity of thermoplastics, hence influencing their phase separation processes therefore the toughening results. However, the main aim of this research work is to demonstrate various routes to deliver CNTs into FRPs, therefore the toughening effect of melt-processed film interleaved specimen was not directly compared with other results from solution methods, but only presented as another route to deliver

CNTs into FRPs. Research works on the topic of curing kinetics and thermodynamics and their effects on toughening effects can be found in [73-75, 115].

5.3.2 Interlaminar toughening using electrospun fibre mat

In this section, both morphological and mechanical properties of phenoxy fibre mat toughened carbon/epoxy laminates are analysed and discussed. The average fibre diameter was around 700 nm. The average thickness of the porous fibre mats varied from 35 to 150 μm and is used for comparison and discussion.

Morphology

The fracture surface of phenoxy veil interleaved specimens after DCB test was examined using SEM (Fig. 5.11). The fractographic results are discussed and compared with data for film interleaved laminates, as well as related studies by other researchers.

As expected, and similar to film based specimens, the introduced fibrous phenoxy phase shows good compatibility with the epoxy phase. At very low phenoxy concentrations (Fig. 5.11a to 5.11b), the fracture surface maintained smooth with some traces of phenoxy nodules, while for slightly higher concentrations, (Fig. 5.11c and 5.11d), evidence of a reaction-induced phase separated morphology consisting of phenoxy nodules and droplets in a continuous epoxy phase can be observed.

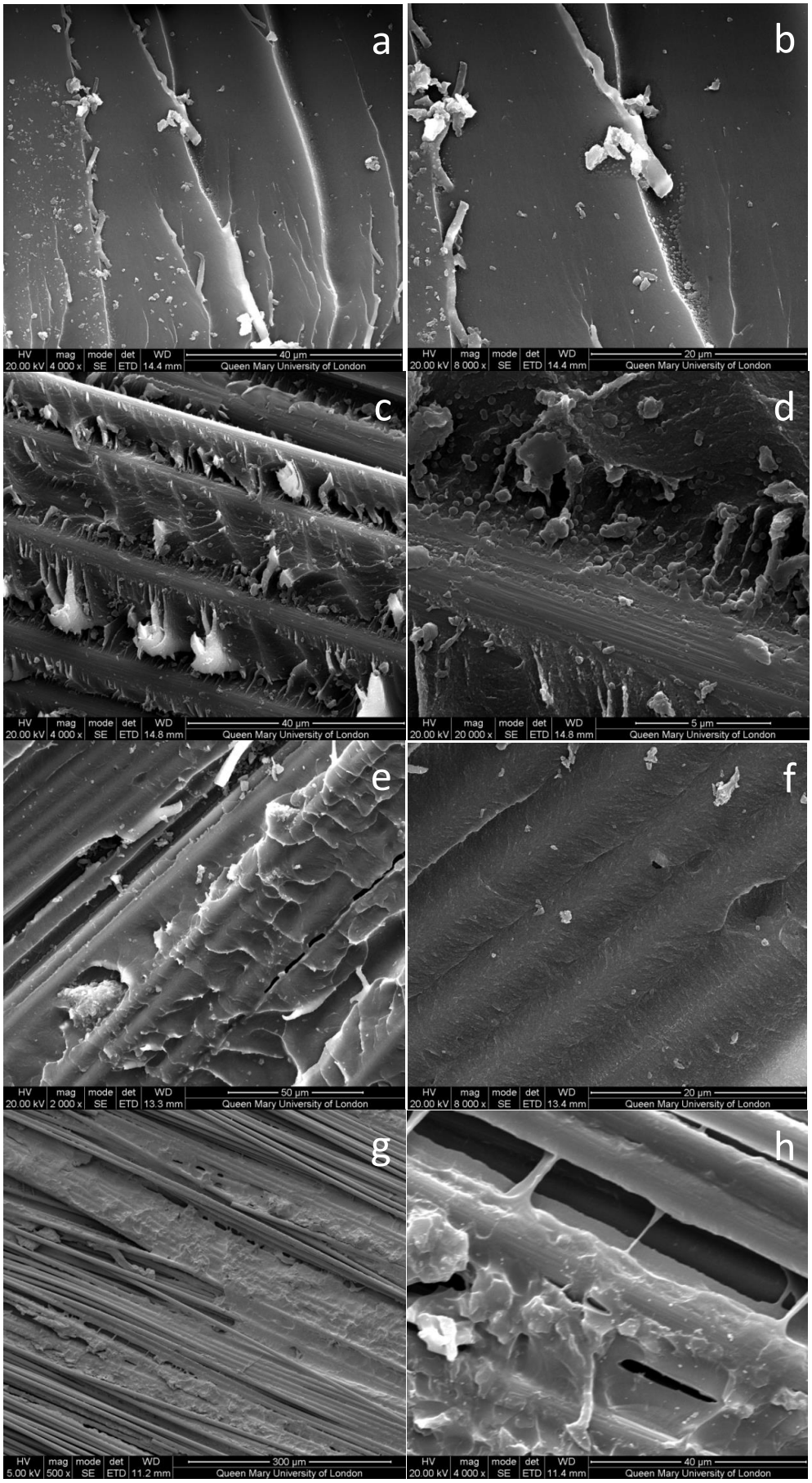
a
HV 20.00 kV | mag 4 000 x | mode SE | det ETD | WD 14.4 mm | 40 µm | Queen Mary University of London
b
HV 20.00 kV | mag 8 000 x | mode SE | det ETD | WD 14.4 mm | 20 µm | Queen Mary University of London
c
HV 20.00 kV | mag 4 000 x | mode SE | det ETD | WD 14.8 mm | 40 µm | Queen Mary University of London
d
HV 20.00 kV | mag 20 000 x | mode SE | det ETD | WD 14.8 mm | 5 µm | Queen Mary University of London
e
HV 20.00 kV | mag 2 000 x | mode SE | det ETD | WD 13.3 mm | 50 µm | Queen Mary University of London
f
HV 20.00 kV | mag 8 000 x | mode SE | det ETD | WD 13.4 mm | 20 µm | Queen Mary University of London
g
HV 5.00 kV | mag 500 x | mode SE | det ETD | WD 11.2 mm | 300 µm | Queen Mary University of London
h
HV 20.00 kV | mag 4 000 x | mode SE | det ETD | WD 11.4 mm | 40 µm | Queen Mary University of London

Fig. 5.11 Mode-I fracture toughness fracture surfaces of phenoxy electrospun fibre mat interleaved specimen, with increasing phenoxy mat thickness (concentration in composite): (a)-(b) 35 μm (0.18 wt.%); (c)-(d) 106 μm (1.14 wt.%); (e)-(f) 150 μm (1.66 wt.%); and (g)-(h) fracture surfaces after removal of the phenoxy phase by DMF.

When the phenoxy concentration is increased, i.e. using thicker electrospun fibre mats, the local phenoxy concentration increases, resulting in a co-continuous polymer blend morphology of phenoxy and epoxy. This morphological change with increasing amount of thermoplastic is consistent with other research works [114, 121, 231]. At the highest phenoxy fibre mat thickness (150 μm), most of the crack surface was covered by a phenoxy-rich phase, revealing evidence of a more ductile deformation mode rather than the brittle failure mode observed in highly crosslinked epoxy based systems. Similar morphologies were found by Magniez *et al.* in their epoxy/phenoxy composites which also exhibited a phase inverted morphology [117]. At some regions with highly-concentrated phenoxy, a continuous phenoxy phase can be found which indicates phase inversion. This morphology was found to be very similar to that of phenoxy film interleaved specimens, as presented in Fig. 5.5. To confirm if carbon fibres were covered by a phenoxy-rich phase, this phase was removed using DMF as a solvent. The resulting morphology is shown in Fig. 5.11g and 5.11h, and reveals exposed carbon fibre surfaces with cavities, and a remaining epoxy phase with rough and diffuse features, indicating a continuous phenoxy-rich phase at the carbon fibre interfacial region. These inverted phenoxy-rich regions are generating larger plastic zones than in highly crosslinked neat epoxy matrices, dissipating more energy as confirmed by the load-displacement curves.

Other researchers also compared the morphological difference between various forms of dissolvable interleaves including nanofibres and films, although the proposed explanations remain inconsistent. Li *et al.* directly electrospun polysulfone (PSF) nanofibres onto prepregs for toughening purposes, and observed homogeneously dispersed spherical PSF domains at fracture surfaces. They also compared PSF film interleaves, which showed a discontinuous dispersion as explained from the high film thickness and resulting poor permeability [232]. In contrast, in another study on the same PSF/epoxy system, Li *et al.* claimed that electrospun PSF nanofibres mats result in an unevenly distributed PSF phase with inhomogeneous phase separation, while film specimens showed a more uniform dispersion of PSF spheres [230].

The fracture surfaces in current work reveal different morphologies from those reported by Li *et al*., showing similar phase separation behaviour and phase inverted blend morphologies for both types of dissolvable interleaves. This might be down to a number of reasons: 1. Phenoxy interleaves are easier to dissolve in epoxy than relatively high T_g thermoplastics such as PSF; 2. Phenoxy concentrations in this study are much lower compared to above research work; 3. Good compatibility exists between phenoxy and epoxy in the current system; 4. Curing kinetic control through the applied cure cycle might ensure and facilitate the phase separation process and formed morphologies.

Load-displacement curves and resistance (R) curves

Representative load-displacement curves and R-curves are plotted for various phenoxy fibre interleaved specimens, together with a carbon/epoxy reference specimen in Fig. 5.12.

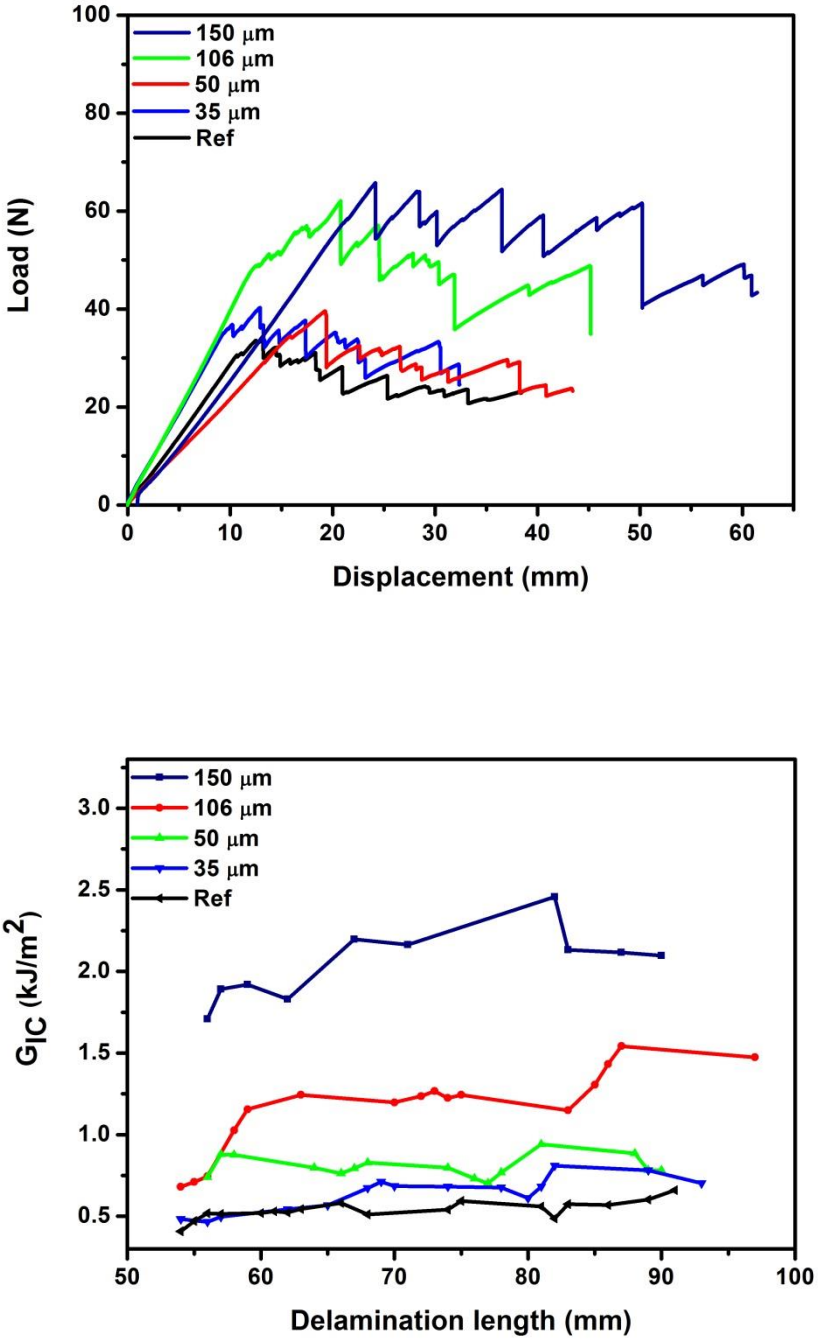

Fig. 5.12 Representative load-displacement curves and R-curves for phenoxy fibre mat interleaved carbon/epoxy laminates with interleaves of different thickness.

A clear increasing trend of load-displacement curves for phenoxy fibre modified CFRP laminates can be observed in this graph. Even at relatively low phenoxy concentrations, the load-displacement curve has shifted towards higher values compared to the reference laminate. Unstable crack growth was found in all specimens during crack propagation, while at higher phenoxy concentrations, larger load steps were observed. This is again believed to be due to an enlarged plastic zone ahead of the crack tip, dissipating more energy during crack propagation, as confirmed from morphological results with highly concentrated phenoxy phase.

Crack resistance curves for different concentrations also show a clear improvement for the laminates with phenoxy fibre interleaves. Average values of resistance curves were used to calculate the average value of crack propagation resistance.

Interlaminar fracture toughness

The interlaminar fracture toughness improvements of phenoxy fibre mat interleaves are summarized in Fig. 5.13. As expected, similar to films there is an increasing trend of G_{IC} values with phenoxy content, especially for G_{IC}-prop values. For 50 µm thick (0.37 wt.% in composite) phenoxy interleaves, the G_{IC}-nl value already improved by 70% (from 0.40 kJ/m^2 to 0.68 kJ/m^2). At the highest mat thickness of 150 µm (1.66 wt.% in composite), the G_{IC}-prop value showed a dramatic increase from 0.56 kJ/m^2 to 1.90 kJ/m^2, i.e. a more than three-fold increase compared to the reference CFRP laminate. The relatively large scatter of G_{IC}-nl values might relate to thickness variations originations from the phenoxy fibre mats.

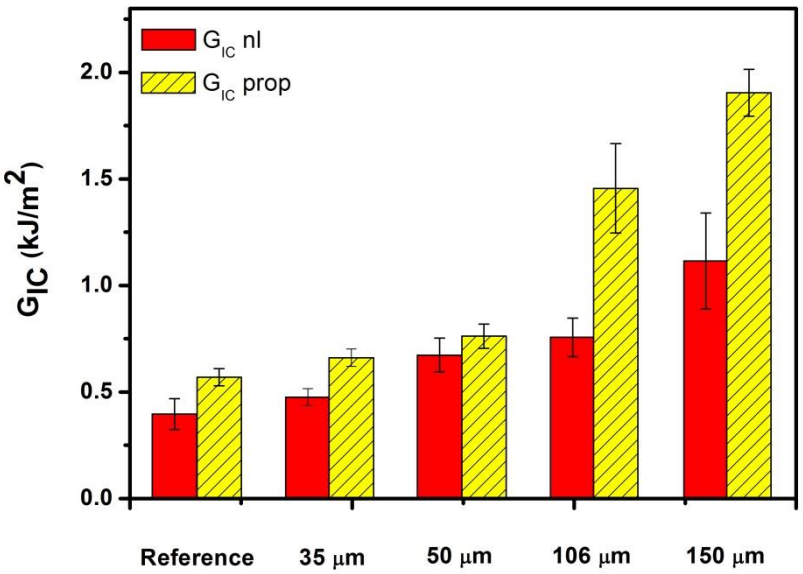

Fig. 5.13 Interlaminar fracture toughness of CFRP laminates with dissolvable electrospun phenoxy fibre mat interleaves of different thickness.

The observed improvements in interlaminar toughness compare very favourable to other research works based on electrospun fibre interleaves used within the mid-plane of composite laminates. Magniez *et al.* directly electrospun 2 wt.% of phenoxy fibres onto carbon fibre prepregs, with the G_{IC} initiation value being increased from a relatively low value of 0.11 kJ/m^2 to a doubled value of 0.21 kJ/m^2, while the G_{IC}-prop value also doubled from 1.00 kJ/m^2 to 2.18 kJ/m^2 [117]. Li *et al.* electrospun polysulfone (PSF) fibres onto carbon fibre prepregs, and reported an increase in G_{IC} value of 58%, 161%, and 181%, for PSF loadings of 1 wt.%, 3 wt.%, and 5 wt.%, respectively [229, 230]. Also Zhang *et al.* electrospun PEK-C fibres directly onto carbon fibre fabrics for interleaf toughening, and reported a G_{IC}-nl increase from 0.15 kJ/m^2 to 0.25 kJ/m^2 with 0.4 wt.% of thermoplastic loading [121]. Zhang *et al*. also compared the effect of fibre diameter (450 nm to 950 nm), and showed that greatest

improvements in out-of-plane properties were achieved with finer fibres [11]. Sihn *et al.* obtained an increase in delamination resistance of 8.1% by introducing a polycarbonate fibre interlayer [116]. Interestingly, Liu *et al.* tried to extend the electrospinning technique to produce an ultrathin epoxy fibrous sheet as interleaf for composites, although no obvious effect on Mode-I delamination resistance was observed [233].

CFRPs in the current study showed for the highest phenoxy fibre loading of 1.66 wt.% to composite (at a mat thickness of 150 μm) a nearly five-fold increase in interlaminate fracture toughness compared to the reference carbon/epoxy laminate which is, to the best of the authors knowledge, the highest reported toughness improvement among all dissolvable thermoplastic fibre interleaf studies so far.

5.3.3 Comparison of toughening effects of films and fibre mats

The interlaminar fracture toughness of electrospun phenoxy fibre mats and bar-coated continuous phenoxy films as interleaves is summarized in this section. Toughening mechanisms for film and fibre mat interleaved specimens, as well as the importance of a balance between curing (kinetics) and phase separation (thermodynamics) are discussed. The proposed explanations are also extended to wider thermoplastic systems which are miscible with epoxy rather than limited to the current phenoxy system.

An important issue that first needs to be addressed is related to the thermoplastic loading in the composites. Similar to other studies reported in literature, here toughening was achieved by introducing a single interleaf at the laminate mid-plane.

This clearly leads to unrealistic low thermoplastic concentrations as thermoplastic is only introduced between two plies of a multi-ply laminate. To provide a more realistic indication of the actual required thermoplastic content in laminated composites the estimated equivalent phenoxy loading in the composites was also calculated on the assumption that interleaves are introduced between all plies of a composite laminate (Table 5.4), by multiplying the local phenoxy fraction between two plies by the number of interfaces between all plies (9 times).

Table 5.4 Summary of interleaved laminates with estimated equivalent phenoxy concentrations.

	Interleaf thickness (μm)	Interleaf surface area (m^2)	Estimated interleave areal density (g/m^2)	Estimated phenoxy concentration with each ply interleaved (wt.%)	Phenoxy concentration in wt.% (vol.%)
Continuous film	6	4.5×10^{-2}	8	1.3	0.15 (0.17)
Continuous film	29	4.5×10^{-2}	34	5.2	0.58 (0.62)
Continuous film	32	4.5×10^{-2}	37	5.6	0.63 (0.67)
Continuous film	62	4.5×10^{-2}	62	10.0	1.13 (1.10)
Electrospun mat	35	9.1×10^{-1}	8	1.6	0.18 (0.22)
Electrospun mat	50	1.8×10^{0}	17	3.3	0.37 (0.43)
Electrospun mat	106	6.3×10^{0}	58	10.3	1.14 (1.11)
Electrospun mat	150	8.2×10^{0}	75	14.9	1.66 (1.45)

In the case of thermoplastic blends its final morphology is mainly controlled by thermodynamics, but for thermoplastic/thermoset blends this is rather more complicated as it involves both thermodynamics and kinetics. Upon curing of epoxy resin, both molecular weight, viscosity and polarity of the system are changing, leading to a decrease in miscibility and ultimately phase separation. These phase separated morphologies have proven to be highly effective in increasing the materials toughness and previous studies have identified a number of toughening mechanisms for phenoxy/epoxy blends [73, 75]. Toughening mechanisms such as crack bridging, crack pinning, crack deflection, microcracking, particle fracture and particle-induced shear yielding have all been proposed, with shear yielding probably being the most important mechanism responsible for improved energy dissipation in these systems. The existence of a thermoplastic phenoxy phase, promotes deformation and plasticity at the crack tip, leading to enhanced energy absorption and increased fracture toughness. The balance between phase separation and epoxy crosslinking is very important for effective toughening. Siddhamalli and Kyu [75] used different curing agents to either facilitate or impede the phase separation of phenoxy, and obtained an increase in tensile toughness for phase separated blends with 20 wt.% phenoxy without sacrificing Young's modulus. Moderate improvements in tensile toughness were also obtained for homogeneous phenoxy/epoxy blends where no apparent phase separation had taken place. At higher phenoxy loadings (40 wt.%) a further increase in toughness was obtained, however at the expense of heat deflection temperature (HDT) as well as tensile strength and modulus [75]. Teng and Chang [73] used an accelerator to control the balance between phase separation and curing kinetics in phenoxy/epoxy blends. They showed that depending on the rate of cure the blends could be either phase

separated or homogeneous. At normal or relatively slow curing rates phase separation occurred with spinodal decomposition being the dominant mechanism over nucleation and growth. Tough homogeneous blends could be obtained at very fast curing rates but at the expense of *Tg* and yield stress due to a decrease in crosslink density.

A brief overview of previously reported phenoxy toughened epoxy systems [75, 76, 115, 117] is presented in Fig. 5.14. Various forms of interleaves including nanofibres, film, and chopped microfibres are included (solid), while bulk phenoxy/epoxy blend systems are also compared (hollow). It can be seen that interleaves provide much better toughening efficiency compared to blend matrix systems, due to localization of the toughening agent within the interlaminar regions.

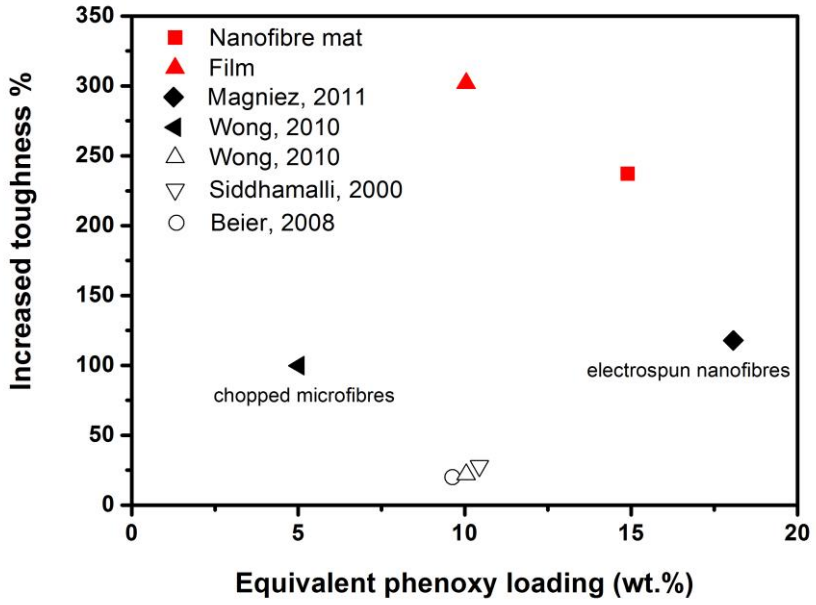

Fig. 5.14 Relative toughness improvement versus equivalent phenoxy concentration in composite. Comparison of current phenoxy toughened interleaf systems (in red)

with various interleaf forms (solid markers) and blend matrix systems (hollow markers) reported in literature [75, 76, 115, 117].

As mentioned before, phase separated systems with interconnected morphologies of thermoplastic and epoxy phases are often found to be more promising for toughening as they do not compromise as much other properties [34, 75, 117]. In the current study the same curing cycle was applied throughout, which resulted in a phase separated and phase inverted morphology as shown in Fig. 5.5 and 5.11. With different interleaf thicknesses, co-continuous morphologies and phase inversion are observed. Therefore, apart from their toughening efficiency, the other main difference between continuous film and electrospun fibre mat interleaves is associated with their different surface-to-volume ratio and its corresponding effect on phenoxy dissolution behaviour and blend stability during composite processing.

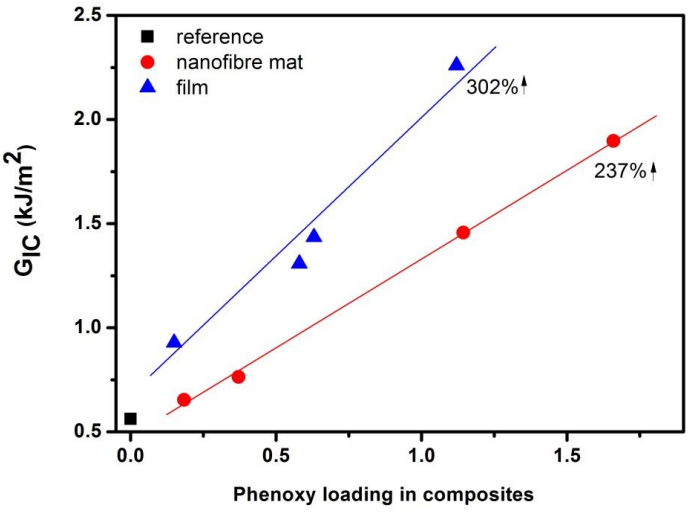

Fig. 5.15 Interlaminar fracture toughness comparison of continuous phenoxy films and electrospun phenoxy fibre mats as interleaves in carbon/epoxy laminates, with

equivalent phenoxy concentration in the composite with only the mid-plane interleaved.

At phenoxy concentrations with only the mid-plane interleaved, the films show a slightly better toughening effect as fibre mat interleaves. At 1.13 wt.% phenoxy film (62 µm), the G_{IC}-prop value has increased to over four-times the reference value, while phenoxy nanofibres show a more than three-times increase at 1.66 wt.% phenoxy (150 µm) in the composites. These improvements are due to the co-continuous thermoplastic phase formed during the phase separation process, particularly for continuous film systems where such a phase exists within the interlaminar region.

As phenoxy is relatively easy to dissolve in epoxy resins, especially at elevated temperatures as encountered during the infusion processes, nanofibre mats with their extremely high surface area will dissolve very fast. This implies that in liquid moulding processes, these phenoxy interleaves will dissolve during the early stages of the infusion process, leading to possible migration of the phenoxy phase together with the epoxy during filling of the mould. This can lead to an inhomogeneous distribution of the phenoxy phase in the composite, and variability in laminate toughness. As such it is highly plausible that in regions away from the resin inlet point, the resin will does not only consist of neat RTM6-2 resin but of a blend of epoxy resin and dissolved phenoxy, potentially leading to an uneven dissolution process from resin inlet to outlet. On the other hand, continuous phenoxy films require longer time to dissolve in epoxy resins, resulting in less migration and a

phenoxy phase that remains within the interlaminar region, where it is highly effective in toughening the composite.

In the current study, the differences in interlaminar fracture toughness of film and fibre interleaved systems are believed to be mainly related to differences in dissolution time of phenoxy in epoxy resin as a result of the differences in surface areas for both systems rather than differences in phase separation mechanisms, as curing cycle and curing agent are identical throughout this work. The main advantage of a continuous film of minimum surface area is to maintain the phenoxy concentration localized within the interlaminar region where it is most effective. It is important to note that for high T_g thermoplastics which are less easy to dissolve in epoxy, this trend might be reversed as here more porous nanofibre mat structures might prove to be more beneficial.

Therefore, apart from apparent important characteristics such as compatibility between thermoplastic and thermoset phases, and curing kinetics, two other aspects need to be considered for optimized toughening using dissolvable interleaves: i) the T_g of the applied thermoplastic and its effect on solubility; and ii) the thermoplastic concentration and surface-to-volume ratio of the interleaf. For relatively low T_g polymers and/or low concentrations, low surface area interleaves (e.g. films) which remain within interlaminar regions during infusion will show better toughening effects, while for relatively high T_g polymers and/or high concentrations, high surface area interleaves (e.g. electrospun nanofibre mats) will facilitate a more rapid dissolution process, leading to better toughening results.

5.3.4 Thermoplastics interleaves with CNTs

Phenoxy films have been employed as carrier for CNTs, with the aim of delivering and localising CNTs into interfacial regions where prone for damage such as delamination. The toughening effect of interleaved thermoplastic/CNTs films has been studied in this section, although the main aim of these interleaves is to deliver CNTs into FRPs.

Morphology

The fracture surface of thermoplastic/CNTs interleaved specimen after DCB tests has been analysed with SEM. For phenoxy/CNTs solution processed film interleaved specimens (Fig. 5.16a to 5.16d), similar morphology was found with pure phenoxy interleaved specimens. No obvious exposure of carbon fibre was found, indicating good adhesion between matrices and reinforcing fibres. The fracture surface has shown deformed morphology rather than brittle smooth failure, which was due to the good compatibility between phenoxy and epoxy phases. Trace of CNTs can be found from fracture surface, with both 1 wt.% and 2 wt.% loadings (to phenoxy/CNTs interleaves). Good dispersion of CNTs was observed, with no obvious agglomeration from the surface. Some of the CNTs had been partially pulled out during the fracture, which has provided the toughening effect, although the length of exposed CNTs was very limited, showing good adhesion between CNTs and matrices. For phenoxy/CNTs melt-processed film interleaved specimen (Fig. 5.16e and 5.16f), local phase inversion can be seen from fracture surface, due to relatively high concentration of phenoxy interleaves. As the CNT loading was as high as 3 wt.% within interleaves, dispersed CNTs can be easily found from fracture surface. The

existence of CNTs has shown percolated network with some agglomerates, making the phenoxy phase more connected compare to relatively low loadings. This might affect the phase separation process between phenoxy and epoxy phases.

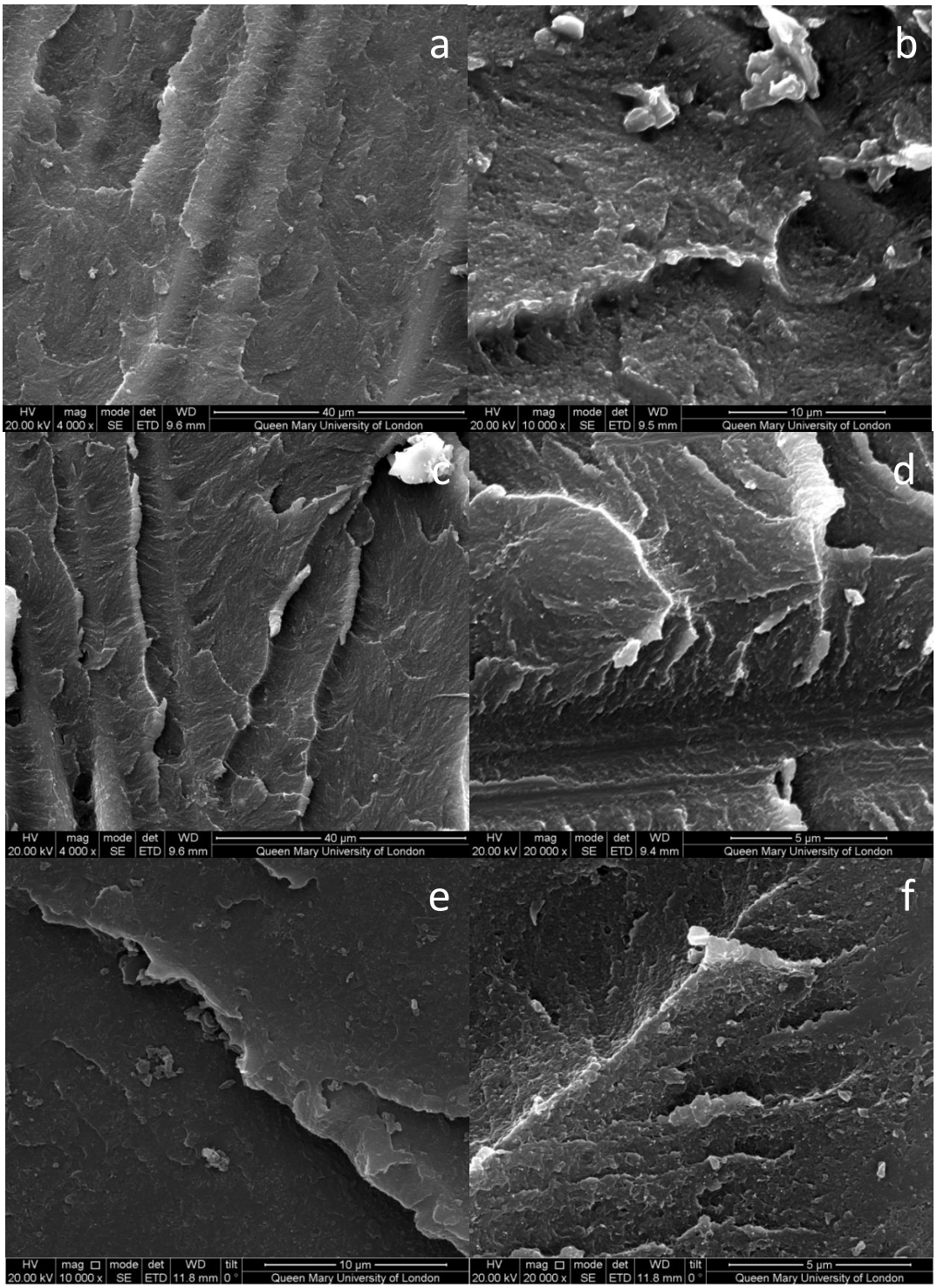

Fig. 5.16 SEM images of phenoxy/CNTs solution processed film interleaved specimen fracture surface, with different CNT loadings within interleaving films: 1 wt.% (a)-(b), and 2 wt.% (c)-(d); and melt-processed film interleaved specimen with 3 wt.% CNT loading within interleaves (e)-(f).

Interlaminar fracture toughness

The interlaminar fracture toughness of interleaves with CNTs has been summarized and analysed in this section. Due to the limited CNT loading to final composites, the main toughening mechanisms are believed still to have been thermoplastics interleaves phase separation rather than nanofillers. Therefore, it is essential to obtain the concentration of interleaves in composites before discussing the mechanical performance of interleaved specimens. As the weight of phenoxy/CNTs films with two CNT loadings was all about 0.7 g, the overall concentrations of interleaves in composites have been calculated with the value about 0.54 wt.%. For melt-processed phenoxy/CNTs films with 3 wt.% CNT loading, the overall concentration of interleaves was about 1.9 wt.%.

Table 5.5 Summary table of thermoplastic/CNTs interleaved specimen.

Interleaves	CNT content within interleaves (wt.%)	Overall loading of interleaves in comp (wt.%)	Abbreviation in comparison graph (Fig. 5.16)
Phenoxy/CNTs solution processed	1	0.54	Ph_1
Phenoxy/CNTs solution processed	2	0.54	Ph_2
Phenoxy/CNTs melt-processed	3	1.9	Ph_3

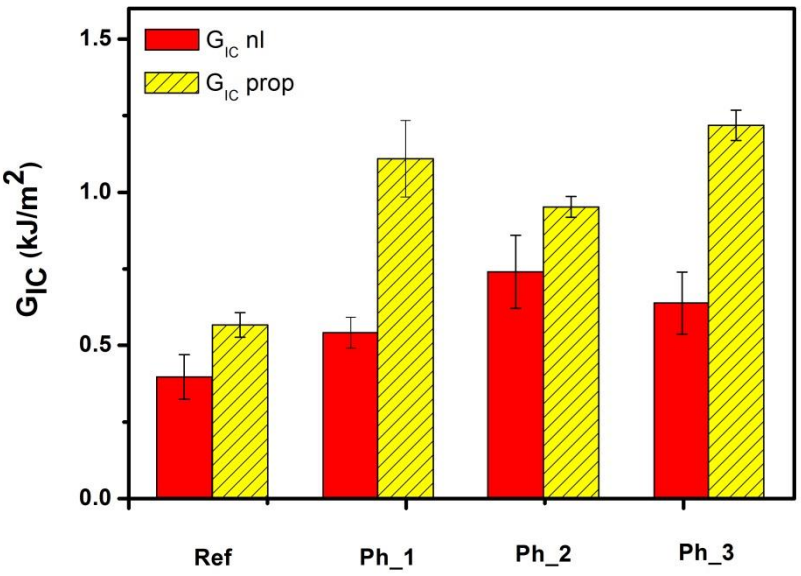

Fig. 5.17 Interlaminar fracture toughness summary of thermoplastic/CNTs interleaved specimens.

With the addition of phenoxy/CNTs interleaves, both the G_{IC}-nl and G_{IC}-prop values have been increased compared to reference specimens (Fig. 5.17). For solution processed interleaves (Ph_1 and Ph_2) with CNT loading from 1 wt.% to 2 wt.%, an increasing trend of G_{IC}-nl was found, although the G_{IC}-prop value was slightly lowered. For melt-processed interleaves (Ph_3), the highest G_{IC}-prop value among all CNT interleaved specimens was obtained, with nearly a 120% increases from the reference specimen. This is due to relatively high interleave concentrations. However, when comparing these composite toughening effects with pure phenoxy interleaved specimen, these increments were lower for CNT loaded specimen, e.g. initial increases from 118% dropped to 87%, and 155% dropped to 70%, for G_{IC}-nl and G_{IC}-prop values, respectively. The high loading of CNTs might lead to agglomerates,

while the presence of CNTs probably also interfered with the phase separation processes. But most importantly, after the delivering of CNTs by thermoplastic films which was the main aim of the work, the mechanical performance is still enhanced as an additional benefit to this methodology, providing great potential of using dissolvable thermoplastics as carriers to deliver CNTs into FRPs for integrated damage sensing and localized toughening.

5.4 Conclusions

The toughening effect of dissolvable thermoplastic and thermoplastic/CNTs interleaves in woven carbon/epoxy laminates has been studied. Various forms of thermoplastics interleaves, including solution processed film, melt-processed film, and electrospun nanofibre mat have been applied. Morphology of fracture surfaces has been examined under SEM, in order to analyse the toughening mechanism of the various interleaves.

For the interleaved carbon/epoxy laminates, both phenoxy film and fibre mats showed significant improvements in interlaminar fracture toughness. In fact, the measured increase in toughness exceeded the highest reported values in literature for these types of blend systems based on electrospun fibrous interleaves. Morphological studies showed good compatibility between the phenoxy and epoxy phase, and a co-continuous phase after reaction-induced phase separation during curing. Increased plasticity at the crack-tip was found to be responsible for the increased energy dissipation and delamination resistance of the interleaved laminates. At current phenoxy concentrations, continuous films seemed to induce a slightly better toughening effect compared to the electrospun fibre mats. This is believed to be not

only due to the formation of a co-continuous phase and some local phase inversion in the case of film systems, but is also affected by the relatively rapid dissolution process of phenoxy in epoxy in the case of fibre mats and possible migration of phenoxy during mould filling. The performed dissolution studies have provided guidelines for subsequent composite manufacturing processes, such as resin infusion processes and curing of epoxy resins. Furthermore, the observed dissolution time scales can provide insight into toughening effects using dissolvable interleaves of different surface-to-volume ratios and/or the use of higher T_g thermoplastics of lower solubility.

CNTs have been successfully delivered into FRPs via dissolvable thermoplastic carriers, without decreasing mechanical performance of composites. The effect of CNTs within thermoplastic interleaves on fracture toughness was not very obvious, which is due to the relatively low overall loading of CNTs to composites. The obtained toughening effect is believed mainly attributed to existence of thermoplastic interleaves. In a subsequent chapter the delivered CNTs will be used as a sensitive tool to detect various composites failure such as delamination.

Chapter 6

Integrated Damage Sensing in Laminated Composites by CNT Networks

6.1 Introduction

The importance and significance of structural health monitoring (SHM) and damage sensing in FRPs is becoming increasingly important for aerospace applications, especially for civil aircraft which require extremely high health and safety standard. Not surprisingly, compared to the outstanding in-plane properties of composite laminates, the relatively weak out-of-plane properties and their associated failures such as delamination need to be better monitored. Not to mention that delamination and matrix cracking normally happen at the early stages of composites failure, which makes them essential to understand and monitor. As a result of this, recently great attention has been placed on developing fully integrated structural health monitoring systems for composite structures [1-5].

Damage monitoring, often referred to as structural health monitoring (SHM), has become a very important topic in composites. Different routes have been followed in SHM, including self-sensing techniques [234-237], embedded sensors [164, 202, 203, 238-240], and various non-destructive testing (NDT) technologies such as acoustic emissions (AE) and ultrasonics. However, the limitation of existed techniques has

triggered researchers to find alternative solutions. For instance, although a number of NDT techniques are available to industry for damage inspection, many are strongly dependent on the experience of manipulating personnel, need of additional equipment, and lead to significant down-time, limiting future applications. Embedded sensors can be localized at damage prone zones, but those sensors normally do not provide any structural contribution. In fact, in many cases they can even lower mechanical performance due to the additional interfaces and stress concentrations generated. Self-sensing concepts can be used in carbon fibre reinforced composites by using the carbon fibre as an electrical sensor, but cannot be applied to wider composite systems such as glass fibre reinforced composites. Moreover, this method is more geared towards fibre dominated failure modes while early matrix- or interface failure is difficult to detect through this method.

Carbon nanotubes (CNTs) were first used in FRPs for SHM purposes by Fiedler *et al.* 2004 [148]. Since then various research works on this topic have been performed [148, 154, 156, 163, 170, 202, 213, 241-244]. CNTs have been utilized as functional fillers for health monitoring and damage sensing in FRPs due to their excellent properties. The percolated CNT networks are acting as conductive pathways, and electrical signals are measured and characterized to identify various composites failure modes under mechanical deformation. Thostenson *et al.* [241], for example, demonstrated that mixing CNTs into an epoxy resin allowed for the evaluation of damage onset and evolution in FRPs. By introducing CNTs into an insulating matrix or by localizing them in certain areas, various matrix-dominated early stage failure modes can be detected by this nerve-like sensory network, thus increasing the safety of composite structures. Additionally, the use of CNT based percolated networks as integrated sensor also provides the possibility to monitor health during service life.

This materials based sensing method overcomes existed challenges such as down-time or need of additional equipment, greatly improving the efficiency of structural composite components for industries such as construction, aerospace or wind turbines.

In this chapter, previously delivered CNT networks in FRPs were used as sensors to detect early stage damage such as delamination during standard composite tests. Electrical method has been utilized for damage detection and sensing. Both epoxy-dissolvable thermoplastic/CNT interleaved specimens, and innovative spray coated specimens were characterized and analysed. The content is divided into sections to DCB (interlaminar fracture toughness) test, and SBS (interlaminar shear strength) test, with sub-sections of different composite systems such as GF/CNTs, CF/ CNTs, CF prepregs/CNTs.

6.2 Experimental

6.2.1 Materials and sample preparation

The GFRP consist of a 2 × 2 twill glass fibre woven fabric (SIGMATEX Ltd., UK), and an epoxy resin system RTM6-2 (HexFlow®). Same curing procedures were applied as described in Chapter 5.

For ILSS specimen, ten plies of carbon fibre fabrics were used to produce the panel. Nine out of ten plies were spray coated with CNT. Standard vacuum assisted infusion processes like other panel production within this work has been applied. The cured panel was cut into specimen with the dimension of 40 × 13 × 3 mm.

For DCB specimens, unlike previous thermoplastic interleaved specimen which was only interleaved at mid-plane of the laminates, all interleaving regions were deposited with CNTs. In other words, when manufacturing the composites panel, apart from the bottom ply which remained uncoated, all plies were spray coated with CNTs and have been placed upside down, in order to facilitate the through-thickness CNT alignment during the resin flow throughout the infusion processes.

Other materials and sample preparation such as CNTs and solvents used, specimen preparation procedures, as well as applied curing conditions for composites, were similar to previous works in this thesis.

Standard DCB and ILSS specimen preparation procedures were applied for specimens, as stated in previous chapters. For DCB specimen, a thin copper wire was positioned along the width of the exposed end-edge of the laminate using silver-loaded epoxy adhesives for electrical damage sensing purposes, as shown in Fig. 6.1a. Two part epoxy adhesive from RS components was hand mixed throughout for 2 min before use. After the wire was attached by adhesive, the specimen was placed into oven at 80 ℃ for 15 min, in order to maximize the electrical conductivity of adhesive. For ILSS specimen, both in-plane and through-the-thickness direction was applied for sensing tests, as shown in Fig. 6.1b. Thin copper wire was positioned at both end of specimen for in-plane measurements, while for through-the-thickness specimen, silver conductive paint (from RS Components) was applied on complete surface and bottom of specimen, before the copper wire was attached by silver-loaded epoxy adhesives.

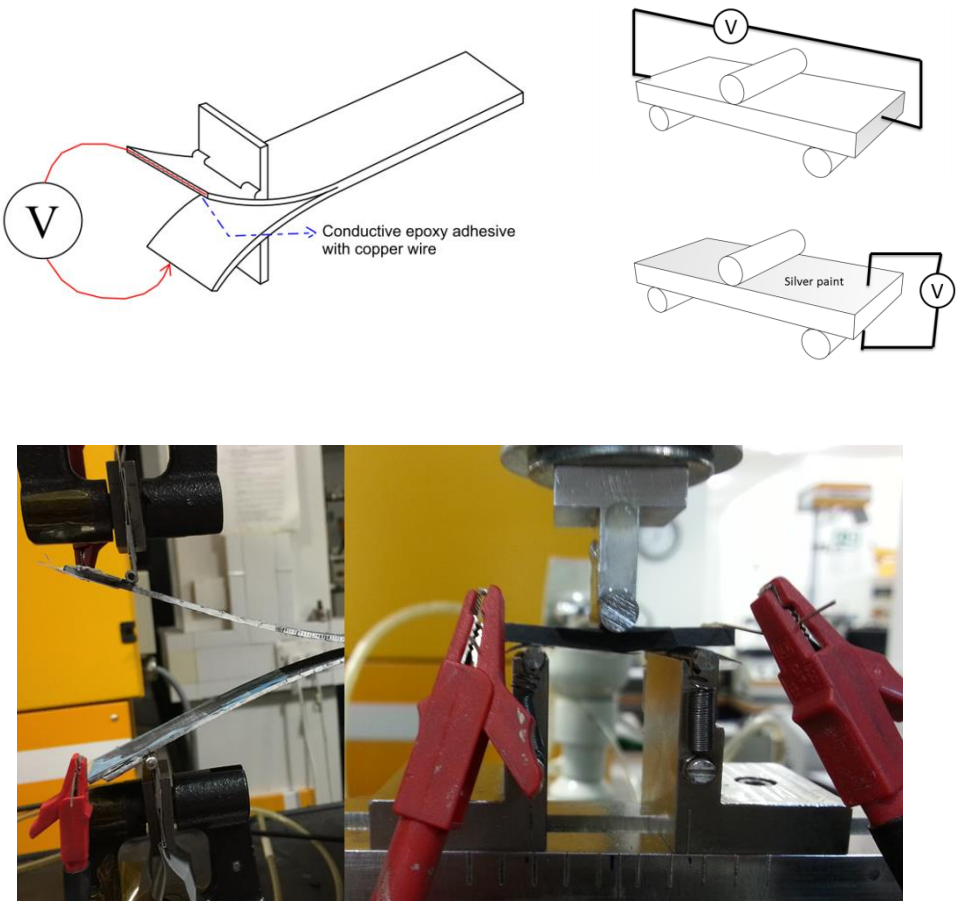

Fig. 6.1 Illustration and pictures of *in-situ* damage sensing setup for DCB and SBS test.

6.2.2 Spray coating

The spraying setup employed in this work was an airbrush system from Iwata Performance (H4001 HP-CPLUS), connected with an Iwata studio series air compressor. An illustration of the spray coating manufacture process is presented in Fig. 6.2. In order to disperse the CNTs in the spraying solution, sonication at 5000 J energy was applied to the CNT/methanol solution at 20% at the maximum amplitude level. After sonication, the solution was connected to an airbrush chamber using a tube to automatically draw the CNT solution from a beaker into the airbrush. The

airbrush was positioned perpendicular to the substrate during the spraying process. The parameters for airbrushing were 30 psi (2.07 bar) for the air pressure during deposition, and a 10 cm distance between spraying nozzle and receiving substrate (e.g. carbon fibre fabrics or prepregs). These parameters were optimized after various trials. A controlled heating stage with a controlled temperature of 50 ℃ was also positioned underneath the prepreg during airbrushing in order to aid the evaporation of solvents. To eliminate the effect of methanol on the prepregs, reference specimen were also been sprayed with the same amount of solvent without CNTs.

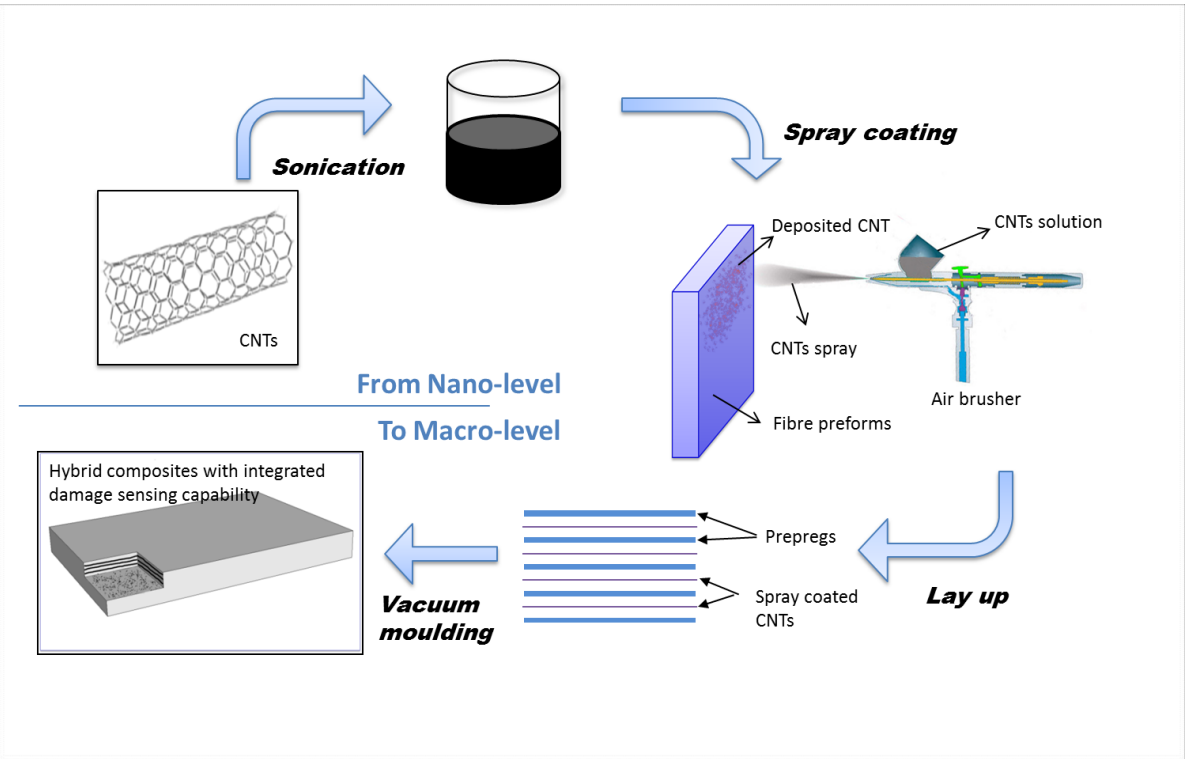

Fig. 6.2 Schematic illustration of spray coating technique for CNT deposition in FRPs.

6.2.3 Interlaminar shear strength test

The interlaminar shear strength of composite panels was evaluated under the short beam strength (SBS) test, in accordance to ASTM D2344. The specimen thickness was around 3 mm, and loading span length-to-specimen thickness ratio was kept to 4.0 as indicated by the ASTM standard.

$$F^{sbs} = 0.75 \times \frac{P_m}{b \times h} \qquad \text{(Equation 6. 1)}$$

After the cutting of specimen into desired dimensions, sand paper was used to polish the both sides of specimen to avoid any notches or uneven surfaces. Then the specimen was placed in between loading noses, and the cross-head speed of testing machine was kept to 1.0 mm/min throughout the test, until the applied load was dropped more than 40%.

The SBS test is widely used due to its simplicity, however, in certain cases it remained controversial due to the possible combination of other failures such as matrix cracking or indentation during test, resulting inaccurate interlaminar shear strength [30]. Therefore, a clear force drop rather than propagating force drop steps need to be observed to maintain the effectiveness of the test.

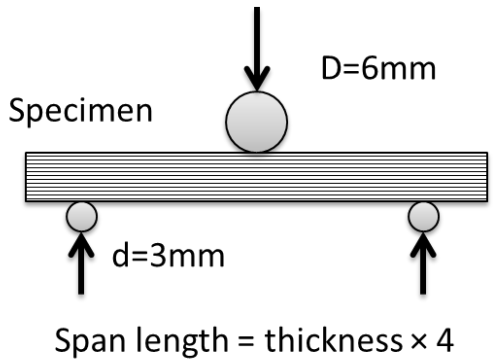

Fig. 6.3 Schematic illustration of SBS test set-up for ILSS.

6.2.4 In-situ damage sensing test

The electrodes were directly connected using copper wire and the volumetric electrical resistance of each specimen was measured and recorded simultaneously with the mechanical data read from the tensile test and an Agilent 34401A digital multi-metre with two probes for real time current measurements. To avoid any effect from fixtures, insulating layers were applied between specimen and clamps for all specimens. Both electrical and mechanical data was recorded by software and later been used to analyse the results.

6.3 Results and discussion

6.3.1 Model study on GFRP

To utilize the effect of conductive CNT networks, and eliminate other conducting effect from system such as carbon fibre, the insulating glass fibre was first used as substrate for *in-situ* damage sensing works. Interlaminar fracture toughness and interlaminar shear strength tests were performed together with *in-situ* electrical measurement, and obtained damage sensing properties are presented and analysed in this section.

Interlaminar fracture toughness test

Surprisingly, at extremely low CNT loadings (0.012 wt.% / 0.013 vol.%), the GF/CNT composites showed already percolation with detectable electrical signals, indicating excellent network formation. This extremely low CNT loading was

chosen due to our previous sensing experience based on percolated networks. Microscopy studies showed that the glass fibre surface was not completely covered by deposited CNTs, indicating potential scope for improved sensing results. The obtained electrical conductivity is believed to be not only attributed to an initial dispersion of CNTs onto the fibre surfaces, but also due to a "dynamic percolation" process [156, 213] to take place after the infusion process but before complete cross-linking of the epoxy resin.

Fig. 6.4a shows the damage sensing results together with a typical load-displacement curve from the DCB test. The successive drops in the load are due to crack propagation. The simultaneously measured resistivity increases with clear steps which directly correlate to the load drops and is due to the percolated CNT network being affected by crack propagation. This correlation confirms that the spray-coated conductive CNT network on the glass fibre fabrics can be used as a sensing tool to detect damage within the composite specimens during mechanical deformation.

To further confirm the correlation between mechanical performance and electrical sensing signals, the relative force- and resistivity change (in percentage) is plotted (Fig. 6.4b). The relative change of force and resistance were taken from data separately, plotting with the displacement. Excellent correlation between these two signals is observed, indicating the reliability of using this technique to detect delamination damage in composite laminates.

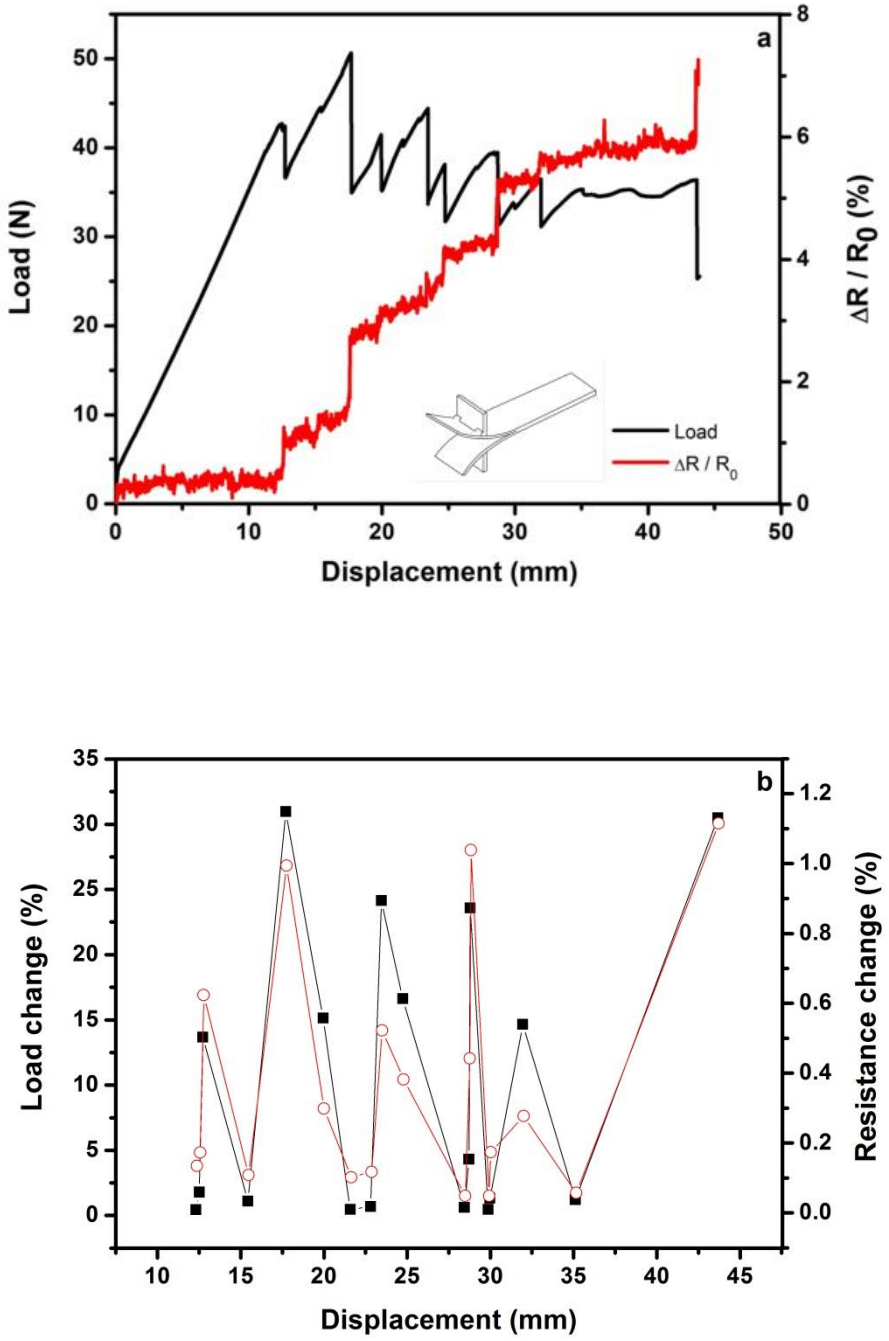

Fig. 6.4 *In-situ* damage sensing data for 0.012 wt.% (0.013 vol.%) CNT loaded GFRPs: (a) Normalized measured volume resistance change of the specimen during the DCB test, accompanied with L-D curve; (b) Correlation between resistance change and force change in normalized values.

In order to better cover the interfacial regions within composites and provide better sensing properties, higher amounts of CNTs were deposited via the same procedures onto glass fibre substrates. 10 mg instead of 4 mg was deposited on each plies, and overall CNT loading was increased to 0.032 wt.% (0.034 vol.%). As shown in Fig. 6.5, unlike previous specimens with extremely low CNT loadings for which the electrical signals were rather unstable, here a much more stable electrical sensing signal is obtained as seen in the normalized graph for the higher amount of CNTs. Furthermore, with each force drop in the loading curve, a clear resistance jump can be seen from the sensing signals. The correlation between force change and resistance change was also presented in terms of a normalized percentage value. Good correlation was found between these two parameters, together with an increased range of changing values. This has led to a more obvious sensing signal when a crack was propagated. It is worth to mention that the measured electrical resistance was also significantly reduced by three orders of magnitude (from 1.097×10^7 to 8.409×10^4) between these two CNT loadings.

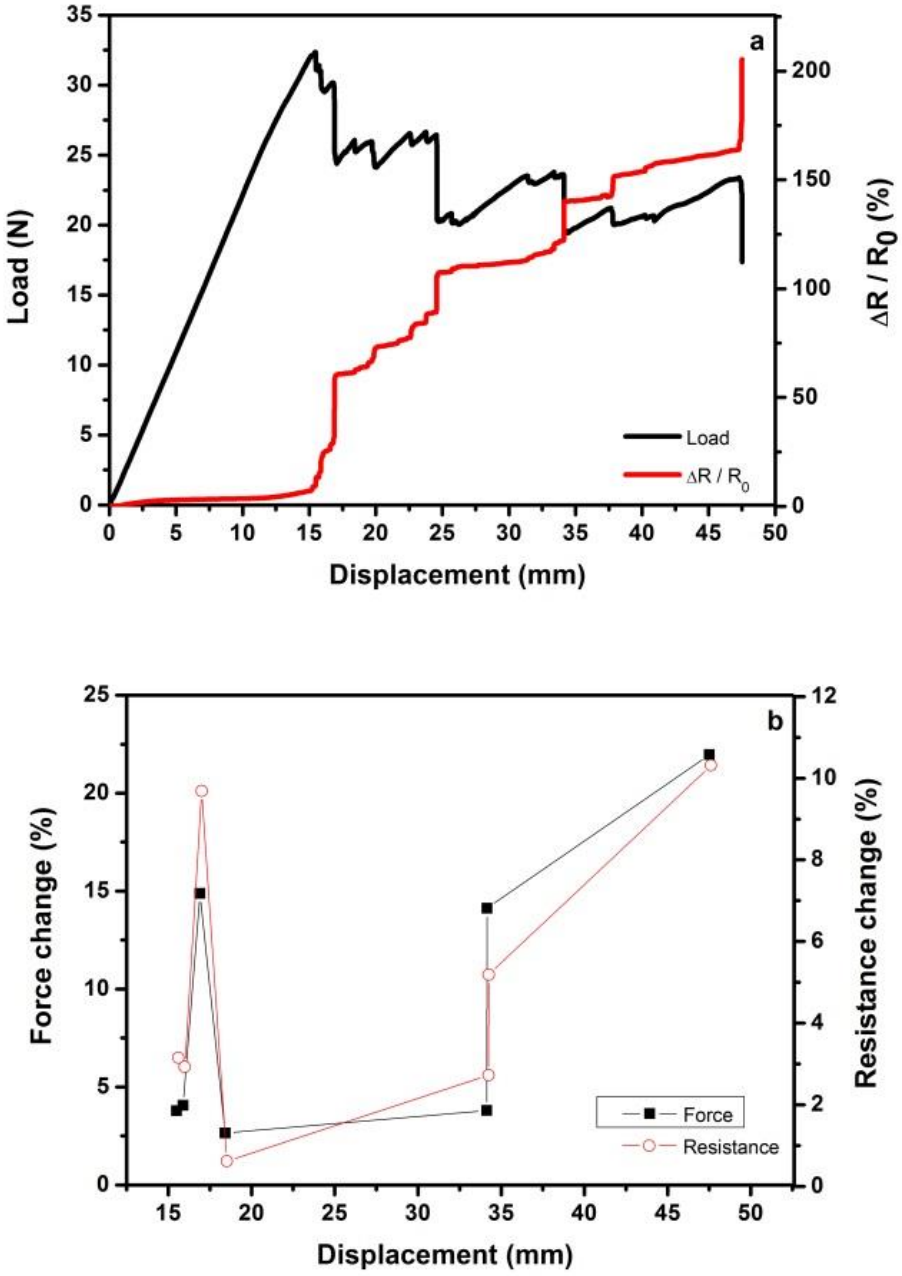

Fig. 6.5 *In-situ* damage sensing results of 0.032 wt.% (0.034 vol.%) CNT deposited GFRPs.

This improvement in sensing signals was attributed to an improved percolating CNT network, which covered more interfacial regions and distributed in adjacent epoxy

matrices. During the test, the crack as well as deformation of the specimen was affecting the CNT network, leading to changes in pathways for electrons which reflected as a change in measured resistance.

Interlaminar shear strength test

The *in-situ* damage sensing work was also performed for the SBS test to examine its effectiveness under flexure loadings. Both in-plane and through-thickness direction was used to apply electric field for sensing test; unfortunately, no electrical signals were obtained from through-thickness specimens. This was believed to be due to two main reasons: i) the relatively low loading of CNTs within composites (0.072 wt.% / 0.076 vol.%), and ii) the resin rich regions at the specimen surface which has a higher electrical resistance. Hence, only in-plane sensing results were successfully obtained and employed to analyse the internal damage of composites during the SBS test.

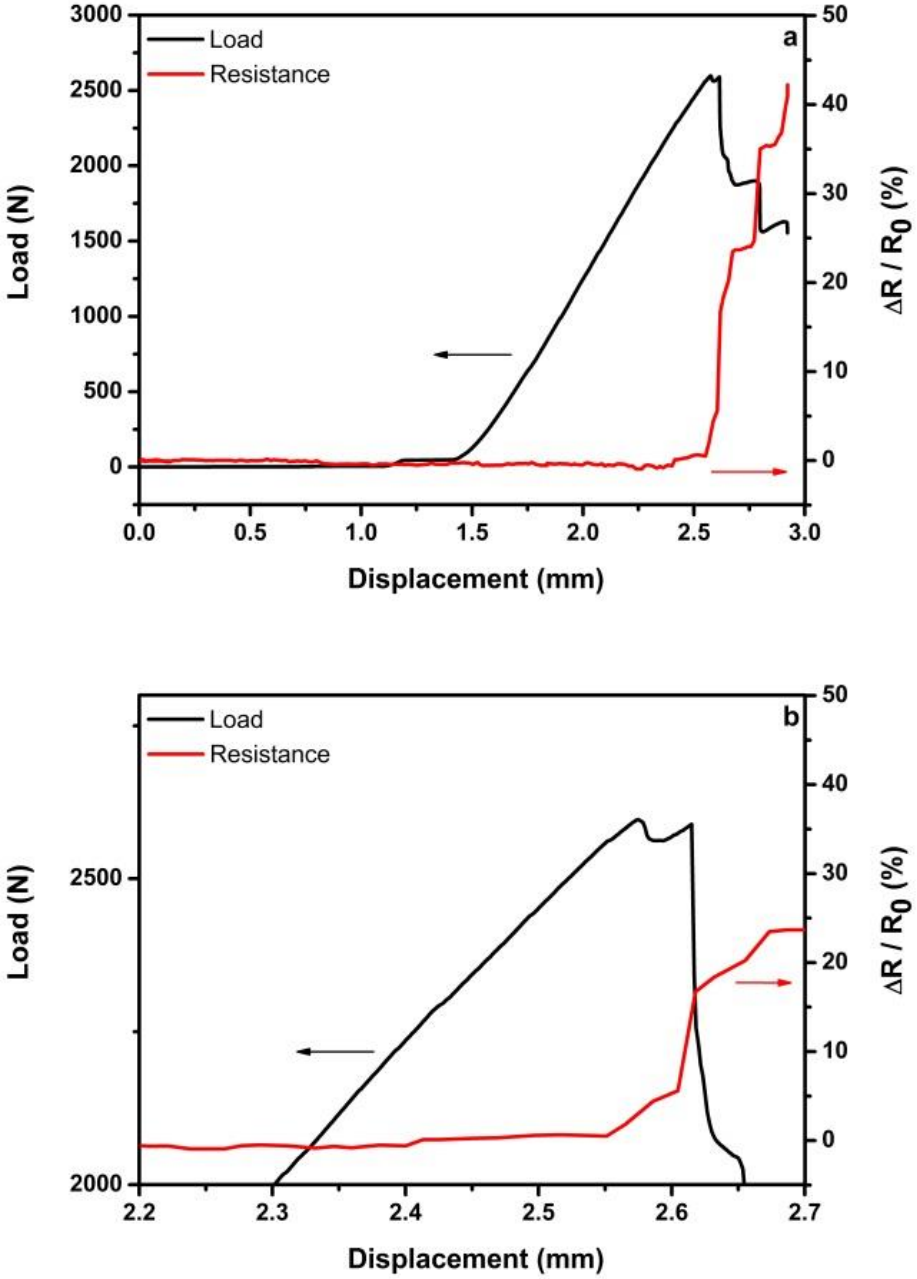

Fig. 6.6 Damage sensing results for ILSS test: (a) load curve with sensing results; (b) zoom in graph at the failure point.

In Fig. 6.6, the load curves together with normalized electrical sensing signals are presented. For SBS tests, the force starts to build up at the beginning of the test, until

interlaminar shear failure occurs which led to an obvious drop in force before the end of the test. Clearly, at the beginning of the test, the sensing signal was not much affected by the applied load but maintained at its starting level. It is worth to note that the electrical resistance was actually slightly reduced with increased loading, which was due to the flexural deformation which partly compresses the specimen and slightly reduces the gap between CNTs within the composites. This finding was consistent with other researcher's results [172, 245]. When interlaminar shear failure takes place, the structure of the internal percolated CNT network is severely affected, leading to a dramatic change in sensing signals. From the enlarged graph at failure point (Fig. 6.6b), it can be seen very clearly that the recorded sensing signals correlate well with the applied load, and a highest relative resistance change was due to the final failure of the specimen.

6.3.2 Carbon fibre prepregs

After successfully demonstrating the spray deposited CNTs as sensing tools for internal damage monitoring in GFRPs, carbon fibre prepregs were used as substrates for *in-situ* damage sensing test. Due to the conducting nature of carbon fibre which can be used as electrical sensor for fibre breakage, special effort has also been made to emphasis the effect of deposited CNT network for sensing delaminations.

In-situ damage sensing tests are performed under Mode-I loading conditions, using electrical methods to detect crack propagation and internal damage. Although electrically conductive carbon fibres by themselves could be used as sensor for damage detection, the existence of localized CNTs is expected to improve not only the through-thickness conductivity, but also sensitivity via changing of sensing

mechanism. During deformation, the percolated CNT networks within the insulating matrix are acting as sensors to detect early stage failure modes such as matrix cracking or delaminations, rather than late stage failure modes such as fibre breakage which could be better directly sensed by the carbon fibres.

To evaluate the effect of the introduction of CNTs into the composites, we compared the electrical property enhancement, as well as the sensing signal stability with different CNT loadings (0.02 and 0.047 wt.% / 0.019 and 0.044 vol.%). The electrical resistance of laminates was reduced from 1.430 Ohm to 0.984 Ohm with the introduction of 0.047 wt.% CNTs. In real applications, a safety threshold is probably required for necessary repair or replacement, which should not vary significantly between different composite laminates or structures. Therefore, the standard deviation of the electrical signals has been compared for the elastic zone among all specimens, in order to better understand the effect of CNTs within the composites during their early stage damage sensing and failure monitoring (Fig. 6.7). The larger the scatter, the less repeatable the sensing signals between different specimens. For each CNT loading, ten specimens are tested and analysed.

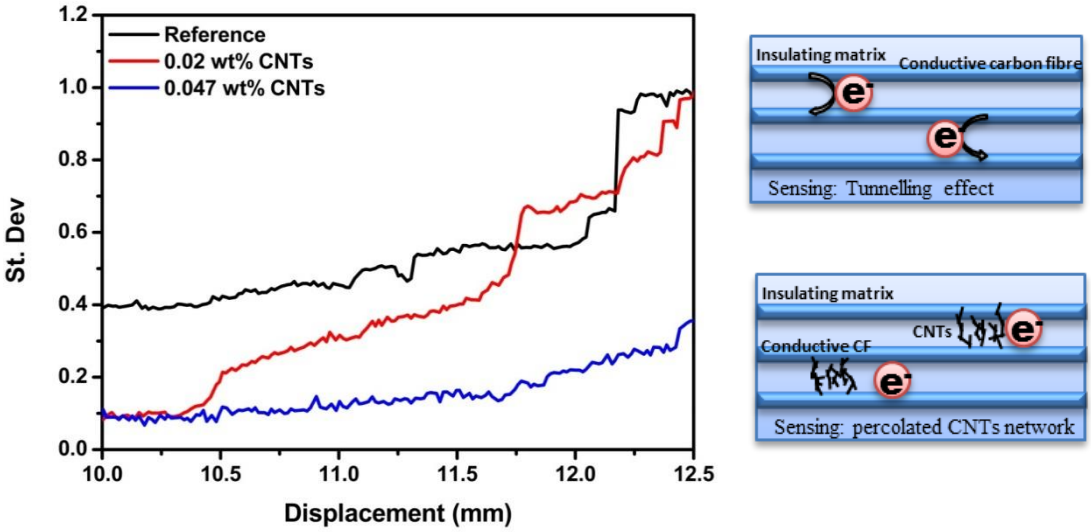

Fig. 6.7 Standard deviation curves for reference, 0.02 wt.% (0.019 vol.%) CNT, and 0.047 wt.% (0.044 vol.%) CNT specimens. The lower the standard deviation value, the more stable the sensing signals. Illustrations on right show the mechanism of electrical sensing.

For the complete elastic deformation zone with various loadings, the displacement is plotted up to 12.5 mm for the sensing signal variation analysis (Fig. 6.7). The average displacement of all specimens became non-linear between 10 and 12 mm. In Fig. 6.7, at a displacement of 10 mm, the sensing signal variation for the reference specimen is about four times compared to that of specimens with CNTs introduced. When the specimen becomes non-linear, the slopes of the variation curve between three concentrations are obviously different. Without CNTs, the standard deviation curve starts to increase dramatically, indicating a large signal variation between different specimens. However, with 0.05 wt.% CNT loaded specimen, the value was only one fourth of the reference, confirming significant improvement in repeatability and stability of the tested electrical sensing signals among different specimens.

This stability improvement is due to the introduction of the spray coated percolated CNT network within the insulating epoxy matrix between conducting carbon fibre fabric plies (as illustrated in Fig. 6.7 inset). During initial elastic deformation, resin rich regions clearly do not contribute to the electrical sensing signals due to their insulating nature. It is well known that CFRPs can be directly used for electrical damage sensing [20], especially with respect to surface resistance changes under flexural loadings [71]. The mechanism is based on the change of degrees of current penetration upon tension or compression [20]. Other damage sensing studies on CFRP were mainly performed in fibre direction, using carbon fibre breakage induced resistance changes [72-74]. For the reference specimen, through-thickness electrical signals are therefore completely attributed to the conductive carbon fibre fabrics and their physical contacts, which results in large sensing signal variability. However, with spray coated CNT networks in between the plies, sensitive CNT networks are introduced in these resin rich regions and reduce the reliance on local physical contacts between carbon fibres, significantly improving the stability and consistence of the sensing signals, allowing them to be used for strain or damage detection, even at small deformations, i.e. elastic deformation.

The *in-situ* damage sensing tests were established using the DCB tests. In Fig. 6.8a, a typical load and displacement curve of a 0.047 wt.% CNT coated specimen is shown. The applied load is increasing linearly to a maximum, followed by a sudden load drop as the crack propagates in a rather unstable manner. This unstable fracture is typical for carbon fabric/epoxy laminates, exhibiting fibre rich and resin rich regions, leading to differences in local toughness and consequently unstable crack propagation. After crack initiation, the force builds up again, until the crack propagates which results in a load drop. This process is carried out until the crack

length of the specimen reaches a certain value. The load-displacement curves can also been analysed to obtain the exact displacement value for each load drop, to be used for further analysis of the damage sensing signals.

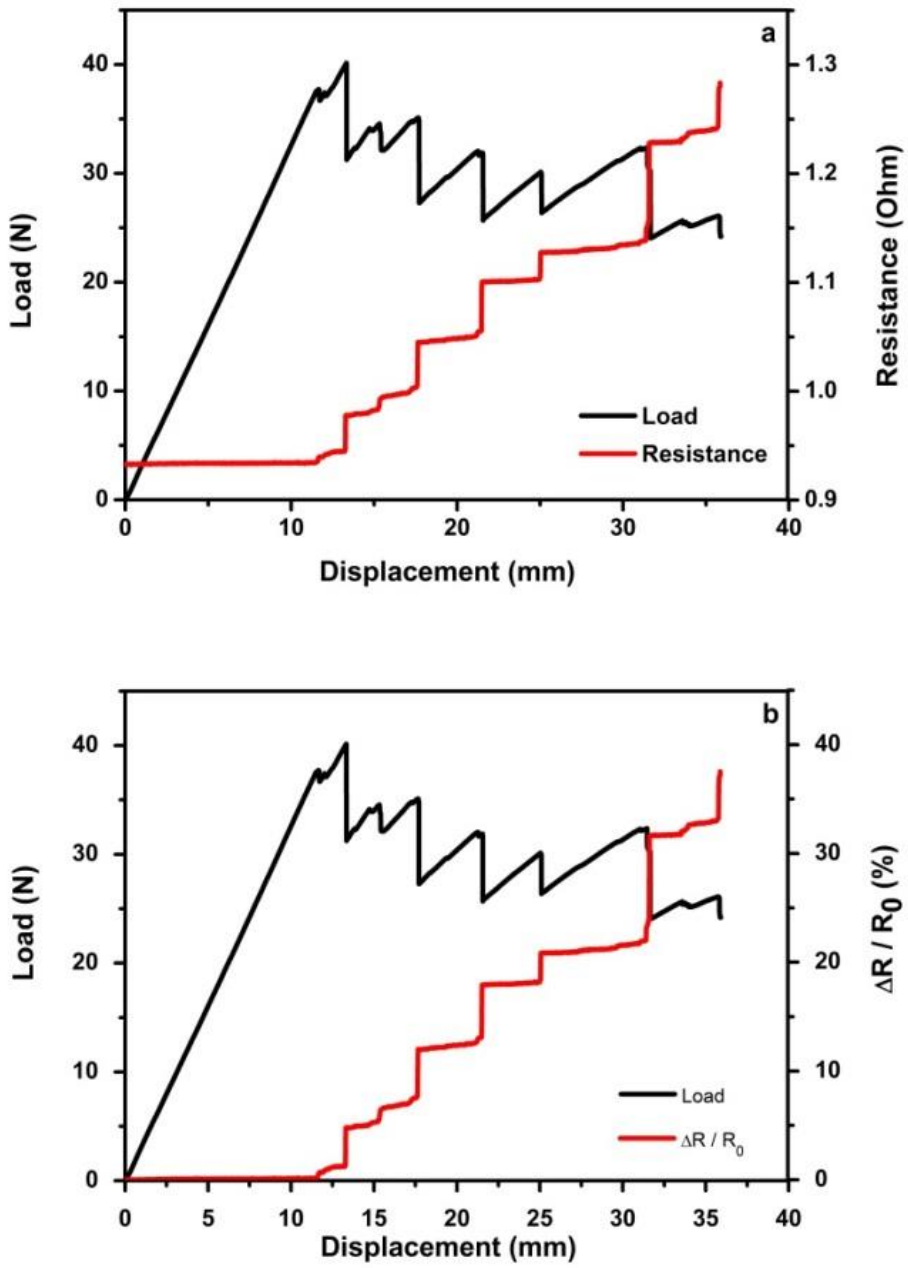

Fig. 6.8 *In-situ* damage sensing graph of 0.047 wt.% (0.044 vol.%) CNT laminates: (a) Load-displacement curve (black) with electrical resistance (red) in absolute

values; (b) Load-displacement curve (black) with electrical resistance (red) in relative percentage change.

As the crack opens, the overall trend of electrical resistance is increasing, which is due to the longer distance for the electrons to "pass-through" the sample. Each load drop is associated with a sudden increase in resistance and indicates a breakdown of the CNT conductive network due to crack propagation. It can be clearly seen that with each load drop, the electrical resistance increases from a starting level to a higher level, which is maintained until the next load drop. Importantly, the increment of the electrical resistance signal attributed to crack initiation and propagation can be correlated to each associated load drop.

Instead of plotting measured volumetric resistance as sensing signals, the resistance change over the original resistance ($\Delta R/R_o$) in percentage is also plotted (Fig. 6.8b), in order to overcome variability between specimens. This way, similar resistance changes are observed for different specimens, confirming the improved stability and consistency of the sensing signals for the laminates with deposited CNTs.

To develop a further understanding of the relationship between measured electrical resistance and internal damage of the specimen, the derivative of the force curves is plotted. From each negative value on these derivative curves, the exact point of cracking can be identified and with this, the resistance change and force change at those locations can be calculated (Fig. 6.9). Only data points with a force change above 0.25 N were collected in order to minimize instrumentation error. Apart from the correlation of force change and resistance which is shown in Fig. 6.9a, the relative change of those two parameters was also plotted as well (Fig. 6.9b).

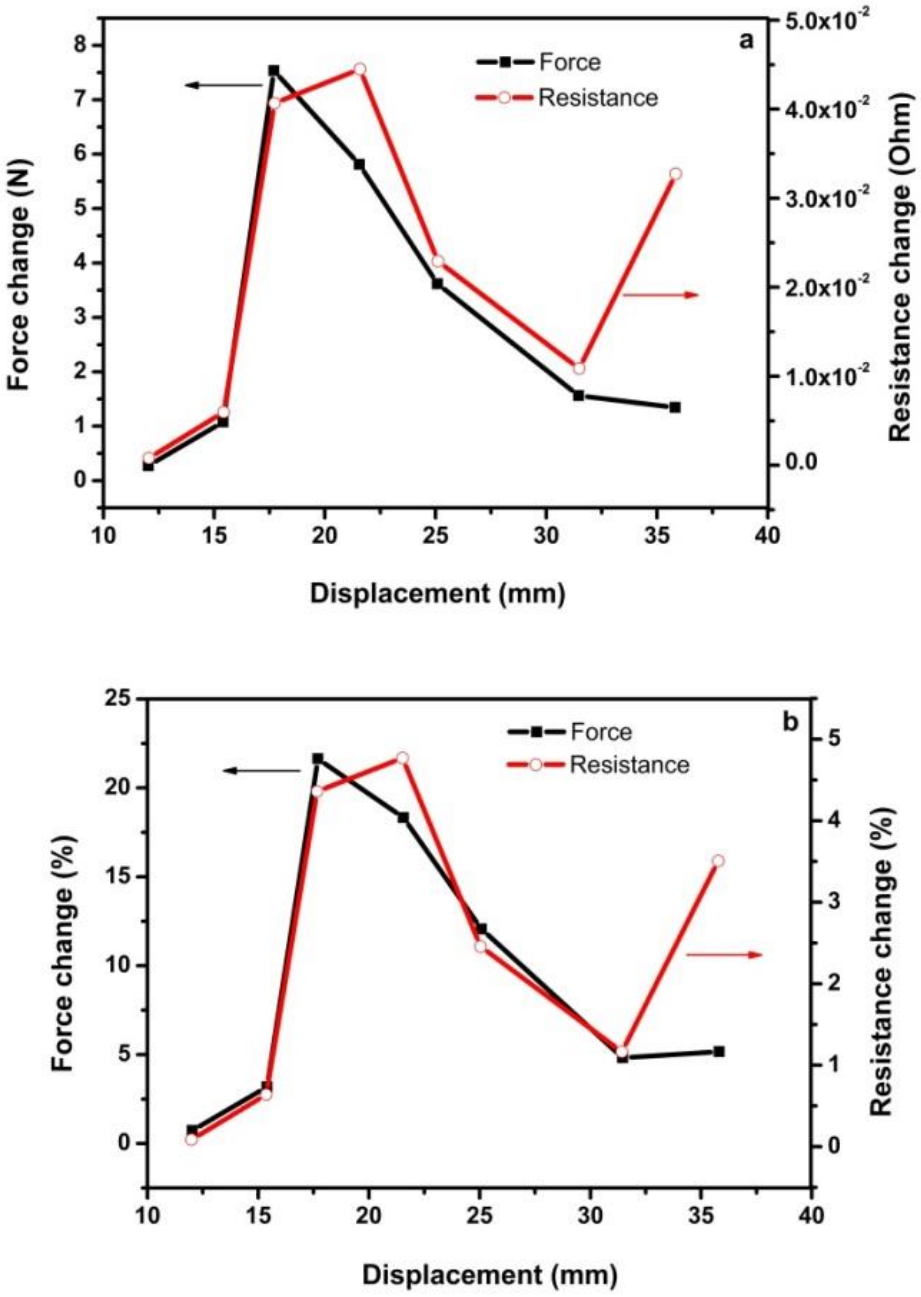

Fig. 6.9 Correlation between applied load and measured resistance of 0.047 wt.% (0.044 vol.%) CNT specimen: (a) in absolute value; (b) in relative percentage change (normalized value).

Fig. 6.9 shows the relationship between force and resistance change at the same location throughout the experiment. The trend of these two parameters matches exactly, especially for the normalized value (Fig. 6.9b), confirming a correlation between the load change and the electrical resistance change as a result of damage. Most of the internal damage can be quantified through the measured change in resistance. Although some data points are not completely consistent with the general trend, this is probably due to the complex CNT network within the composites. For instance, certain connected pathways in a CNT network are weaker than others, leading to a significant resistance change at relatively small load changes. In fact, according to previous studies on CNT based damage sensing networks [156-158], even more diluted networks could lead here to greater sensitivity with the ability to detect even smaller internal damage such as microscopic matrix cracks and/or interfacial debonds. Although in real application, optimum CNT amounts should be employed to provide not only percolated but more sensitive network for internal damage monitoring.

6.3.3 Phenoxy/CNTs interleaved CFRPs

Compression moulded and solution cast phenoxy/CNTs films were used as interleaves at the mid-plane to build up localized CNT networks for damage sensing measurements. In order to better compare the effect of CNTs, electrical sensing signals of virgin thermoplastic film interleaved specimen were also recorded and compared, although the insulating thermoplastic layers are expected to interfere with the electrical signals through the specimen.

Phenoxy/CNTs film interleaved specimen

The melt-processed phenoxy film interleaved specimen was characterized for damage sensing properties to build up the baseline. Not surprisingly, the insulating phenoxy layer within the mid-plane severely affected the electrical signals. At the beginning of the DCB test, no obvious electrical signal changes were observed, even with crack propagating and sudden force drops. As the test continued, some of the specimen has shown sudden resistance jump from original level to higher level together with a force, although the electrical signals remained no obvious correlation with force drops after sudden increment (Fig. 6.10a). In other cases, the electrical signals remained at their initial level without any significant changes throughout the DCB test, regardless of crack propagating status. Therefore, no reliable information can be obtained from the electrical sensing results for phenoxy film interleaved specimens.

As previously presented, both melt-processing and solution processing methods were employed to incorporate CNTs into thermoplastic carrier for CNT delivery in FRPs. These interleaved specimens were characterized together with standard DCB test.

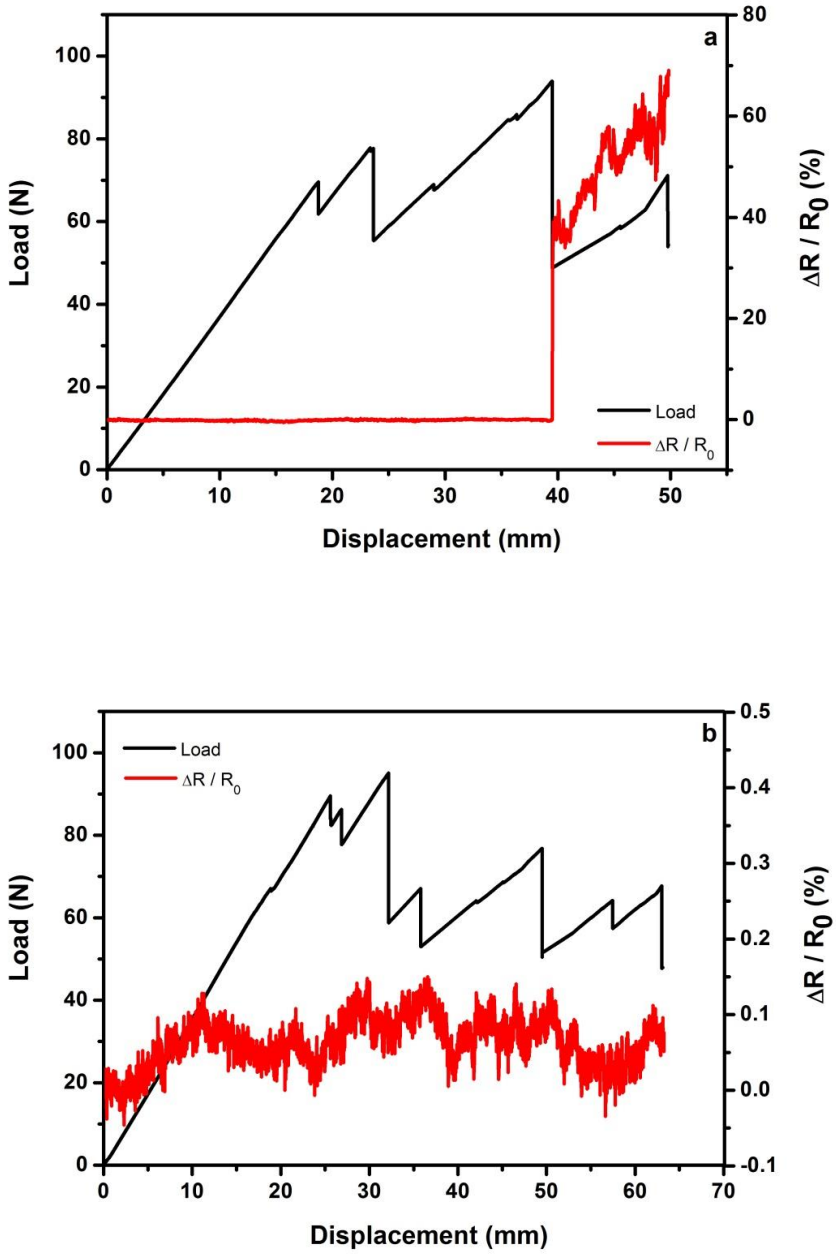

Fig. 6.10 *In-situ* damage sensing results of phenoxy film interleaved specimens.

The in-situ damage sensing results with typical load-displacement curve was plotted in Fig. 6.11 for phenoxy/CNT film interleaved specimens, for both melt-processed and solution processed interleaves. Apparently, due to the presence of a CNT percolated network in the composites, the electrical sensing signals were clear and

stable, and maintained at an initial value during the beginning of the test, while slightly increasing when the specimen yielded with increasing loading force. With each force drop, the sensing signal obviously jumped to a higher level, until the next force drop where the crack was propagating. Very good correlation between each force drop and sensing signal jump can be found from both graphs, indicating the potential of using this methodology for internal damage monitoring in composites. It is worth noting that the average value of measured electrical resistance of phenoxy/CNTs interleaved specimens was also reduced, for instance, from 178.7 Ohm to 1.49 Ohm compared to virgin phenoxy film interleaved specimen, due to the introduction of conductive CNTs. Interestingly, the sensitivity of solution-processed interleaved specimen seems higher than those of melt-processed interleaved specimen, as shown in Fig. 6.11. This was believed to be due to the different amount of CNTs in the specimen. In percolated networks, an additional amount of conductive fillers normally lead to a lower sensitivity, since there are more possible pathways for electrons to pass through.

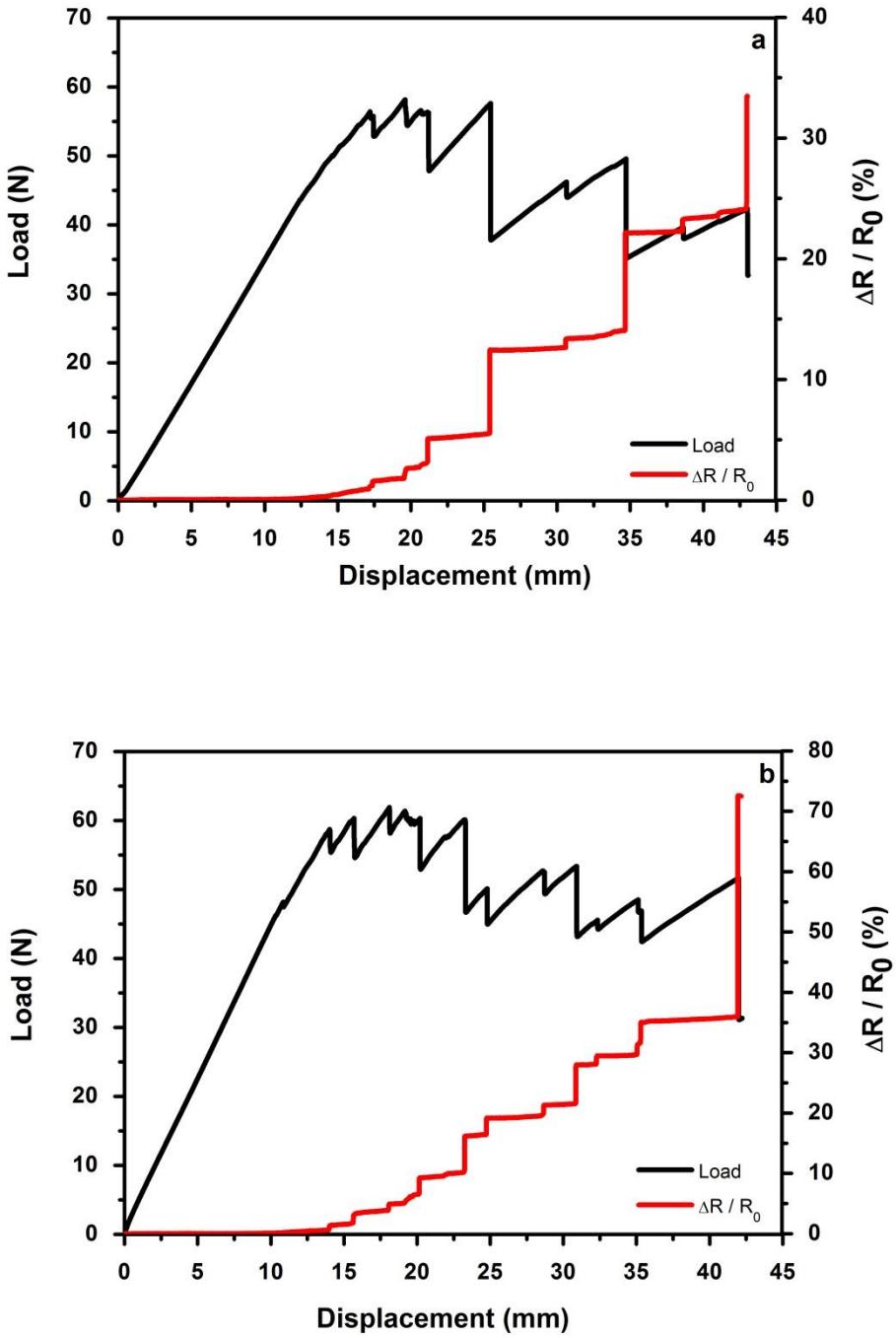

Fig. 6.11 *In-situ* damage sensing results: (a) melt-processed phenoxy/CNTs interleaved specimen with 3 wt.% (2.15 vol.%) CNTs; (b) solution-processed phenoxy/CNTs interleaved specimen with 1 wt.% (0.71 vol.%) CNTs.

6.3.4 CNT Spray coated CFRP

As out-of-autoclave processes such as vacuum assisted infusion have become more popular due to their various advantages over traditional autoclave processes such as reduced overall cost and higher integration functions, carbon fibre fabrics with spray coated CNTs were employed to produce composite panels by vacuum assisted infusion processes. The *in-situ* electrical sensing tests were performed alongside both DCB and SBS standard tests. The overall concentrations of CNTs in Mode-I specimen and ILSS specimen were 0.13 wt.% (0.12 vol.%) and 0.08 wt.% (0.07 vol.%), respectively. Sensing results together with load curve are presented in this section.

Interlaminar fracture toughness test

Typical load curve with electrical sensing curve are presented in Fig. 6.12a. As expected, a very clear and correlated sensing curve was obtained. As the force starts to build up, sensing signals remained unchanged, until a slight increase can be observed at specimen yielding. With each subsequent load drop throughout the test, sensing signals clearly jumped to a higher level. This was due to break-down of the percolated CNT network resulting from internal crack propagation, leading to a reduced number of possible pathways for electrons to pass through the specimen.

To obtain a clear correlation between sensing signals and mechanical performance, a correlation graph was plotted in Fig. 6.12b. Excellent correlation between two load and resistivity with crack growth were observed, confirming the reliability of this damage sensing method.

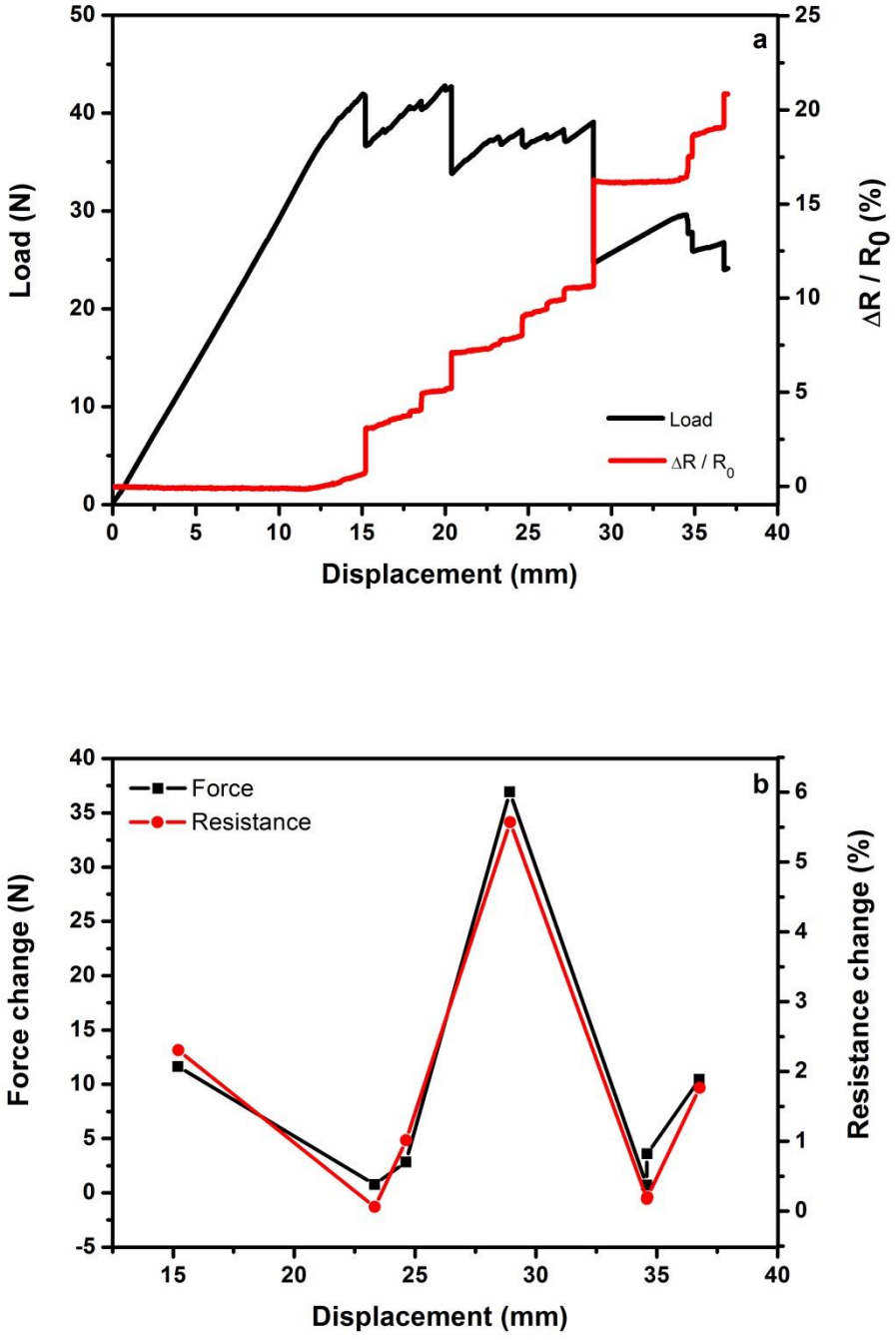

Fig. 6.12 *In-situ* damage sensing results for CF/CNTs composites: (a) sensing signals with load curve; (b) correlation between sensing signals and force drops.

Interlaminar shear strength test

The SBS test was performed to obtain ILSS values of CNT modified CFRP, while electrical measurements were taken in both through-thickness and in-plane direction for damage sensing. Both reference specimen (without CNTs) and CNT deposited specimen were tested, and their results are compared to examine the effect of CNTs on the sensing results.

Due to the conductive nature of carbon fibres, the reference specimen without CNTs can be directly applied to the electrical sensing method. However, due to the insulating layers of epoxy resins, the conductivity is completely relying on carbon fibre and connections between them. As stated in earlier section, this direct sensing measurement based on carbon fibre without percolated CNTs might lead to more scattered signals and less reliability.

The in-situ damage sensing results of reference specimens are presented in Fig. 6.13, for both in-plane (a) and through-thickness (b) measurement. As mentioned earlier, the electrical conducting nature of carbon fibres allows the reference specimen to be directly used for such an electrical damage sensing method. However, due to the insulating layers of epoxy resin between the carbon fibre fabric plies, the conductivity is completely relying on interconnects between individual carbon fibres or tows. Therefore, a direct sensing method based on carbon fibre without CNTs to improve network formation may lead to more scattered signals and less reliability [203]. CNT modified specimen may improve small-scale tunnelling effects, leading to an improvement in sensitivity of the electrical damage sensing method.

For the in-plane measurement, the electrical sensing signal of the unmodified CFRP laminate showed some unstable readings during SBS testing, with a slight reduction in resistance being even observed with increased loading. This small reduction was

attributed to the deformation of the specimen, which may result from a reduction in gap distance between conductive carbon fibres as a results of the compressive load applied in the three-point bending experiment. This was found consistent with other research [148, 202, 238, 239]. No obvious resistance change was observed with increasing load, due to the dominating conductive character of the carbon fibre phase. At failure the sensing signal shows a sudden increase in resistivity, which is due to a break-down of interlaminar conductive pathways as well as fibre breakage. However, once a composite structure has reached the fibre breakage stage, the component is too near the end of its life-time for this kind of damage sensing to be useful.

In the case of through-thickness measurements, unlike previously reported results [5, 6] where the sensing signal remained unchanged until final failure, here the measured electrical sensing signals increased continuously with load. At final failure of the specimen, also a sudden jump is observed in resistivity, however, this sudden jump is preceded by progressive damage accumulation, making this a more interesting experiment from a structural health monitoring (SHM) point of view. It is also worth noting that the observed relative resistivity change was much greater for the through-thickness measurements (14%) than for the in-plane measurements (4%) (see Fig. 6.13a and 6.13b).

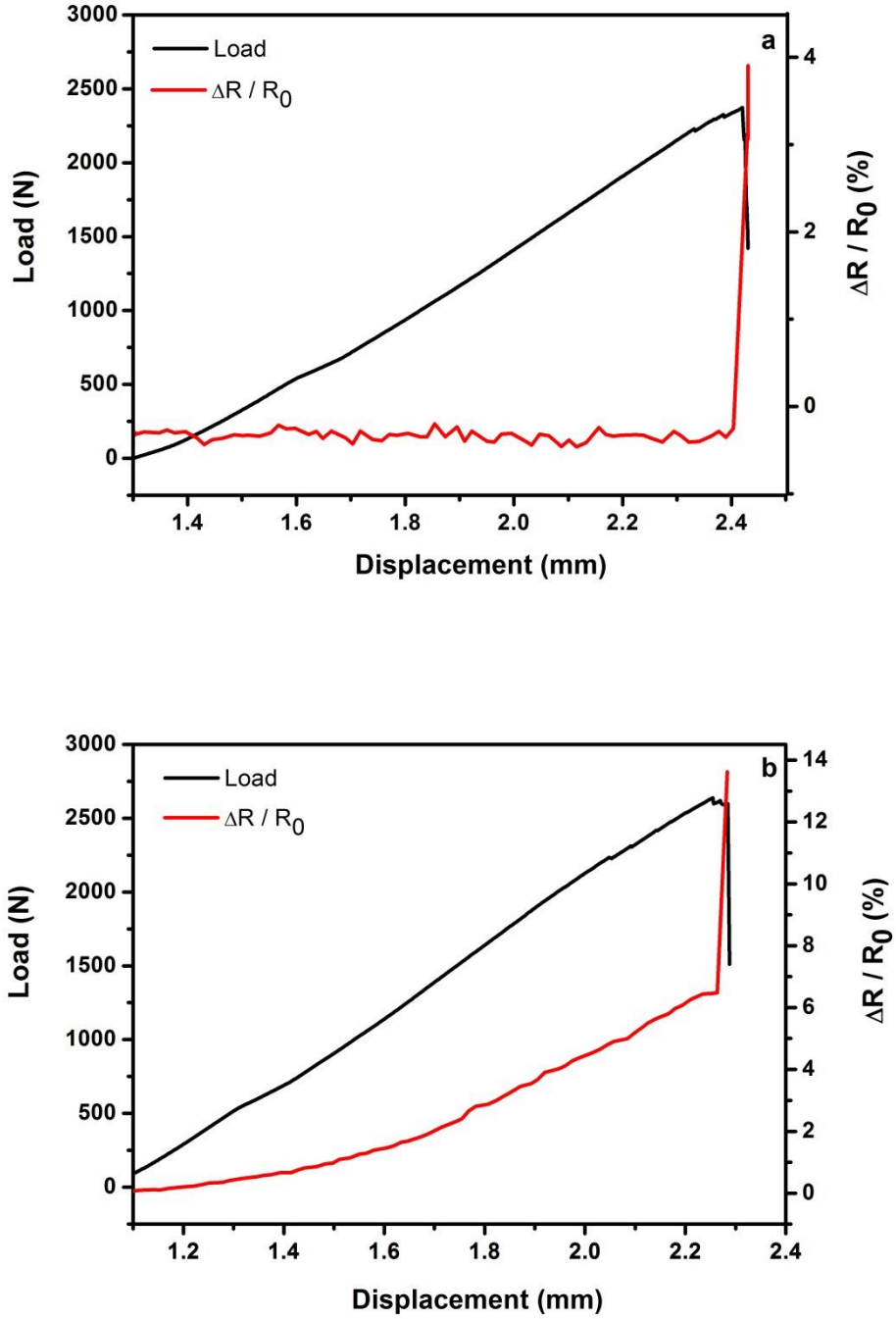

Fig. 6.13 *In-situ* damage sensing results for CFRPs reference specimen with: (a) in-plane measurement; (b) through-thickness measurment.

The sensing results of CNT spray-coated specimen are presented in Fig. 6.14, for both in-plane (a) and through-thickness (b) electrical measurements. Typical load-displacement curves for the ILSS tests are shown in the graphs, together with normalized resistance change values as sensing signals. For in-plane measurements, the sensing signals remain constant without any obvious change until final failure of the specimen where a sudden jump in electrical resistance was found. Similar to the reference CFRP specimens, this sudden jump was mainly due to breakage of conductive carbon fibres, which dominate the overall electrical properties. In the case of through-thickness measurements, the sensing signal continuously increased with loading similar to the reference specimen, with another sudden increment being observed at final failure of the specimen.

For both reference and CNT deposited CFRP specimen, the in-plane sensing signals remained fairly unaffected with increasing load until final failure of the specimen, while through-thickness sensing signals progressively changed with increasing loading. These finding are in agreement with expected SBS failure modes as in-plane resistivity is dominated by the conductive carbon fibres, while the out-of-plane measurements are matrix and/or interface dominated. These finding are different to previous ILSS damage sensing works [238, 239] where through-thickness resistivity was not affected by loading.

In order to monitor the structural health condition of composites components, here the through-thickness method is better than the in-plane method, as it provides a possibility to in-situ monitor the internal deformation and damage before catastrophic failure. Moreover, it agrees with expected failure modes in such a test, which should be either dominated by matrix cracking or interfacial debonding, rather than fibre breakage.

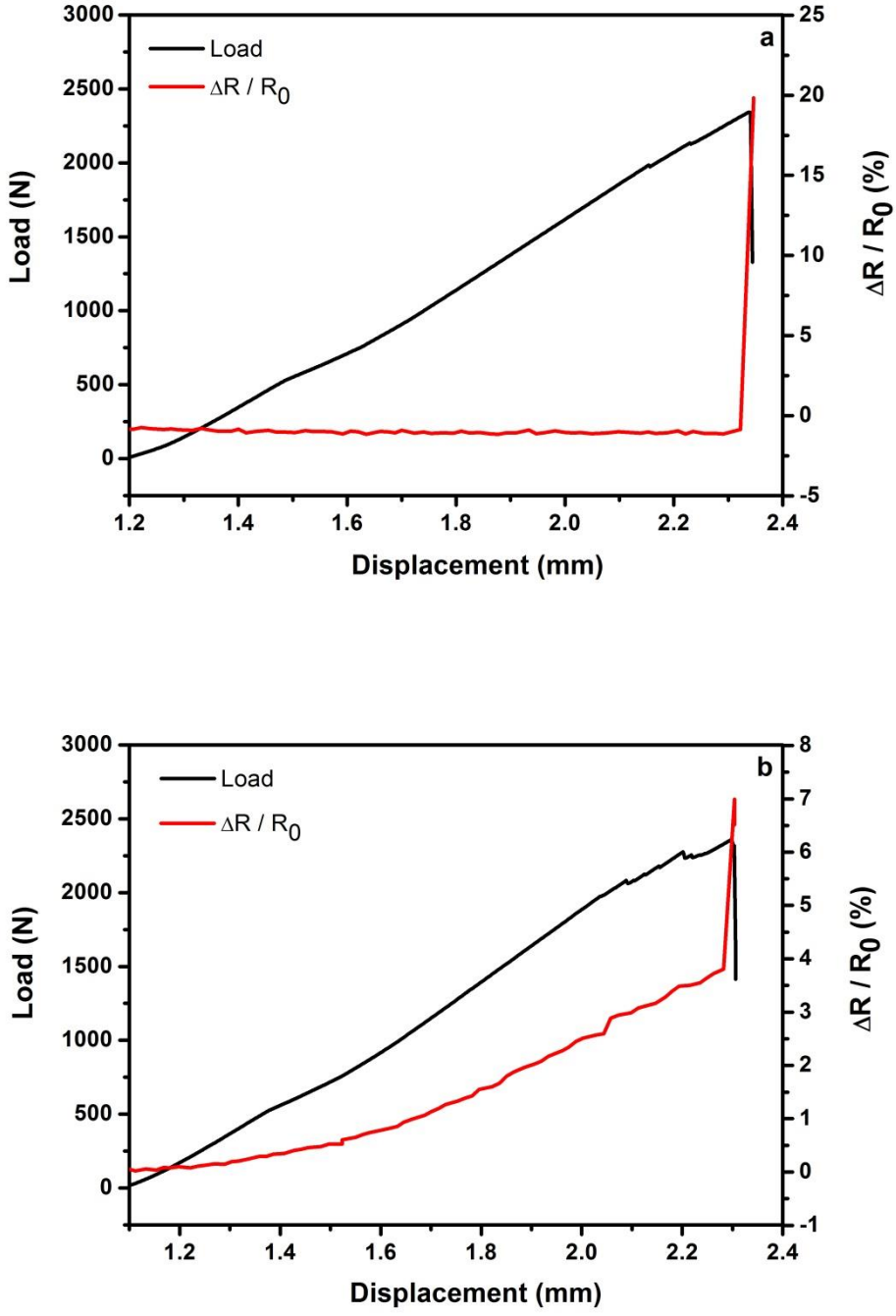

Fig. 6.14 *In-situ* damage sensing results for CNTs deposited CFRPs specimen with: (a) in-plane measurement; (b) through-thickness measurement.

In order to confirm the obtained *in-situ* sensing results, especially progressive damage monitored via through-thickness method, acoustic emission was also performed separately for specimens during SBS test. With internal damage initiating and propagating, energy generated signals are collected by piezoelectric sensor attached on specimens. In Fig. 6.15, it can be seen clearly that with increasing load during the test, the specimen was experiencing progressive internal damages, as confirmed by AE data and previous demonstrated through-thickness electrical sensing signals.

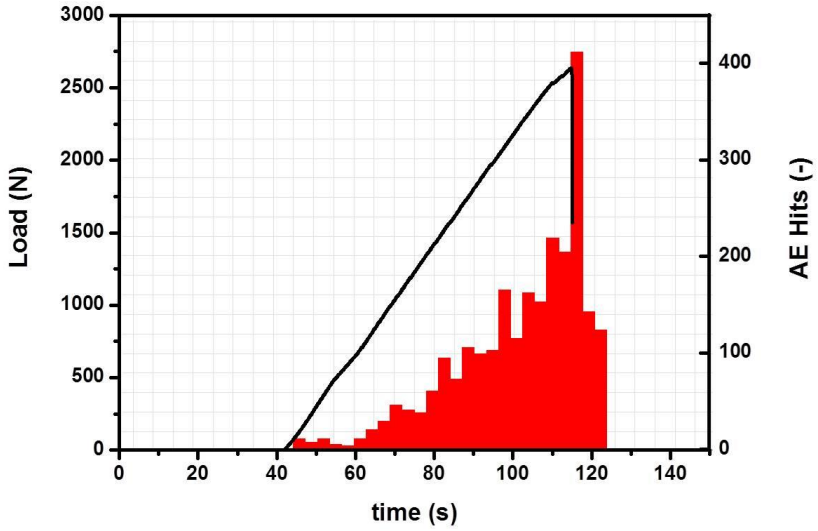

Fig. 6.15 Acoustic emission data with load curve to confirm progressive internal damage during ILSS test.

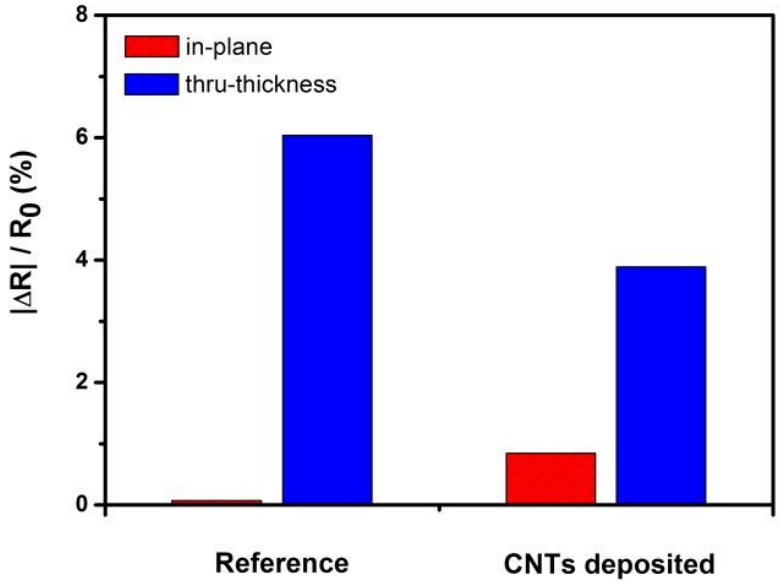

Fig. 6.16 Comparison of maximum sensing signals before failure between reference and CNT coated specimen

To evaluate the effect of the introduction of CNTs on the sensing properties of the specimen, the average values of the maximum sensing signals before failure are presented in Fig. 6.16. Compared to the reference CFRP specimen, the maximum sensing signals slightly improved with the introduction of a CNT network for the in-plane method, while surprisingly the sensitivity of the through-thickness signals was slightly reduced by 35%. The increment in in-plane sensitivity is believed to be due to the additional conductive pathways for electrons and is not solely based on conducting carbon fibres but also on the deposited CNT network. Hence the interruption of the in-plane conductive network will result in a greater resistance change at the final point of failure. On the other hand, the conduction mechanism in the case of through-thickness measurements seems to be dominated by physical contacts between carbon fibres, while the addition of CNTs between carbon fibre

plies does little to improve the damage sensing behaviour. In SBS testing the specimen are subjected to flexural loading combined with high compressive contact stresses, which may maintain electrical conductive pathways even in plain CFRP laminates. This is in contrast to our previous mode-I delamination studies, where obviously such contact stresses are absent and CNTs greatly enhanced the sensitivity towards interlaminar failure.

6.4 Conclusions

Percolated CNT networks have been utilized as a sensing tool in composites for internal health monitoring. Various composite systems have been evaluated for in-situ damage sensing, including insulating glass fibre, conducting carbon fibre fabrics, and carbon fibre prepregs. Both thermoplastic delivered and directly spray coated CNT networks have been evaluated as potential methods to introduce CNTs in composite laminates for electrical damage sensing measurements.

For the first time, standard interlaminar fracture toughness tests (DCB) have been applied for in-situ damage detection. The same methodology has also been extent to other standard composites test such as interlaminar shear strength test (SBS).

The localized CNT sensing network can simultaneously respond to macro-deformation, and provide an indication of internal health condition including damage initiation and propagation. Excellent correlation between electrical sensing signals and mechanical performance during the test was observed for all tests.

For thermoplastic interleaved specimen, the insulating thermoplastic interleaves were found to significantly affect the electrical sensing signals, as the electron

cannot travel through this interlayer. The overall trend of measured resistance during DCB tests shows no correlation with internal crack propagation status. This was overcome by the introduction of CNTs into the interleaves.

For electrical sensing during ILSS tests, the through-thickness measurement was found to be more effective to monitor the health condition throughout the test, especially to monitor damage before final interlaminar shear failure takes place.

Chapter 7

Conclusions and Future works

7.1 Summary

The continuous market expansion of carbon fibre reinforced plastics (CFRPs) has attracted growing attention to health monitoring and damage sensing functionalities. Carbon nanotubes (CNTs) have shown great potential to detect various composite failures using percolated network [162, 171, 185] and could be of interest as a multifunctional filler in CFRP simultaneously improving mechanical properties and introducing sensing capablities. However, due to the associated problems of introducing CNTs into FRPs such as increased resin viscosity and filtering effect [246], innovative routes are still required for introducing CNTs into FRPs with the potential of industrial scale-up. This thesis mainly focused on using CNTs in fibre reinforced composites for integrated damage sensing properties, and two main routes were explored to deliver CNTs into FRPs. First, thermoplastic phenoxy was employed as a dissolvable carrier for CNT delivery and localization, with additional benefits of added toughening in composite laminates. Secondly, a simple spray coating technique was utilized to directly deposit CNTs on fibre preforms, resulting in localized toughening and integrated percolated networks for damage sensing at extremely low CNT concentrations.

Some of the key findings from this thesis are listed below:

- Recent advance on utilizing percolated CNT network for electrical damage sensing and structural health monitoring has been reviewed;
- Different toughening routes for fibre-reinforced plastics has been reviewed;
- Binary system of thermoplastic phenoxy and CNTs was studied, with lowest reported percolation threshold observed for current system. The temperature dependence of the conductive network was studied;
- Binary system of thermoplastic and thermoset has been studied on the system of phenoxy and RTM6-2. The dissolution behaviour with different temperature profiles were studied, and simple relationship between dissolution time, initial fibre diameter, and temperature has been proposed;
- The toughening effect of phenoxy interleaf with various surface-to-volume ratio has been studied, while a highest reported toughness improvement compared to literature data was obtained for the current system;
- The difference in toughening effects between phenoxy film and nanofibre mat were explained in relation to differences in dissolution time;
- Simple and versatile spray coating technique was applied to deposit and localize CNTs onto fibre preform for damage sensing purposes;
- Phenoxy interleaves were used as CNT carriers for localized delivery, overcoming nanoparticle related resin infusion problems such as filtration or uneven distribution;

- *In-situ* damage sensing test was set up for standard DCB and SBS test, and delamination as well as interlaminar shearing failures were successfully monitored by electrical sensing methods.

The binary system of thermoplastic phenoxy and CNTs has been studied first (Chapter 3). The percolation curve of melt processed phenoxy/CNTs nanocomposites has been obtained, showing a low percolation threshold of 0.58 wt.% after processing parameter optimization, while a lowest reported percolation threshold value of about 0.20 wt.% was obtained for specimen after annealing. The temperature dependence of the conductive network formation and resulted electrical conductivities has been analysed and explained by a dynamic percolation process.

After the binary study of thermoplastic/CNTs, the other binary system of thermoplastic/thermoset was studied in Chapter 4 and 5. The dissolution behaviour of phenoxy in epoxy resins was studied using optical microscopy, and the effect of temperature and initial thermoplastic fibre diameter on dissolution time was analysed (Chapter 4). These finding provided fundamental information for the development of a dissolvable interleaf system, and insight into toughening effects for dissolvable interleaves with different surface-to-volume ratios. With different forms of phenoxy interleaves, the difference in surface-to-volume ratios resulted in Mode-I interlaminar toughness improvements which were studied in Chapter 5. A highest reported toughness improvement compared to literature data was obtained for the current system based on electrospun phenoxy nanofibre interleaves, while differences in toughening effects between film and nanofibre mat were explained in relation to differences in dissolution time.

Apart from using dissolvable thermoplastics as a CNT carrier, spray coating was also employed for localized CNT deposition on fibre preforms due to its simplicity and versatility. The spray coating method also overcomes traditional limitations such as increased resin viscosity by CNTs or uneven distribution and filtering during resin infusion processes.

Finally, the main focus of this thesis, the development of an integrated damage sensing capability for FRPs using CNT networks was evaluated in Chapter 7. Model studies on insulating glass fibre laminates were carried out in order to emphasise the importance of the conductive CNT network for sensing, while an electrical sensing method was successfully demonstrated for both double-cantilever beam tests and short beam strength tests. Spray coated carbon fibre prepregs and fabrics were also manufactured, which showed a good correlation between internal damage state and electrical sensing signals. The dissolvable thermoplastic phenoxy film delivered CNT networks also demonstrated good correlation between damage and sensing signals, while reference specimen of phenoxy film interleaves without CNTs showed no electrical sensing signals until sample failure. It was also found that out-of-plane measurements were more effective for detecting interlaminar shear damage, as it provided more progressive sensing signals.

Compared to traditional CF/CNT hybrid composite, the other obvious advantage of this work is CNT localization and innovative delivery systems. Unlike top-down methods which disperse CNTs into epoxy resins for composite manufacturing, the use of dissolvable thermoplastic carriers and direct spray coating deposition has overcome important issues such as increased viscosity and filtering effects, providing good spatial control of CNT deposition in composites. Meanwhile, these

delivery routes avoid relatively complex procedures (e.g. *in-situ* growth or chemical deposition), providing excellent feasibility for industrial scale up.

In short, hierarchically engineered micro-nanocomposite systems have been developed with integrated damage sensing capabilities. Outstanding mechanical and electrical sensing properties were obtained, and innovative nanoparticle delivery systems were demonstrated for such hybrid systems.

7.2 Applications and Future works

In this thesis, carbon fibre/carbon nanotube hybrid composites with integrated damage sensing capabilities were successfully manufactured and characterized. The established in-situ damage sensing method under standard composite test has shown excellent correlation between composite internal damage and electrical sensing signals, especially for out-of-plane failures such as delamination and interlaminar shearing. With the extensive use of composite laminates in various structural applications like aircraft and wind turbines, the presented nano-engineered composites can be used for structural health monitoring throughout components service life without requirements of extra equipment. With in-service damage detection, the current approach of overdesigning composite components can be partially solved. Furthermore, the low fracture interlaminar toughness of composite - laminates as one of its main limitations can be improved simultaneously.

In aerospace and railway industry, a sufficient level of electrical conductivity in composite components is required for both electromagnetic interference and lighting strike protection (LSP). Currently aerospace parts employ a layer of a metallic

(bronze/copper) mesh for such function without any structural contribution, taking few hundreds of kilograms weight penalty in modern aircraft. In collaboration with industrial partner (FIDAMC), the developed CNT spray coating method demonstrated potential for partially replacing existing metallic mesh with significant weight savings.

Table 7.1 compares the LST results between a reference CFRP laminate without metallic mesh layer, and a laminate with CNTs spray coated on the top surface. A reduction in maximum temperature, damage area, as well as electrical resistance can be seen. Especially with respect to the damage area, a reduction of around 30% was observed for a laminate with only the surface fabric been spray coated with CNTs. These promising results show great potential of using spray coating for partial removal of the metallic mesh in aerospace applications, potentially leading to significant weight reductions.

Table 7.1 Simulated LST results between reference and CNT deposited laminates, test performed at zone 2A, in accordance with EUROCAE ED-105.

	Maximum temperature reached (℃)	Maximum damage area (mm^2)	Elec. resistance before test (mΩ)	Elec. resistance after test (mΩ)
Reference	130	9500	1138	1135
CNT deposited at top surface	120	6675	430	431

Although all spray coating works were carried out in a fume cupboard, considerable amount of organic solvent was used. Life cycle analysis should be performed to compare this technique with others, and solvent recovery should also been

considered. From a health and safety point of view, minimization of the effect of airborne nanoparticles during manufacturing is another important consideration, especially the handling and lay up step after spray coating deposition. Compatible thin resin films could be used as a solution to secure the deposited CNTs in place on the fibre preforms.

As the current spray coating studies mainly focused on the deposition of CNTs onto fabrics, a further utilization of the current technique to deliver CNTs not only on fabrics surfaces but also more within fibre bundles could be beneficial for other through-thickness properties of composite laminates and transverse matrix cracking. Longer evaporation times with vacuum pulling systems at the other side of fabrics might be able to achieve this, although good CNT dispersion needs to be maintained. Higher amounts of CNTs could also be used in the composite laminates, in order to partially replace the copper mesh in current aircraft design for lighting strike protection, contributing to weight reduction.

Apart from CNTs, graphene has been extensively studied during the last couple of years. The established CNT delivery system, together with in-situ damage sensing characterization could be adapted from 1D filler to 2D graphene, with potential of some improved performances.

References

1. S. Black, in Composites World. (2012), vol. March 2012. http://www.carbonfiber.gr.jp/english/field/craft.html.
2. T. J. C. F. M. Association. http://www.compositesworld.com/articles/structural-health-monitoring-composites-get-smart
3. J. Y. Rho, L. Kuhn-Spearing, P. Zioupos, Mechanical properties and the hierarchical structure of bone. *Medical Engineering & Physics* **20**, 92-102 (Mar, 1998) 10.1016/s1350-4533(98)00007-1.
4. E. T. Thostenson, W. Z. Li, D. Z. Wang, Z. F. Ren, T. W. Chou, Carbon nanotube/carbon fiber hybrid multiscale composites. *J. Appl. Phys.* **91**, 6034-6037 (May 1, 2002) 10.1063/1.1466880.
5. E. Bekyarova *et al.*, Multiscale carbon nanotube-carbon fiber reinforcement for advanced epoxy composites. *Langmuir* **23**, 3970-3974 (Mar 27, 2007) 10.1021/la062743p.
6. H. Qian, E. S. Greenhalgh, M. S. P. Shaffer, A. Bismarck, Carbon nanotube-based hierarchical composites: a review. *Journal of Materials Chemistry* **20**, 4751-4762 (2010, 2010) 10.1039/c000041h.
7. H. Speckmann, Structural health monitoring: Composites get smart. *CompositesWorld*, (9/9/2008, 2008)
8. J. A. Nairn, in *Polymer Matrix Composites*. (Elsevier Science, Salt Lake City, Utah, USA, 2000), vol. 2.
9. J. A. N. a. S. Hu, Micromechanics of Damage: A Case Study of Matrix Microcracking. *Damage Mechanics of Composite Materials*, 187-243 (1994, 1994)
10. K. W. G. a. J. E. Bailey, Multiple Transverse Fracture in 90^{o} Cross-Ply Laminates of a Glass Fibre-Reinforced Polyester. *J. Mat. Sci* **12**, 157-168 (1977)
11. K. W. G. a. J. E. Bailey, The Efiect of Resin Failure Strain on the Tensile Properties of Glass Fiber-Reinforced Cross-Ply Laminates. *J. Mat. Sci.* **12**, 2189-2194 (1977)
12. K. W. G. A. Parvizi, and J. E. Bailey, Constrained Cracking in Glass Fiber-Reinforced Epoxy Cross-Ply Laminates. *J. Mat. Sci.* **13**, 195-201 (1978)
13. S. W. T. a. E. M. Wu, A General Theory of Strength for Anisotropic Materials. *J. Comp. Mater.*, 58-80 (1971)
14. M. C. Lafarie-Frenot, C. Henaff-Gardin, D. Gamby, Matrix cracking induced by cyclic ply stresses in composite laminates. *Compos. Sci. Technol.* **61**, 2327-2336 (2001, 2001) 10.1016/s0266-3538(01)00125-7.
15. M. Y. Kashtalyan, C. Soutis, Mechanisms of internal damage and their effect on the behavior and properties of cross-ply composite laminates.

International Applied Mechanics **38**, 641-657 (Jun, 2002) 10.1023/a:1020456726805.

16. J. K. Kim, C. Baillie, Y. W. Mai, INTERFACIAL DEBONDING AND FIBER PULL-OUT STRESSES .1. CRITICAL COMPARISON OF EXISTING THEORIES WITH EXPERIMENTS. *J. Mater. Sci.* **27**, 3143-3154 (Jun 15, 1992) 10.1007/bf01116004.

17. X. F. Zhou, J. A. Nairn, H. D. Wagner, Fiber-matrix adhesion from the single-fiber composite test: nucleation of interfacial debonding. *Compos. Pt. A-Appl. Sci. Manuf.* **30**, 1387-1400 (1999, 1999) 10.1016/s1359-835x(99)00043-3.

18. H. Zhang, M. L. Ericson, J. Varna, L. A. Berglund, Transverse single-fibre test for interfacial debonding in composites .1. Experimental observations. *Compos. Pt. A-Appl. Sci. Manuf.* **28**, 309-315 (1997, 1997) 10.1016/s1359-835x(96)00123-6.

19. B. W. Kim, J. A. Nairn, Observations of fiber fracture and interfacial debonding phenomena using the fragmentation test in single fiber composites. *J. Compos Mater.* **36**, 1825-1858 (2002, 2002) 10.1177/0021998302036015243.

20. L. T. Drzal, M. Madhukar, FIBER MATRIX ADHESION AND ITS RELATIONSHIP TO COMPOSITE MECHANICAL-PROPERTIES. *J. Mater. Sci.* **28**, 569-610 (Feb, 1993) 10.1007/bf01151234.

21. C. A. Wood, W. L. Bradley, Determination of the effect of seawater on the interfacial strength of an interlayer E-glass/graphite/epoxy composite by in situ observation of transverse cracking in an environmental SEM. *Compos. Sci. Technol.* **57**, 1033-1043 (1997, 1997) 10.1016/s0266-3538(96)00170-4.

22. D. Hull, T. W. Clyne, *An introduction to composite materials*. (Cambridge University Press, Cambridge, ed. 2nd ed., 1996), pp. xvi,326p.

23. N. Sela, O. Ishai, Interlaminar fracture-toughness and toughening of laminated composite-materials - a review. *Composites* **20**, 423-435 (Sep, 1989) 10.1016/0010-4361(89)90211-5.

24. J. K. Kim, M. L. Sham, Impact and delamination failure of woven-fabric composites. *Compos. Sci. Technol.* **60**, 745-761 (2000) 10.1016/s0266-3538(99)00166-9.

25. G. A. Bibo, P. J. Hogg, The role of reinforcement architecture on impact damage mechanisms and post-impact compression behaviour. *J. Mater. Sci.* **31**, 1115-1137 (Mar, 1996) 10.1007/bf00353091.

26. J. K. Kim, Methods for improving impact damage resistance of CFRPs. *Impact Response and Dynamic Failure of Composites and Laminate Materials, Pts 1 and 2* **141-1**, 149-168 (1998)

27. P. Davies, B. R. K. Blackman, A. J. Brunner, Standard test methods for delamination resistance of composite materials: Current status. *Appl. Compos. Mater.* **5**, 345-364 (Nov, 1998) 10.1023/a:1008869811626.

28. ISO. (the International Organization for Standardization, 2001).

29. A. D. 5528-01. (ASTM International, 2001), pp. 12.

30. N. Chikhi, S. Fellahi, M. Bakar, Modification of epoxy resin using reactive liquid (ATBN) rubber. *Eur. Polym. J.* **38**, 251-264 (Feb, 2002) 10.1016/s0014-3057(01)00194-x.

31. Z. N. Sanjana, L. Kupchella, DYNAMIC MECHANICAL ANALYSIS OF RUBBER TOUGHENED EPOXY-RESINS. *Polym. Eng. Sci.* **25**, 1148-1154 (Dec, 1985) 10.1002/pen.760251807.

32. A. J. Kinloch, S. J. Shaw, D. L. Hunston, Deformation and fracture-behavior of a rubber-toughened epoxy .2. failure criteria. *Polymer* **24**, 1355-1363 (1983, 1983) 10.1016/0032-3861(83)90071-x.

33. A. J. Kinloch, S. J. Shaw, D. A. Tod, D. L. Hunston, Deformation and fracture-behavior of a rubber-toughened epoxy .1. microstructure and fracture studies. *Polymer* **24**, 1341-1354 (1983, 1983) 10.1016/0032-3861(83)90070-8.

34. K. Yamanaka, Y. Takagi, T. Inoue, Reaction-induced phase-separation in rubber-modified epoxy-resins. *Polymer* **30**, 1839-1884 (Oct, 1989) 10.1016/0032-3861(89)90355-8.

35. R. A. Pearson, A. F. Yee, INFLUENCE OF PARTICLE-SIZE AND PARTICLE-SIZE DISTRIBUTION ON TOUGHENING MECHANISMS IN RUBBER-MODIFIED EPOXIES. *J. Mater. Sci.* **26**, 3828-3844 (Jul 15, 1991) 10.1007/bf01184979.

36. S. Kunzdouglass, P. W. R. Beaumont, M. F. Ashby, A MODEL FOR THE TOUGHNESS OF EPOXY-RUBBER PARTICULATE COMPOSITES. *J. Mater. Sci.* **15**, 1109-1123 (1980, 1980) 10.1007/bf00551799.

37. S. C. Kunz, J. A. Sayre, R. A. Assink, MORPHOLOGY AND TOUGHNESS CHARACTERIZATION OF EPOXY-RESINS MODIFIED WITH AMINE AND CARBOXYL TERMINATED RUBBERS. *Polymer* **23**, 1897-1906 (1982, 1982) 10.1016/0032-3861(82)90215-4.

38. R. Bagheri, R. A. Pearson, Role of particle cavitation in rubber-toughened epoxies .1. Microvoid toughening. *Polymer* **37**, 4529-4538 (Sep, 1996) 10.1016/0032-3861(96)00295-9.

39. J. Lee, A. F. Yee, Fracture of glass bead/epoxy composites: on micro-mechanical deformations. *Polymer* **41**, 8363-8373 (Nov, 2000) 10.1016/s0032-3861(00)00187-7.

40. J. Lee, A. F. Yee, Role of inherent matrix toughness on fracture of glass bead filled epoxies. *Polymer* **41**, 8375-8385 (Nov, 2000) 10.1016/s0032-3861(00)00186-5.

41. J. Lee, A. F. Yee, Inorganic particle toughening II: toughening mechanisms of glass bead filled epoxies. *Polymer* **42**, 589-597 (Jan, 2001) 10.1016/s0032-3861(00)00398-0.

42. J. Lee, A. F. Yee, Inorganic particle toughening I: micro-mechanical deformations in the fracture of glass bead filled epoxies. *Polymer* **42**, 577-588 (Jan, 2001) 10.1016/s0032-3861(00)00397-9.

43. S.-Y. Fu, X.-Q. Feng, B. Lauke, Y.-W. Mai, Effects of particle size, particle/matrix interface adhesion and particle loading on mechanical

properties of particulate-polymer composites. *Compos. Pt. B-Eng.* **39**, 933-961 (Sep, 2008) 10.1016/j.compositesb.2008.01.002.

44. R. A. Pearson, A. F. Yee, Toughening mechanisms in thermoplastic-modified epoxies .1. modification using poly(phenylene oxide). *Polymer* **34**, 3658-3670 (1993, 1993) 10.1016/0032-3861(93)90051-b.

45. J. L. Hedrick *et al.*, Chemical modification of matrix resin networks with engineering thermoplastics .1. synthesis, morphology, physical behavior and toughening mechanisms of poly(arylene ether sulfone) modified epoxy networks. *Polymer* **32**, 2020-2032 (1991, 1991) 10.1016/0032-3861(91)90168-i.

46. D. J. Hourston, J. M. Lane, N. A. Macbeath, TOUGHENING OF EPOXY-RESINS WITH THERMOPLASTICS .2. TETRAFUNCTIONAL EPOXY-RESIN POLYETHERIMIDE BLENDS. *Polymer International* **26**, 17-21 (1991, 1991) 10.1002/pi.4990260104.

47. D. J. Hourston, J. M. Lane, The toughening of epoxy-resins with thermoplastics .1. trifunctional epoxy-resin polyetherimide blends. *Polymer* **33**, 1379-1383 (1992, 1992) 10.1016/0032-3861(92)90110-i.

48. B. G. Min, Z. H. Stachurski, J. H. Hodgkin, MICROSTRUCTURAL EFFECTS AND THE TOUGHENING OF THERMOPLASTIC MODIFIED EPOXY-RESINS. *J. Appl. Polym. Sci.* **50**, 1511-1518 (Dec 5, 1993) 10.1002/app.1993.070500904.

49. D. J. Hourston, J. M. Lane, H. X. Zhang, Toughening of epoxy resins with thermoplastics .3. An investigation into the effects of composition on the properties of epoxy resin blends. *Polymer International* **42**, 349-355 (Apr, 1997) 10.1002/(sici)1097-0126(199704)42:4<349::aid-pi710>3.0.co;2-3.

50. J. H. Hodgkin, G. P. Simon, R. J. Varley, Thermoplastic toughening of epoxy resins: a critical review. *Polymers for Advanced Technologies* **9**, 3-10 (Jan, 1998)

51. H. Wu, J. Xu, Y. Liu, P. Heiden, Investigation of readily processable thermoplastic-toughened thermosets. V. Epoxy resin toughened with hyperbranched polyester. *J. Appl. Polym. Sci.* **72**, 151-163 (Apr 11, 1999) 10.1002/(sici)1097-4628(19990411)72:2<151::aid-app1>3.0.co;2-0.

52. G. Ragosta, M. Abbate, P. Musto, G. Scarinzi, L. Mascia, Epoxy-silica particulate nanocomposites: Chemical interactions, reinforcement and fracture toughness. *Polymer* **46**, 10506-10516 (Nov 14, 2005) 10.1016/j.polymer.2005.08.028.

53. P. Rosso, L. Ye, K. Friedrich, S. Sprenger, A toughened epoxy resin by silica nanoparticle reinforcement. *J. Appl. Polym. Sci.* **100**, 1849-1855 (May 5, 2006) 10.1002/app.22805.

54. B. Wetzel, P. Rosso, F. Haupert, K. Friedrich, Epoxy nanocomposites - fracture and toughening mechanisms. *Eng. Fract. Mech.* **73**, 2375-2398 (Nov, 2006) 10.1016/j.engfracmech.2006.05.018.

55. H. Zhang, Z. Zhang, K. Friedrich, C. Eger, Property improvements of in situ epoxy nanocomposites with reduced interparticle distance at high nanosilica

content. *Acta Materialia* **54**, 1833-1842 (Apr, 2006) 10.1016/j.actamat.2005.12.009.

56. B. B. Johnsen, A. J. Kinloch, R. D. Mohammed, A. C. Taylor, S. Sprenger, Toughening mechanisms of nanoparticle-modified epoxy polymers. *Polymer* **48**, 530-541 (Jan 12, 2007) 10.1016/j.polymer.2006.11.038.

57. C. Chen, R. S. Justice, D. W. Schaefer, J. W. Baur, Highly dispersed nanosilica-epoxy resins with enhanced mechanical properties. *Polymer* **49**, 3805-3815 (Aug 11, 2008) 10.1016/j.polymer.2008.06.023.

58. T. H. Hsieh *et al.*, The toughness of epoxy polymers and fibre composites modified with rubber microparticles and silica nanoparticles. *J. Mater. Sci.* **45**, 1193-1210 (Mar, 2010) 10.1007/s10853-009-4064-9.

59. S. C. Tjong, Structural and mechanical properties of polymer nanocomposites. *Materials Science & Engineering R-Reports* **53**, 73-197 (Aug 30, 2006) 10.1016/j.mser.2006.06.001.

60. B. Fiedler, F. H. Gojny, M. H. G. Wichmann, M. C. M. Nolte, K. Schulte, Fundamental aspects of nano-reinforced composites. *Compos. Sci. Technol.* **66**, 3115-3125 (Dec, 2006) 10.1016/j.compscitech.2005.01.014.

61. R. F. Gibson, A review of recent research on mechanics of multifunctional composite materials and structures. *Compos. Struct.* **92**, 2793-2810 (Nov, 2010) 10.1016/j.compstruct.2010.05.003.

62. W. G. Perkins, Polymer toughness and impact resistance. *Polym. Eng. Sci.* **39**, 2445-2460 (Dec, 1999) 10.1002/pen.11632.

63. R. Thomas *et al.*, Miscibility, morphology, thermal, and mechanical properties of a DGEBA based epoxy resin toughened with a liquid rubber. *Polymer* **49**, 278-294 (Jan 10, 2008) 10.1016/j.polymer.2007.11.030.

64. C. Yan, K. Q. Xiao, L. Ye, Y. W. Mai, Numerical and experimental studies on the fracture behavior of rubber-toughened epoxy in bulk specimen and laminated composites. *J. Mater. Sci.* **37**, 921-927 (Mar 1, 2002) 10.1023/a:1014335511515.

65. M. Todo, P. Jar, Study of mode-I interlaminar crack growth in DCB specimens of fibre-reinforced composites. *Compos. Sci. Technol.* **58**, 105-118 (1998) 10.1016/s0266-3538(97)00102-4.

66. A. J. Kinloch, M. L. Yuen, S. D. Jenkins, Thermoplastic-toughened epoxy polymers. *J. Mater. Sci.* **29**, 3781-3790 (Jul, 1994) 10.1007/bf00357349.

67. A. J. Mackinnon, S. D. Jenkins, P. T. McGrail, R. A. Pethrick, A dielectric, mechanical, rheological, and electron-microscopy study of cure and properties of a thermoplastic-modified epoxy-resin. *Macromolecules* **25**, 3492-3499 (Jun 22, 1992) 10.1021/ma00039a029.

68. R. A. Pethrick *et al.*, Dielectric, mechanical and structural, and water absorption properties of a thermoplastic-modified epoxy resin: Poly(ether sulfone)-amine cured epoxy resin. *Macromolecules* **29**, 5208-5214 (Jul 15, 1996) 10.1021/ma9518464.

69. G. DiPasquale *et al.*, New high-performance thermoplastic toughened epoxy thermosets. *Polymer* **38**, 4345-4348 (Aug, 1997) 10.1016/s0032-3861(96)01031-2.

70. P. Huang, S. X. Zheng, J. Y. Huang, Q. P. Guo, W. Zhu, Miscibility and mechanical properties of epoxy resin polysulfone blends. *Polymer* **38**, 5565-5571 (Oct, 1997) 10.1016/s0032-3861(97)00104-3.

71. R. W. Venderbosch, T. Peijs, H. E. H. Meijer, P. J. Lemstra, Fibre-reinforced composites with tailored interphases using PPE/epoxy blends as a matrix system. *Compos. Pt. A-Appl. Sci. Manuf.* **27**, 895-905 (1996, 1996) 10.1016/1359-835x(96)00043-7.

72. A. Saalbrink, A. Lorteije, T. Peijs, The influence of processing parameters on interphase morphology in polymer composites based on phase-separating thermoplast/epoxy blends. *Compos. Pt. A-Appl. Sci. Manuf.* **29**, 1243-1250 (1998) 10.1016/s1359-835x(98)00043-8.

73. K. C. Teng, F. C. Chang, Single-phase and multiple-phase thermoplastic/thermoset polyblends .2. Morphologies and mechanical properties of phenoxy/epoxy blends. *Polymer* **37**, 2385-2394 (Jun, 1996) 10.1016/0032-3861(96)85350-x.

74. E. M. Woo, K. L. Mao, Interlaminar morphology effects on fracture resistance of amorphous polymer-modified epoxy/carbon fibre composites. *Compos. Pt. A-Appl. Sci. Manuf.* **27**, 625-631 (1996, 1996) 10.1016/1359-835x(96)00028-0.

75. S. K. Siddhamalli, T. Kyu, Toughening of thermoset/thermoplastic composites via reaction-induced phase separation: Epoxy/phenoxy blends. *J. Appl. Polym. Sci.* **77**, 1257-1268 (Aug 8, 2000) 10.1002/1097-4628(20000808)77:6<1257::aid-app10>3.0.co;2-z.

76. D. W. Y. Wong, L. Lin, P. T. McGrail, T. Peijs, P. J. Hogg, Improved fracture toughness of carbon fibre/epoxy composite laminates using dissolvable thermoplastic fibres. *Compos. Pt. A-Appl. Sci. Manuf.* **41**, 759-767 (Jun, 2010) 10.1016/j.compositesa.2010.02.008.

77. J. C. Hedrick, N. M. Patel, J. E. McGrath, Toughening of epoxy-resin networks with functionalized engineering thermoplastics. *Advances in Chemistry Series*, 293-304 (1993, 1993)

78. C. B. Bucknall, I. K. Partridge, Phase-separation in epoxy-resins containing polyethersulfone. *Polymer* **24**, 639-644 (1983) 10.1016/0032-3861(83)90120-9.

79. B. J. Cardwell, A. F. Yee, Toughening of epoxies through thermoplastic crack bridging. *J. Mater. Sci.* **33**, 5473-5484 (Nov 15, 1998) 10.1023/a:1004427123388.

80. H. Kishi, K. Uesawa, S. Matsuda, A. Murakami, Adhesive strength and mechanisms of epoxy resins toughened with pre-formed thermoplastic polymer particles. *Journal of Adhesion Science and Technology* **19**, 1277-1290 (2005, 2005) 10.1163/156856105774784402.

81. C. B. Bucknall, A. H. Gilbert, Toughening tetrafunctional epoxy-resins using polyetherimide. *Polymer* **30**, 213-217 (Feb, 1989) 10.1016/0032-3861(89)90107-9.

82. J. L. Hedrick, M. J. Jurek, I. Yilgor, J. E. McGrath, Chemical modification of matrix resin networks with engineering thermoplastics .3. synthesis and properties of epoxy networks modified with amine terminated poly(aryl ether sulfone) oligomers. *Abstracts of Papers of the American Chemical Society* **190**, 106-POY (1985, 1985)

83. S. Iijima, Helical microtubules of graphitic carbon. *Nature* **354**, 56-58 (Nov 7, 1991) 10.1038/354056a0.

84. C. Y. Li, T. W. Chou, A structural mechanics approach for the analysis of carbon nanotubes. *Int. J. Solids Struct.* **40**, 2487-2499 (May, 2003) 10.1016/s0020-7683(03)00056-8.

85. C. Y. Li, T. W. Chou, Elastic moduli of multi-walled carbon nanotubes and the effect of van der Waals forces. *Compos. Sci. Technol.* **63**, 1517-1524 (Aug, 2003) 10.1016/s0266-3538(03)00072-1.

86. E. Hernandez, C. Goze, P. Bernier, A. Rubio, Elastic properties of C and BxCyNz composite nanotubes. *Physical Review Letters* **80**, 4502-4505 (May 18, 1998) 10.1103/PhysRevLett.80.4502.

87. E. W. Wong, P. E. Sheehan, C. M. Lieber, Nanobeam mechanics: Elasticity, strength, and toughness of nanorods and nanotubes. *Science* **277**, 1971-1975 (Sep 26, 1997) 10.1126/science.277.5334.1971.

88. S. J. Tans *et al.*, Individual single-wall carbon nanotubes as quantum wires. *Nature* **386**, 474-477 (Apr 3, 1997) 10.1038/386474a0.

89. R. H. Baughman, A. A. Zakhidov, W. A. de Heer, Carbon nanotubes - the route toward applications. *Science* **297**, 787-792 (Aug 2, 2002) 10.1126/science.1060928.

90. M. Moniruzzaman, K. I. Winey, Polymer nanocomposites containing carbon nanotubes. *Macromolecules* **39**, 5194-5205 (Aug 8, 2006) 10.1021/ma060733p.

91. O. Becker, R. Varley, G. Simon, Morphology, thermal relaxations and mechanical properties of layered silicate nanocomposites based upon high-functionality epoxy resins. *Polymer* **43**, 4365-4373 (Jul, 2002) Pii s0032-3861(02)00269-010.1016/s0032-3861(02)00269-0.

92. D. Ratna, O. Becker, R. Krishnamurthy, G. P. Simon, R. J. Varley, Nanocomposites based on a combination of epoxy resin, hyperbranched epoxy and a layered silicate. *Polymer* **44**, 7449-7457 (Nov, 2003) 10.1016/j.polmer.2003.08.035.

93. L. Le Pluart, J. Duchet, H. Sautereau, Epoxy/montmorillonite nanocomposites: influence of organophilic treatment on reactivity, morphology and fracture properties. *Polymer* **46**, 12267-12278 (Dec 12, 2005) 10.1016/j.polymer.2005.10.089.

94. K. Wang *et al.*, Epoxy nanocomposites with highly exfoliated clay: Mechanical properties and fracture mechanisms. *Macromolecules* **38**, 788-800 (Feb 8, 2005) 10.1021/ma048465n.

95. S. Deng, J. Zhang, L. Ye, J. Wu, Toughening epoxies with halloysite nanotubes. *Polymer* **49**, 5119-5127 (Oct 30, 2008) 10.1016/j.polymer.2008.09.027.

96. T. H. Hsieh, A. J. Kinloch, K. Masania, A. C. Taylor, S. Sprenger, The mechanisms and mechanics of the toughening of epoxy polymers modified with silica nanoparticles. *Polymer* **51**, 6284-6294 (Dec 10, 2010) 10.1016/j.polymer.2010.10.048.

97. S. Zhao, L. S. Schadler, R. Duncan, H. Hillborg, T. Auletta, Mechanisms leading to improved mechanical performance in nanoscale alumina filled epoxy. *Compos. Sci. Technol.* **68**, 2965-2975 (Nov, 2008) 10.1016/j.compscitech.2008.01.009.

98. A. Haque, M. Shamsuzzoha, F. Hussain, D. Dean, S2-glass/epoxy polymer nanocomposites: Manufacturing, structures, thermal and mechanical properties. *J. Compos Mater.* **37**, 1821-1837 (2003, 2003) 10.1177/0021998303035186.

99. F. H. Gojny, M. H. G. Wichmann, B. Fiedler, W. Bauhofer, K. Schulte, Influence of nano-modification on the mechanical and electrical properties of conventional fibre-reinforced composites. *Compos. Pt. A-Appl. Sci. Manuf.* **36**, 1525-1535 (2005, 2005) 10.1016/j.compositesa.2005.02.007.

100. Y. X. Zhou, F. Pervin, S. Jeelani, P. K. Mallick, Improvement in mechanical properties of carbon fabric-epoxy composite using carbon nanofibers. *J. Mater. Process. Technol.* **198**, 445-453 (Mar, 2008) 10.1016/j.jmatprotec.2007.07.028.

101. F. P. Inam, Ton, Re-agglomeration of carbon nanotubes in two-component epoxy system. *Journal of Nanostructured Polymers and Nanocomposites* **2**, 9 (2006)

102. S. Singh, I. K. Partridge, Mixed-mode fracture in an interleaved carbon-fibre epoxy composite. *Compos. Sci. Technol.* **55**, 319-327 (1995, 1995) 10.1016/0266-3538(95)00062-3.

103. A. Aksoy, L. A. Carlsson, Interlaminar shear fracture of interleaved graphite epoxy composites. *Compos. Sci. Technol.* **43**, 55-69 (1992, 1992) 10.1016/0266-3538(92)90133-n.

104. M. Hojo *et al.*, Modes I and II interlaminar fracture toughness and fatigue delamination of CF/epoxy laminates with self-same epoxy interleaf. *International Journal of Fatigue* **28**, 1154-1165 (Oct, 2006) 10.1016/j.ijfatigue.2006.02.004.

105. F. Ozdil, L. A. Carlsson, MODE-I INTERLAMINAR FRACTURE OF INTERLEAVED GRAPHITE EPOXY. *J. Compos Mater.* **26**, 432-459 (1992, 1992) 10.1177/002199839202600306.

106. F. Gao, G. Jiao, Z. Lu, R. Ning, Mode II delamination and damage resistance of carbon/epoxy composite laminates interleaved with thermoplastic particles. *J. Compos Mater.* **41**, 111-123 (Jan, 2007) 10.1177/0021998306063356.

107. S. N. Yadav, V. Kumar, S. K. Verma, Fracture toughness behaviour of carbon fibre epoxy composite with Kevlar reinforced interleave. *Materials Science and Engineering B-Solid State Materials for Advanced Technology* **132**, 108-112 (Jul 25, 2006) 10.1016/j.mseb.2006.02.026.

108. S. S. Wicks, R. G. de Villoria, B. L. Wardle, Interlaminar and intralaminar reinforcement of composite laminates with aligned carbon nanotubes. *Compos. Sci. Technol.* **70**, 20-28 (Jan, 2010) 10.1016/j.compscitech.2009.09.001.

109. E. J. Garcia, B. L. Wardle, A. J. Hart, N. Yamamoto, Fabrication and multifunctional properties of a hybrid laminate with aligned carbon nanotubes grown In Situ. *Composites Science and Technology* **68**, 2034-2041 (Jul, 2008) 10.1016/j.compscitech.2008.02.028.

110. R. a. H. Evans, K. (American Cyanamid Company). (United States 1986), vol. Patent No. 4,604,319.

111. R. F. Gibson, Y. Chen, H. Zhao, Improvement of vibration damping capacity and fracture toughness in composite laminates by the use of polymeric interleaves. *J. Eng. Mater. Technol.-Trans. ASME* **123**, 309-314 (Jul, 2001) 10.1115/1.1370385.

112. R. Fracasso, M. Rink, A. Pavan, R. Frassine, The effects of strain-rate and temperature on the interlaminar fracture toughness of interleaved PEEK/CF composites. *Compos. Sci. Technol.* **61**, 57-63 (2001, 2001) 10.1016/s0266-3538(00)00153-6.

113. M. Yasaee, I. P. Bond, R. S. Trask, E. S. Greenhalgh, Mode I interfacial toughening through discontinuous interleaves for damage suppression and control. *Compos. Pt. A-Appl. Sci. Manuf.* **43**, 198-207 (Jan, 2012) 10.1016/j.compositesa.2011.10.009.

114. N. G. Yun, Y. G. Won, S. C. Kim, Toughening of carbon fiber/epoxy composite by inserting polysulfone film to form morphology spectrum. *Polymer* **45**, 6953-6958 (Sep 16, 2004) 10.1016/j.polymer.2004.08.020.

115. U. Beier *et al.*, Mechanical performance of carbon fibre-reinforced composites based on preforms stitched with innovative low-melting temperature and matrix soluble thermoplastic yarns. *Compos. Pt. A-Appl. Sci. Manuf.* **39**, 1572-1581 (Sep, 2008) 10.1016/j.compositesa.2008.06.003.

116. S. Sihn, R. Y. Kim, W. Huh, K.-H. Lee, A. K. Roy, Improvement of damage resistance in laminated composites with electrospun nano-interlayers. *Compos. Sci. Technol.* **68**, 673-683 (Mar, 2008) 10.1016/j.compscitech.2007.09.015.

117. K. Magniez, T. Chaffraix, B. Fox, Toughening of a Carbon-Fibre Composite Using Electrospun Poly(Hydroxyether of Bisphenol A) Nanofibrous Membranes Through Inverse Phase Separation and Inter-Domain Etherification. *Materials* **4**, 1967-1984 (Nov, 2011) 10.3390/ma4111967.

118. G. Pena *et al.*, Control of morphologies and mechanical properties of thermoplastic-modified epoxy matrices by addition of a second thermoplastic. *Polymer International* **52**, 1444-1453 (Sep, 2003) 10.1002/pi.1209.

119. L. Li, P. LeeSullivan, K. M. Liew, The influence of thermoplastic film interleaving on the interlaminar shear strength and mode I fracture of laminated composites. *J. Eng. Mater. Technol.-Trans. ASME* **118**, 302-309 (Jul, 1996) 10.1115/1.2806810.

120. Y. Dzenis, and D. Reneker. (U.S., 2001), vol. 6,265,333.

121. J. Zhang, T. Lin, X. Wang, Electrospun nanofibre toughened carbon/epoxy composites: Effects of polyetherketone cardo (PEK-C) nanofibre diameter and interlayer thickness. *Compos. Sci. Technol.* **70**, 1660-1666 (Oct 15, 2010) 10.1016/j.compscitech.2010.06.019.

122. M. Kuwata, P. J. Hogg, Interlaminar toughness of interleaved CFRP using non-woven veils: Part 1. Mode-I testing. *Compos. Pt. A-Appl. Sci. Manuf.* **42**, 1551-1559 (Oct, 2011) 10.1016/j.compositesa.2011.07.016.

123. M. Kuwata, P. J. Hogg, Inter laminar toughness of interleaved CFRP using non-woven veils: Part 2. Mode-II testing. *Compos. Pt. A-Appl. Sci. Manuf.* **42**, 1560-1570 (Oct, 2011) 10.1016/j.compositesa.2011.07.017.

124. R. Palazzetti *et al.*, Influence of electrospun Nylon 6,6 nanofibrous mats on the interlaminar properties of Gr-epoxy composite laminates. *Compos. Struct.* **94**, 571-579 (Jan, 2012) 10.1016/j.compstruct.2011.08.019.

125. S. H. Lee, H. Noguchi, Y. B. Kim, S. K. Cheong, Effect of interleaved non-woven carbon tissue on interlaminar fracture toughness of laminated composites: Part I - Mode II. *J. Compos Mater.* **36**, 2153-2168 (2002, 2002) 10.1106/002199802026981.

126. S. H. Lee, H. Noguchi, S. K. Cheong, Tensile properties and fatigue characteristics of hybrid composites with non-woven carbon tissue. *International Journal of Fatigue* **24**, 397-405 (Feb-Apr, 2002) Pii s0142-1123(01)00095-010.1016/s0142-1123(01)00095-0.

127. S. H. Lee, H. Noguchi, Y. B. Kim, S. K. Cheong, Effect of interleaved non-woven carbon tissue on interlaminar fracture toughness of laminated composites: Part II - Mode I. *J. Compos Mater.* **36**, 2169-2181 (2002, 2002) 10.1106/002199802026980.

128. V. P. Veedu *et al.*, Multifunctional composites using reinforced laminae with carbon-nanotube forests. *Nat. Mater.* **5**, 457-462 (Jun, 2006) 10.1038/nmat1650.

129. M. Arai, Y. Noro, K. I. Sugimoto, M. Endo, Mode I and mode II interlaminar fracture toughness of CFRP laminates toughened by carbon nanofiber interlayer. *Compos. Sci. Technol.* **68**, 516-525 (Feb, 2008) 10.1016/j.compscitech.2007.06.007.

130. Q. An, A. N. Rider, E. T. Thostenson, Electrophoretic deposition of carbon nanotubes onto carbon-fiber fabric for production of carbon/epoxy composites with improved mechanical properties. *Carbon* **50**, 4130-4143 (Sep, 2012) 10.1016/j.carbon.2012.04.061.

131. Q. An, A. N. Rider, E. T. Thostenson, Hierarchical Composite Structures Prepared by Electrophoretic Deposition of Carbon Nanotubes onto Glass Fibers. *ACS Appl. Mater. Interfaces* **5**, 2022-2032 (Mar 27, 2013) 10.1021/am3028734.

132. S. Hamer *et al.*, Mode I and Mode II fracture energy of MWCNT reinforced nanofibrilmats interleaved carbon/epoxy laminates. *Compos. Sci. Technol.* **90**, 48-56 (Jan, 2014) 10.1016/j.compscitech.2013.10.013.

133. K. L. White, H.-J. Sue, Delamination toughness of fiber-reinforced composites containing a carbon nanotube/polyamide-12 epoxy thin film interlayer. *Polymer* **53**, 37-42 (Jan 5, 2012) 10.1016/j.polymer.2011.11.022.

134. A. J. S. Russell, K.N., FACTORS AFFECTING THE INTERLAMINAR FRACTURE ENERGY OF GRAPHITE/EPOXY LAMINATES. *Proc. ICCM-IV, Progress in Science and Engineering of Composites, Tokyo*, 8 (1982)

135. W. D. Bascom, J. L. Bitner, R. J. Moulton, A. R. Siebert, INTERLAMINAR FRACTURE OF ORGANIC-MATRIX, WOVEN REINFORCEMENT COMPOSITES. *Composites* **11**, 9-18 (1980, 1980) 10.1016/0010-4361(80)90016-6.

136. J. G. F. J. W. Deaton, The interlaminar fracture toughness of graphite/epoxy composites. *NASA Technical peper 2950*, (1989)

137. J. G. S. Funk, G. F., The effects of radiation on the interlaminar fracture toughness of a graphite/epoxy composite. *Journal of Composites Technology and Research* **8**, 92-97 (1986)

138. B. Schrauwen, T. Peijs, Influence of matrix ductility and fibre architecture on the repeated impact response of glass-fibre-reinforced laminated composites. *Appl. Compos. Mater.* **9**, 331-352 (Nov, 2002) 10.1023/a:1020267013414.

139. T. Ebeling, A. Hiltner, E. Baer, I. M. Fraser, M. L. Orton, Delamination failure of a woven glass fiber composite. *J. Compos Mater.* **31**, 1318-1333 (1997, 1997)

140. T. Ebeling, A. Hiltner, E. Baer, I. M. Fraser, M. L. Orton, Delamination failure of a single yarn glass fiber composite. *J. Compos Mater.* **31**, 1302-1317 (1997, 1997)

141. S. L. Bazhenov, STRONG BENDING IN THE DCB INTERLAMINAR TEST OF THIN, E-GLASS WOVEN-FABRIC-REINFORCED LAMINATES. *Composites* **22**, 275-280 (Jul, 1991) 10.1016/0010-4361(91)90002-x.

142. B. J. Briscoe, R. S. Court, D. R. Williams, THE EFFECTS OF FABRIC WEAVE AND SURFACE TEXTURE ON THE INTERLAMINAR FRACTURE-TOUGHNESS OF ARAMID EPOXY LAMINATES. *Compos. Sci. Technol.* **47**, 261-270 (1993, 1993) 10.1016/0266-3538(93)90035-f.

143. A. P. Mouritz, K. H. Leong, I. Herszberg, A review of the effect of stitching on the in-plane mechanical properties of fibre-reinforced polymer composites. *Compos. Pt. A-Appl. Sci. Manuf.* **28**, 979-991 (1997, 1997) 10.1016/s1359-835x(97)00057-2.

144. K. Dransfield, C. Baillie, Y. W. Mai, IMPROVING THE DELAMINATION RESISTANCE OF CFRP BY STITCHING - A REVIEW. *Compos. Sci. Technol.* **50**, 305-317 (1994) 10.1016/0266-3538(94)90019-1.

145. M. Kupke, K. Schulte, R. Schuler, Non-destructive testing of FRP by d.c. and a.c. electrical methods. *Compos. Sci. Technol.* **61**, 837-847 (2001, 2001) 10.1016/s0266-3538(00)00180-9.

146. R. Schueler, S. P. Joshi, K. Schulte, Damage detection in CFRP by electrical conductivity mapping. *Compos. Sci. Technol.* **61**, 921-930 (2001) 10.1016/s0266-3538(00)00178-0.

147. A. S. E2533. (ASTM International, West Conshohocken, PA, 2009).

148. B. Fiedler, F. H. Gojny, M. H. G. Wichmann, W. Bauhofer, K. Schulte, Can carbon nanotubes be used to sense damage in composites? *Ann. Chim.-Sci. Mat.* **29**, 81-94 (Nov-Dec, 2004) 10.3166/acsm.29.6.81-94.

149. T. W. Ebbesen *et al.*, Electrical conductivity of individual carbon nanotubes. *Nature* **382**, 54-56 (Jul, 1996) 10.1038/382054a0.

150. M. M. J. Treacy, T. W. Ebbesen, J. M. Gibson, Exceptionally high Young's modulus observed for individual carbon nanotubes. *Nature* **381**, 678-680 (Jun, 1996) 10.1038/381678a0.

151. S. Iijima, T. Ichihashi, Single-shell carbon nanotubes of 1-nm diameter. *Nature* **363**, 603-605 (Jun 17, 1993) 10.1038/363603a0.

152. S. Iijima, C. Brabec, A. Maiti, J. Bernholc, Structural flexibility of carbon nanotubes. *Journal of Chemical Physics* **104**, 2089-2092 (Feb 1, 1996) 10.1063/1.470966.

153. E. T. Thostenson, Z. F. Ren, T. W. Chou, Advances in the science and technology of carbon nanotubes and their composites: a review. *Compos. Sci. Technol.* **61**, 1899-1912 (2001) 10.1016/s0266-3538(01)00094-x.

154. J. M. Park, D. S. Kim, J. R. Lee, T. W. Kim, Nondestructive damage sensitivity and reinforcing effect of carbon nanotube/epoxy composites using electro-micromechanical technique. *Mater. Sci. Eng. C-Biomimetic Supramol. Syst.* **23**, 971-975 (Dec 15, 2003) 10.1016/j.msec.2003.09.131.

155. J.-M. Park *et al.*, Inherent sensing and interfacial evaluation of carbon nanofiber and nanotube/epoxy composites using electrical resistance measurement and micromechanical technique. *Compos. Pt. B-Eng.* **38**, 847-861 (2007, 2007) 10.1016/j.compositesb.2006.12.004.

156. E. Bilotti *et al.*, Controlling the dynamic percolation of carbon nanotube based conductive polymer composites by addition of secondary nanofillers: The effect on electrical conductivity and tuneable sensing behaviour. *Compos. Sci. Technol.* **74**, 85-90 (Jan, 2013) 10.1016/j.compscitech.2012.10.008.

157. E. Bilotti, R. Zhang, H. Deng, M. Baxendale, T. Peijs, Fabrication and property prediction of conductive and strain sensing TPU/CNT nanocomposite fibres. *Journal of Materials Chemistry* **20**, 9449-9455 (2010, 2010) 10.1039/c0jm01827a.

158. R. Zhang *et al.*, Strain sensing behaviour of elastomeric composite films containing carbon nanotubes under cyclic loading. *Compos. Sci. Technol.* **74**, 1-5 (Jan, 2013) 10.1016/j.compscitech.2012.09.016.

159. H. Zhang, E. Bilotti, W. Tu, C. Y. Lew, T. Peijs, Static and dynamic percolation of phenoxy/carbon nanotube nanocomposites. *Eur. Polym. J.* **68**, 128-138 (2015) http://dx.doi.org/10.1016/j.eurpolymj.2015.04.022.

160. J.-M. Park *et al.*, Self-sensing and dispersive evaluation of single carbon fiber/carbon nanotube (CNT)-epoxy composites using electro-micromechanical technique and nondestructive acoustic emission. *Compos. Pt. B-Eng.* **39**, 1170-1182 (Oct-Dec, 2008) 10.1016/j.compositesb.2008.03.004.

161. J. Zhang *et al.*, Functional interphases with multi-walled carbon nanotubes in glass fibre/epoxy composites. *Carbon* **48**, 2273-2281 (Jul, 2010) 10.1016/j.carbon.2010.03.001.

162. S.-l. Gao, R.-C. Zhuang, J. Zhang, J.-W. Liu, E. Maeder, Glass Fibers with Carbon Nanotube Networks as Multifunctional Sensors. *Adv. Funct. Mater.* **20**, 1885-1893 (Jun 23, 2010) 10.1002/adfm.201000283.

163. J. Rausch, E. Mader, Health monitoring in continuous glass fibre reinforced thermoplastics: Manufacturing and application of interphase sensors based on carbon nanotubes. *Composites Science and Technology* **70**, 1589-1596 (Oct, 2010) 10.1016/j.compscitech.2010.05.018.

164. J. Rausch, E. Mader, Health monitoring in continuous glass fibre reinforced thermoplastics: Tailored sensitivity and cyclic loading of CNT-based interphase sensors. *Composites Science and Technology* **70**, 2023-2030 (Nov, 2010) 10.1016/j.compscitech.2010.08.003.

165. J. R. Wood *et al.*, Mechanical response of carbon nanotubes under molecular and macroscopic pressures. *Journal of Physical Chemistry B* **103**, 10388-10392 (Nov 25, 1999) 10.1021/jp992136t.

166. J. R. Wood *et al.*, Carbon nanotubes: From molecular to macroscopic sensors. *Phys. Rev. B* **62**, 7571-7575 (Sep 15, 2000) 10.1103/PhysRevB.62.7571.

167. E. T. Thostenson, T.-W. Chou, Carbon nanotube-based health monitoring of mechanically fastened composite joints. *Compos. Sci. Technol.* **68**, 2557-2561 (Sep, 2008) 10.1016/j.compscitech.2008.05.016.

168. V. Kostopoulos, A. Vavouliotis, P. Karapappas, P. Tsotra, A. Paipetis, Damage Monitoring of Carbon Fiber Reinforced Laminates Using Resistance Measurements. Improving Sensitivity Using Carbon Nanotube Doped Epoxy Matrix System. *Journal of Intelligent Material Systems and Structures* **20**, 1025-1034 (Jun, 2009) 10.1177/1045389x08099993.

169. L. M. Gao, T. W. Chou, E. T. Thostenson, Z. G. Zhang, M. Coulaud, In situ sensing of impact damage in epoxy/glass fiber composites using percolating carbon nanotube networks. *Carbon* **49**, 3382-3385 (Aug, 2011) 10.1016/j.carbon.2011.04.003.

170. L. M. Gao, E. T. Thostenson, Z. Zhang, T. W. Chou, Sensing of Damage Mechanisms in Fiber-Reinforced Composites under Cyclic Loading using Carbon Nanotubes. *Adv. Funct. Mater.* **19**, 123-130 (Jan, 2009) 10.1002/adfm.200800865.

171. E. T. Thostenson, T.-W. Chou, Carbon nanotube networks: Sensing of distributed strain and damage for life prediction and self healing. *Adv. Mater.* **18**, 2837-+ (Nov 3, 2006) 10.1002/adma.200600977.

172. L. Boeger, M. H. G. Wichmann, L. O. Meyer, K. Schulte, Load and health monitoring in glass fibre reinforced composites with an electrically conductive nanocomposite epoxy matrix. *Compos. Sci. Technol.* **68**, 1886-1894 (Jun, 2008) 10.1016/j.compscitech.2008.01.001.

173. L. Boeger, J. Sumfleth, H. Hedemann, K. Schulte, Improvement of fatigue life by incorporation of nanoparticles in glass fibre reinforced epoxy. *Compos. Pt. A-Appl. Sci. Manuf.* **41**, 1419-1424 (Oct, 2010) 10.1016/j.compositesa.2010.06.002.

174. G. Pandey, M. Wolters, E. T. Thostenson, D. Heider, Localized functionally modified glass fibers with carbon nanotube networks for crack sensing in composites using time domain reflectometry. *Carbon* **50**, 3816-3825 (Aug, 2012) 10.1016/j.carbon.2012.04.008.

175. K. J. Kim *et al.*, Damage characterization of 3D braided composites using carbon nanotube-based in situ sensing. *Compos. Pt. A-Appl. Sci. Manuf.* **41**, 1531-1537 (Oct, 2010) 10.1016/j.compositesa.2010.06.016.

176. A. S. Wu *et al.*, Sensing of damage and healing in three-dimensional braided composites with vascular channels. *Compos. Sci. Technol.* **72**, 1618-1626 (Aug, 2012) 10.1016/j.compscitech.2012.06.012.

177. Y. Song *et al.*, Carbon nanotube sensor thread for distributed strain and damage monitoring on IM7/977-3 composites. *Smart Materials and Structures* **23**, (Jul, 2014) 07500810.1088/0964-1726/23/7/075008.

178. Z. Zhang, H. Wei, Y. Liu, J. Leng, Self-sensing properties of smart composite based on embedded buckypaper layer. *Structural Health Monitoring-an International Journal* **14**, 127-136 (Mar, 2015) 10.1177/1475921714568405.

179. A. Hehr, M. Schulz, V. Shanov, Y. Song, Micro-crack detection and assessment with embedded carbon nanotube thread in composite materials. *Structural Health Monitoring-an International Journal* **13**, 512-524 (Sep, 2014) 10.1177/1475921714532987.

180. S. D. Luo, W. Obitayo, T. Liu, SWCNT-thin-film-enabled fiber sensors for lifelong structural health monitoring of polymeric composites - From manufacturing to utilization to failure. *Carbon* **76**, 321-329 (Sep, 2014) 10.1016/j.carbon.2014.04.083.

181. W. K. Li, D. L. He, Z. M. Dang, J. B. Bai, In situ damage sensing in the glass fabric reinforced epoxy composites containing CNT-Al2O3 hybrids. *Compos. Sci. Technol.* **99**, 8-14 (Jul, 2014) 10.1016/j.compscitech.2014.05.005.

182. J. Sebastian *et al.*, Health monitoring of structural composites with embedded carbon nanotube coated glass fiber sensors. *Carbon* **66**, 191-200 (Jan, 2014) 10.1016/j.carbon.2013.08.058.

183. L. Gao, E. T. Thostenson, Z. Zhang, T.-W. Chou, Coupled carbon nanotube network and acoustic emission monitoring for sensing of damage

development in composites. *Carbon* **47**, 1381-1388 (Apr, 2009) 10.1016/j.carbon.2009.01.030.

184. L. Gao, T.-W. Chou, E. T. Thostenson, Z. Zhang, A comparative study of damage sensing in fiber composites using uniformly and non-uniformly dispersed carbon nanotubes. *Carbon* **48**, 3788-3794 (Nov, 2010) 10.1016/j.carbon.2010.06.041.

185. E. T. Thostenson, T.-W. Chou, Real-time in situ sensing of damage evolution in advanced fiber composites using carbon nanotube networks. *Nanotechnology* **19**, (May 28, 2008) 21571310.1088/0957-4484/19/21/215713.

186. L. Gao, T.-W. Chou, E. T. Thostenson, Z. Zhang, M. Coulaud, In situ sensing of impact damage in epoxy/glass fiber composites using percolating carbon nanotube networks. *Carbon* **49**, 3382-3385 (Aug, 2011) 10.1016/j.carbon.2011.04.003.

187. S. Yesil, C. Winkelrnann, G. Bayram, V. La Saponara, Surfactant-modified multiscale composites for improved tensile fatigue and impact damage sensing. *Materials Science and Engineering a-Structural Materials Properties Microstructure and Processing* **527**, 7340-7352 (Oct 25, 2010) 10.1016/j.msea.2010.07.105.

188. H. Zhang, Y. Liu, M. Kuwata, E. Bilotti, T. Peijs, Improved fracture toughness and integrated damage sensing capability by spray coated CNTs on carbon fibre prepreg. *Compos. Pt. A-Appl. Sci. Manuf.* **70**, 102-110 (Mar, 2015) 10.1016/j.compositesa.2014.11.029.

189. L. Arronche, V. La Saponara, S. Yesil, G. Bayram, Impact damage sensing of multiscale composites through epoxy matrix containing carbon nanotubes. *J. Appl. Polym. Sci.* **128**, 2797-2806 (Jun, 2013) 10.1002/app.38448.

190. M. Monti, M. Natali, R. Petrucci, J. M. Kenny, L. Torre, Impact Damage Sensing in Glass Fiber Reinforced Composites Based on Carbon Nanotubes by Electrical Resistance Measurements. *J. Appl. Polym. Sci.* **122**, 2829-2836 (Nov, 2011) 10.1002/app.34412.

191. A. Naghashpour, S. Van Hoa, A technique for real-time detection, location and quantification of damage in large polymer composite structures made of electrically non-conductive fibers and carbon nanotube networks. *Nanotechnology* **24**, (Nov, 2013) 45550210.1088/0957-4484/24/45/455502.

192. B. R. Loyola *et al.*, Detection of spatially distributed damage in fiber-reinforced polymer composites. *Structural Health Monitoring-an International Journal* **12**, 225-239 (May, 2013) 10.1177/1475921713479642.

193. K. J. Loh, T.-C. Hou, J. P. Lynch, N. A. Kotov, Carbon Nanotube Sensing Skins for Spatial Strain and Impact Damage Identification. *Journal of Nondestructive Evaluation* **28**, 9-25 (Mar, 2009) 10.1007/s10921-009-0043-y.

194. C. S. Grimmer, C. K. H. Dharan, High-cycle fatigue of hybrid carbon nanotube/glass fiber/polymer composites. *J. Mater. Sci.* **43**, 4487-4492 (Jul, 2008) 10.1007/s10853-008-2651-9.

195. M. Nofar, S. V. Hoa, M. D. Pugh, Failure detection and monitoring in polymer matrix composites subjected to static and dynamic loads using

carbon nanotube networks. *Compos. Sci. Technol.* **69**, 1599-1606 (Aug, 2009) 10.1016/j.compscitech.2009.03.010.

196. J. Zhang *et al.*, Single MWNT-Glass Fiber as Strain Sensor and Switch. *Adv. Mater.* **23**, 3392-+ (Aug 9, 2011) 10.1002/adma.201101104.

197. L. Gao, E. T. Thostenson, Z. Zhang, T.-W. Chou, Sensing of Damage Mechanisms in Fiber-Reinforced Composites under Cyclic Loading using Carbon Nanotubes. *Adv. Funct. Mater.* **19**, 123-130 (Jan 9, 2009) 10.1002/adfm.200800865.

198. S. A. Grammatikos, A. S. Paipetis, On the electrical properties of multi scale reinforced composites for damage accumulation monitoring. *Compos. Pt. B-Eng.* **43**, 2687-2696 (Sep, 2012) 10.1016/j.compositesb.2012.01.077.

199. J. Rausch, E. Maeder, Health monitoring in continuous glass fibre reinforced thermoplastics: Manufacturing and application of interphase sensors based on carbon nanotubes. *Compos. Sci. Technol.* **70**, 1589-1596 (Oct 15, 2010) 10.1016/j.compscitech.2010.05.018.

200. J. Rausch, E. Maeder, Health monitoring in continuous glass fibre reinforced thermoplastics: Tailored sensitivity and cyclic loading of CNT-based interphase sensors. *Compos. Sci. Technol.* **70**, 2023-2030 (Nov 15, 2010) 10.1016/j.compscitech.2010.08.003.

201. J. Rausch, E. Maeder, Carbon nanotube coated glass fibres for interphase health monitoring in textile composites. *Materials Technology* **26**, 153-158 (Jul, 2011) 10.1179/175355511x13007211259042.

202. N. D. Alexopoulos, C. Bartholome, P. Poulin, Z. Marioli-Riga, Structural health monitoring of glass fiber reinforced composites using embedded carbon nanotube (CNT) fibers. *Compos. Sci. Technol.* **70**, 260-271 (Feb, 2010) 10.1016/j.compscitech.2009.10.017.

203. N. D. Alexopoulos, C. Bartholome, P. Poulin, Z. Marioli-Riga, Damage detection of glass fiber reinforced composites using embedded PVA-carbon nanotube (CNT) fibers. *Compos. Sci. Technol.* **70**, 1733-1741 (Oct 31, 2010) 10.1016/j.compscitech.2010.07.004.

204. N. D. Alexopoulos, C. Jaillet, C. Zakri, P. Poulin, S. K. Kourkoulis, Improved strain sensing performance of glass fiber polymer composites with embedded pre-stretched polyvinyl alcohol-carbon nanotube fibers. *Carbon* **59**, 65-75 (Aug, 2013) 10.1016/j.carbon.2013.02.055.

205. S. A. Grammatikos, E. Z. Kordatos, T. E. Matikas, A. S. Paipetis, Real-Time Debonding Monitoring of Composite Repaired Materials via Electrical, Acoustic, and Thermographic Methods. *Journal of Materials Engineering and Performance* **23**, 169-180 (Jan, 2014) 10.1007/s11665-013-0672-2.

206. I. Blanco, G. Cicala, C. Lo Faro, A. Recca, Development of a toughened DGEBS/DDS system toward improved thermal and mechanical properties by the addition of a tetrafunctional epoxy resin and a novel thermoplastic. *J. Appl. Polym. Sci.* **89**, 268-273 (Jul 5, 2003) 10.1002/app.12179.

207. H. Kim, K. Char, Effect of phase separation on rheological properties during the isothermal curing of epoxy toughened with thermoplastic polymer.

Industrial & Engineering Chemistry Research **39**, 955-959 (Apr, 2000) 10.1021/ie990536x.

208. M. D. Gilchrist, N. Svensson, A fractographic analysis of delamination within multidirectional carbon/epoxy laminates. *Compos. Sci. Technol.* **55**, 195-207 (1995, 1995) 10.1016/0266-3538(95)00099-2.

209. K. Mimura, H. Ito, H. Fujioka, Improvement of thermal and mechanical properties by control of morphologies in PES-modified epoxy resins. *Polymer* **41**, 4451-4459 (Jun, 2000) 10.1016/s0032-3861(99)00700-4.

210. J. Sandler *et al.*, Development of a dispersion process for carbon nanotubes in an epoxy matrix and the resulting electrical properties. *Polymer* **40**, 5967-5971 (Oct, 1999) 10.1016/s0032-3861(99)00166-4.

211. J. K. W. Sandler, J. E. Kirk, I. A. Kinloch, M. S. P. Shaffer, A. H. Windle, Ultra-low electrical percolation threshold in carbon-nanotube-epoxy composites. *Polymer* **44**, 5893-5899 (Sep, 2003) 10.1016/s0032-3861(03)00539-1.

212. I. P. R. T. p. o. PKHH. InChem.

213. R. Zhang, A. Dowden, H. Deng, M. Baxendale, T. Peijs, Conductive network formation in the melt of carbon nanotube/thermoplastic polyurethane composite. *Compos. Sci. Technol.* **69**, 1499-1504 (2009) 10.1016/j.compscitech.2008.11.039.

214. D. Stauffer, A. Aharony, *Introduction to percolation theory*. (Taylor & Francis, 1994).

215. S. Vionnet-Menot, C. Grimaldi, T. Maeder, S. Strassler, P. Ryser, Tunneling-percolation origin of nonuniversality: Theory and experiments. *Phys. Rev. B* **71**, (Feb, 2005) 06420110.1103/PhysRevB.71.064201.

216. R. Zhang, M. Baxendale, T. Peijs, Universal resistivity-strain dependence of carbon nanotube/polymer composites. *Phys. Rev. B* **76**, (Nov, 2007) 19543310.1103/PhysRevB.76.195433.

217. W. Bauhofer, J. Z. Kovacs, A review and analysis of electrical percolation in carbon nanotube polymer composites. *Compos. Sci. Technol.* **69**, 1486-1498 (Aug, 2009) 10.1016/j.compscitech.2008.06.018.

218. J. F. Feller, I. Linossier, Y. Grohens, Conductive polymer composites: comparative study of poly(ester)-short carbon fibres and poly(epoxy)-short carbon fibres mechanical and electrical properties. *Mater. Lett.* **57**, 64-71 (Nov, 2002) 10.1016/s0167-577x(02)00700-0.

219. J. Bouchard, A. Cayla, E. Devaux, C. Campagne, Electrical and thermal conductivities of multiwalled carbon nanotubes-reinforced high performance polymer nanocomposites. *Compos. Sci. Technol.* **86**, 177-184 (Sep 24, 2013) 10.1016/j.compscitech.2013.07.017.

220. H. Deng, R. Zhang, E. Bilotti, J. Loos, T. Peijs, Conductive Polymer Tape Containing Highly Oriented Carbon Nanofillers. *J. Appl. Polym. Sci.* **113**, 742-751 (Jul 15, 2009) 10.1002/app.29624.

221. H. Deng, R. Zhang, C. T. Reynolds, E. Bilotti, T. Peijs, A Novel Concept for Highly Oriented Carbon Nanotube Composite Tapes or Fibres with High

Strength and Electrical Conductivity. *Macromol. Mater. Eng.* **294**, 749-755 (Nov 12, 2009) 10.1002/mame.200900151.

222. H. Deng *et al.*, Preparation of High-Performance Conductive Polymer Fibers through Morphological Control of Networks Formed by Nanofillers. *Adv. Funct. Mater.* **20**, 1424-1432 (May 10, 2010) 10.1002/adfm.200902207.

223. J. Doshi, D. H. Reneker, ELECTROSPINNING PROCESS AND APPLICATIONS OF ELECTROSPUN FIBERS. *Journal of Electrostatics* **35**, 151-160 (Aug, 1995) 10.1016/0304-3886(95)00041-8.

224. D. H. Reneker, I. Chun, Nanometre diameter fibres of polymer, produced by electrospinning. *Nanotechnology* **7**, 216-223 (Sep, 1996) 10.1088/0957-4484/7/3/009.

225. H. Fong, I. Chun, D. H. Reneker, Beaded nanofibers formed during electrospinning. *Polymer* **40**, 4585-4592 (Jul, 1999) 10.1016/s0032-3861(99)00068-3.

226. J. S. Kim, D. H. Reneker, Mechanical properties of composites using ultrafine electrospun fibers. *Polym. Compos.* **20**, 124-131 (Feb, 1999) 10.1002/pc.10340.

227. M. Bognitzki *et al.*, Nanostructured fibers via electrospinning. *Adv. Mater.* **13**, 70-+ (Jan 5, 2001) 10.1002/1521-4095(200101)13:1<70::aid-adma70>3.3.co;2-8.

228. A. Greiner, J. H. Wendorff, Electrospinning: A fascinating method for the preparation of ultrathin fibres. *Angewandte Chemie-International Edition* **46**, 5670-5703 (2007, 2007) 10.1002/anie.200604646.

229. G. Li *et al.*, Novel carbon fiber/epoxy composite toughened by electrospun polysulfone nanofibers. *Mater. Lett.* **62**, 511-514 (Feb 15, 2008) 10.1016/j.matlet.2007.05.080.

230. G. Li *et al.*, Inhomogeneous toughening of carbon fiber/epoxy composite using electrospun polysulfone nanofibrous membranes by in situ phase separation. *Compos. Sci. Technol.* **68**, 987-994 (Mar, 2008) 10.1016/j.compscitech.2007.07.010.

231. H. S. Min, S. C. Kim, Fracture toughness of polysulfone/epoxy semi-IPN with morphology spectrum. *Polym. Bull.* **42**, 221-227 (Feb, 1999) 10.1007/s002890050456.

232. I. 15024. (2001).

233. L. Liu, Y. M. Liang, G. Y. Xu, H. S. Zhang, Z. M. Huang, Mode I interlaminar fracture of composite laminates incorporating with ultrathin fibrous sheets. *Journal of Reinforced Plastics and Composites* **27**, 1147-1162 (Jul, 2008) 10.1177/0731684407086504.

234. D. Brooks, S. Hayes, N. Khan, K. Zolfaghar, G. F. Fernando, *Self-sensing E-glass fibre reinforced composites*. R. O. Claus, Ed., Smart Sensing, Processing, and Instrumentation - Smart Structures and Materials 1997 (Spie - Int Soc Optical Engineering, Bellingham, 1997), vol. 3042, pp. 111-119.

235. G. Kister, B. Ralph, G. F. Fernando, Damage detection in glass fibre-reinforced plastic composites using self-sensing E-glass fibres. *Smart Mater. Struct.* **13**, 1166-1175 (Oct, 2004) 10.1088/0964-1726/13/5/021.

236. D. D. L. Chung, Carbon materials for structural self-sensing, electromagnetic shielding and thermal interfacing. *Carbon* **50**, 3342-3353 (Aug, 2012) 10.1016/j.carbon.2012.01.031.

237. D. J. Wang, D. D. L. Chung, Through-thickness piezoresistivity in a carbon fiber polymer-matrix structural composite for electrical-resistance-based through-thickness strain sensing. *Carbon* **60**, 129-138 (Aug, 2013) 10.1016/j.carbon.2013.04.005.

238. G. P. Carman, M. Mitrovic, *Health monitoring techniques for composite-materials employing thermal parameters and fiber optic sensors*. J. S. Sirkis, Ed., Smart Sensing, Processing, and Instrumentation: Smart Structures and Materials 1994 (Spie - Int Soc Optical Engineering, Bellingham, 1994), vol. 2191, pp. 244-256.

239. Y. Okabe, S. Yashiro, T. Kosaka, N. Takeda, Detection of transverse cracks in CFRP composites using embedded fiber Bragg grating sensors. *Smart Mater. Struct.* **9**, 832-838 (Dec, 2000) 10.1088/0964-1726/9/6/313.

240. B. R. Loyola, V. La Saponara, K. J. Loh, In situ strain monitoring of fiber-reinforced polymers using embedded piezoresistive nanocomposites. *J. Mater. Sci.* **45**, 6786-6798 (Dec, 2010) 10.1007/s10853-010-4775-y.

241. E. T. Thostenson, T. W. Chou, Carbon nanotube networks: Sensing of distributed strain and damage for life prediction and self healing. *Adv. Mater.* **18**, 2837-+ (Nov, 2006) 10.1002/adma.200600977.

242. T. W. Chou, L. M. Gao, E. T. Thostenson, Z. G. Zhang, J. H. Byun, An assessment of the science and technology of carbon nanotube-based fibers and composites. *Compos. Sci. Technol.* **70**, 1-19 (Jan, 2010) 10.1016/j.compscitech.2009.10.004.

243. E. T. Thostenson, T. W. Chou, Real-time in situ sensing of damage evolution in advanced fiber composites using carbon nanotube networks. *Nanotechnology* **19**, (May, 2008) 21571310.1088/0957-4484/19/21/215713.

244. C. Li, E. T. Thostenson, T. W. Chou, Sensors and actuators based on carbon nanotubes and their composites: A review. *Compos. Sci. Technol.* **68**, 1227-1249 (May, 2008) 10.1016/j.compscitech.2008.01.006.

245. T. Takeda, Y. Shindo, T. Fukuzaki, F. Narita, Short beam interlaminar shear behavior and electrical resistance-based damage self-sensing of woven carbon/epoxy composite laminates in a cryogenic environment. *J. Compos Mater.* **48**, 119-128 (Jan, 2014) 10.1177/0021998312469240.

246. E. F. R. da Costa, A. A. Skordos, I. K. Partridge, A. Rezai, RTM processing and electrical performance of carbon nanotube modified epoxy/fibre composites. *Compos. Pt. A-Appl. Sci. Manuf.* **43**, 593-602 (Apr, 2012) 10.1016/j.compositesa.2011.12.019.

List of Publications

1. **Han Zhang**, Yi Liu, Manabu Kuwata, Emiliano Bilotti, Ton Peijs, Improved fracture toughness and integrated damage sensing capability by spray coated CNTs on carbon fibre prepreg. ***Composites Part A: Applied Science and Manufacturing.*** 2015, 70, 102-110.
2. **Han Zhang**, Manabu Kuwata, Emiliano Bilotti, Ton Peijs, Integrated damage sensing in fibre-reinforced composites with extremely low carbon nanotube loadings***. Journal of Nanomaterials.*** 2015, Article Number: 785834.
3. **Han Zhang**, Emiliano Bilotti, Wei Tu, Chun Yee Lew, Ton Peijs, Static and dynamic percolation of phenoxy/carbon nanotube nanocomposites. ***European Polymer Journal.*** 2015, 68, 128-138.
4. **Han Zhang**, Yi Liu, Emiliano Bilotti, Ton Peijs, In-situ monitoring of interlaminar shear damage in carbon fibre composites, ***Advanced Composites Letters,*** 2015, Accepted.
5. **Han Zhang**, Emiliano Bilotti, Ton Peijs, The use of carbon nanotubes for damage sensing and structural health monitoring in laminated composites: A review. ***Nanocomposites***, 2015, Accepted.
6. **Han Zhang**, Anisha Bharti, Zheng Li, Sixuan Du, Emiliano Bilotti, Ton Peijs, Localized toughening of carbon/epoxy laminates using dissolvable thermoplastic interleaves and electrospun fibres. ***Composites Part A: Applied Science and Manufacturing***, 2015, Accepted.
7. **Han Zhang**, Emiliano Bilotti, Ton Peijs, Dissolvable thermoplastic interleaves as a delivery system for CNTs in CFRP. 2015, Paper in preparation.
8. **Han Zhang**, Manabu Kuwata, Emiliano Bilotti, Ton Peijs, Damage sensing in fibre-reinforced composites using carbon nanotube networks by spray coating. ***ECCM15 Conference Proceedings***, Venice, Italy, 2012.
9. **Han Zhang**, Emiliano Bilotti, Ton Peijs, Damage sensing in fibre-reinforced composites using carbon nanotube networks by spray coating. ***ICCM19 Conference Proceedings***, Montreal, Canada, 2013.
10. **Han Zhang**, Manabu Kuwata, Emiliano Bilotti, Ton Peijs, Damage sensing and improved fracture toughness in fibre-reinforced composites using percolated CNT networks. ***Composites Week @ Leuven Conference Proceedings***, Leuven, Belgium, 2013
11. Manabu Kuwata, **Han Zhang**, Emiliano Bilotti, Ton Peijs, Interlaminar toughness improvement of carbon fibre/epoxy composite laminates by electrospun nanofibre interleaves, ***ECCM15 Conference Proceedings***, Venice, Italy, 2012.